Exploring the role of the H4-S4 loop and of the N-terminal His-tag in stabilizing quaternary structure of enolase from *Streptococcus pyogenes*

Veronica P. Quiros

A Thesis

In the Department

of

Chemistry and Biochemistry

Presented in Partial Fulfillment of the Requirements

For the Degree of Master of Science at

Concordia University

Montreal, Quebec, Canada

September 2010

CONCORDIA UNIVERSITY
School of Graduate Studies

This is to certify that the thesis prepared

By: Veronica P. Quiros

Entitled: Exploring the role of the H4-S4 loop and of the N-terminal His-tag in stabilizing quaternary structure of enolase from *Streptococcus pyogenes*

and submitted in partial fulfillment of the requirements for the degree of

Master of Science (Chemistry)

complies with the regulations of the University and meets the accepted standards with respect to originality and quality.

Signed by the final examining committee:

Dr. Guillaume Lamoureux Chair

Dr. Peter Pawelek Examiner

Dr. Paul Joyce Examiner

Dr. Judith Kornblatt Supervisor

Approved by _____
Chair of Department or Graduate Program Director

_____
Dean of Faculty

Date September 27, 2010

ABSTRACT

Exploring the role of the H4-S4 Loop and of the N-terminal His-tag in stabilizing quaternary structure of *S. Pyogenes*

Veronica P. Quiros

Yeast (*Saccharomyces cerevisiae*) enolase is known to be a dimer of identical monomers while *Streptococcus pneumoniae* enolase is a tetramer of dimers. Dimeric enolase is a well-studied ubiquitous protein; however, not much is known about the octameric protein. Therefore, understanding the amino acids that determine quaternary structure could provide important information regarding its role. Based on the crystal structure of both enolases, it was hypothesized that the loop connecting helix 4 (H4) and strand 4 (S4) could be responsible for preventing formation of octamers in yeast enolase (Ehinger *et al.*, 2004). In the octameric enolase this loop contributes to the dimer-dimer interface; however, in yeast enolase this loop is shorter due to the presence of an extra turn at the end of H4. The goal of my project is to understand if the extra turn at the end of H4 will destroy the dimer-dimer interface and prevent the formation of octameric enolase.

In order to study the effects of the extra turn in the octameric enolase, site-directed mutagenesis was performed on the H4-S4 loop. Residues 135-138 were changed from GGFN to ADLS, which corresponds to the amino acid sequence of yeast enolase. The same amino acids were also changed to AAAA, since alanine is known as a helix-forming amino acid. Characterization of the quaternary structure by analytical ultracentrifugation (AUC) showed that the variant enolase proteins are formed by a

mixture of octamers, monomers, dimers and possibly other intermediates. Consistent with this observation, the specific activity of the variant proteins decreased considerably compared to the wild-type, due to a lower percentage of octamers. These results suggest that those amino acids in the extra turn play an important role in quaternary structure.

The second goal of this project is to determine if the polyhistidine tag (His-tag) affects the stability of octameric enolase. This protein is expressed with an N-terminal polyhistidine tag (His-tag) to facilitate the purification processes. The enolase gene also was inserted into a vector which carries a C-terminal His-tag with a thrombin recognition site, permitting removal of the tag. In order to study stabilization, sodium perchlorate, a weak chaotrope, was used to dissociate the octameric enolase (Karbassi *et al.*, 2010). This dissociation was monitored by sedimentation velocity using AUC. Although, His-tagged proteins are commonly used to facilitate purification, we have observed that the His-tag at the N-terminus stabilizes the octameric structure.

Acknowledgments

I especially thank my research supervisor Dr. Mary Judith Kornblatt for her invaluable help, patience and guidance during the completion of this project. Dr Kornblatt's supervision was a vital instrument to transmit her vast knowledge and experience, facilitating my learning process and understanding of biochemistry, in particular of enolase.

I also want to make a special note for Dr. Jack A. Kornblatt. This project would never become true without his financial support. His passion for science drives him beyond the technical expertise to invest in projects like mine. My sincere gratitude for believing in this project.

I would like to thank my committee members Dr. Paul Joyce and Dr. Peter Pawelek for their excellent suggestions and efforts in following the progress of my work. Their insights provided exciting directions to investigate and analyze, enriching my research about enolase.

I would like to thank Nadia Schoonhoven for her sincere friendship and for amazing help editing this thesis. Our long days at the Lab and the office are finally paying off with this thesis.

There are no words to thank my husband Luis for his unconditional love, support, encouragement and patience, especially when I couldn't spend enough time with him. I am really fortunate and blessed to have such a wonderful friend as a life partner.

I also must extend the warmest expression of gratitude to my parents and brothers for their continued love and encouragement as I achieved each small step toward my goal. My mom and dad were always there to support me whenever I called them, and willing to listen and boost my confidence.

Last but not least, I want to thanks my friends for all their support and companionship. Hanging out with them was always refreshing. They helped me clear my mind, take a break, and see things in a different perspective.

Table of Contents

List of Figures

List of Tables

List of Abbreviation

2-PGA	2-Phosphoglyceric acid
A.C.S.	American Chemical Society
Amp	Ampicillin
APS	Ammonium persulfate
AUC	Analytical Ultracentrifugation
bp	Base pair
CD	Circular Dichroism
CIAP	Calf intestinal alkaline phosphatase
dH_2O	Distilled water
DLS	Dynamic light scattering
DNA	Deoxyribonucleic acid
dNTP	deoxyribonucleotide triphosphate
ε	Molecular extinction coefficient
E. coli	*Escherichia coli*
EDTA	Ethylenediaminetetraacetic acid
ESI-Q-TOF	Electrospray ionization- Quadrupole time-of-flight
EtOH	Ethanol
FPLC	Fast protein liquid chromatography
g	Gravity, units for centrifugal force
HEPES	4-(2-hydroxyethyl)-1-piperazineethanesulfonic acid
His-Tag	Polyhistidine-tag

k_{cat}	Turnover number
K_d	Dissociation constant
K_i	Inhibitory constant
K_m	Michaelis constant
LB	Luria-Bertani medium
MES	2-morpholinoethanesulfonic acid
$Mg(OAc)_2$	Magnesium acetate
NCBI	National Center for Biotechnology Information
NTA	Nitrilotriacetic acid
OD	Optical density
PCR	Polymerase chain reaction
PEP	Phosphoenolpyruvate
PhAH	Phosphonoacetohydroxamate
SDS-PAGE	Sodium dodecyl sulfate polyacrylamide gel electrophoresis
TAE	Tris/Acetate/EDTA
TEMED	N,N,N`,N`-tetra-methylethylenediamine
T_m	Melting temperature
Tris	Tris (hydroxymethyl) aminomethane
UV	Ultraviolet
V_{max}	Maximum velocity

Chapter 1 Introduction

1.1 General introduction: glycolysis and gluconeogenesis

Glycolysis is the metabolic pathway that converts one molecule of glucose into two molecules of pyruvate. In this process there is a net production of two molecules of ATP (form of energy for the cell), and two molecules of NADH (which can produce additional molecules of ATP). Under aerobic condition, pyruvate enters the tricarboxylic acid cycle to produce additional ATP and NADH. In contrast, gluconeogenesis is the synthesis of glucose from pyruvate, with the consumption of ATP, NADH, GTP and water (Berg *et al.*, 2002). The process of glycolysis is carried out by ten different catalytic reactions while gluconeogenesis is a pathway consisting of eleven reactions. There is only one step in the glycolytic and gluconeogenesis pathways that catalyze a dehydration/hydration reaction. This reversible dehydration reaction is carried out by an enzyme called enolase (Garret *et al.*, 2005).

1.2 Enolase

Enolase (2-phospho-D-glycerate-hydrolase; EC 4.2.1.11) is a ubiquitous enzyme responsible for the interconversion of 2-phosphoglyceric acid (2-PGA) and phosphoenolpyruvate (PEP). The enolase reaction in glycolysis involves the removal of a water molecule to form the enol structure of PEP, while in gluconeogenesis it catalyzed the reverse reaction (Figure 1). Enolase is a metalloenzyme, which has an indispensable requirement for certain divalent metal ions as cofactors for its activity. The natural cofactor Mg^{2+} gives the highest activity (Wold, 1957). In addition to their roles in the

catalytic reaction, it appears that the metals have an important structural function in the stabilization of the active form of the enzyme (Brewer *et al.*, 1983; Brewer, 1985).

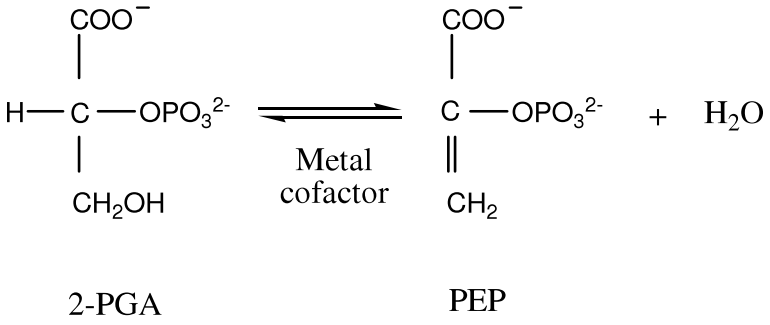

Figure 1 Reaction catalyzed by enolase.

Enolase has been purified and characterized from many biological sources since 1941 when it was first purified from brewers' yeast (Westhead *et al.*, 1964). Enolase may be the most characterized glycolytic protein, and the detailed structural studies have provided a strong basis for understanding fundamental aspects of biochemistry.

Enolase from most species exists as a dimeric protein with a molecular mass ranging from 80 to 100 kDa depending on the organism. Surprisingly, in 1973 *Thermus aquaticus* enolase was discovered to exist as an octamer having a mass of about 350 kDa, in its native form (Stellwagen *et al.*, 1973).

1.2.1. Yeast enolase

The most widely studied enolase is derived from yeast (*Saccharomyces cerevisiae)*. Yeast enolase is a dimeric protein with 436 residues per subunit and a molecular mass of approximately 88 kDa. There are two well-known genes in yeast enolase which have been found to code for two isozymes, enolase 1 (ENO1) and enolase

2 (ENO2) (Holland *et al.*, 1981). Enolase 1 and 2 demonstrate 95% sequence identity and their sequence differ at only 20 of 436 amino acids (Chin *et al.*, 1981). Enolase 1 is the form which has been best characterized and most extensively studied. More recently, the yeast genome has revealed that there are three other genes for enolase called Enolase-Related Repeat (ERR1, ERR2 and ERR3) (Pryde *et al.*, 1995). ERRs have been found to show high sequence identity with both the ENO1 and ENO2 genes (Liti *et al.*, 2005).

In the late 1980's and early 1990's it was confirmed that enolase is composed of two identical subunits facing each other in an anti-parallel manner (Lebioda *et al.*, 1988; Stec *et al.*, 1990). There is a significant amount of information about yeast enolase including its mechanism and structure. Several crystal structures for yeast enolase have been solved including enolase complexes with/without substrate, and complexes with inhibitors and with different metals bound like magnesium, manganese, calcium, and zinc and these structures are available in the Protein Data Bank (http://www.pdb.org).

1.2.2. Octameric enolase

Octameric enolase has been found in a few prokaryotic species such as: *Bacillus stearothermophilus* (Veronese *et al.*, 1984), *Thermotoga maritima (Schurig et al., 1995)*, *Bacillus subtilis (C. K. Brown et al., 1998)*, *Streptococcus pneumonia (Ehinger et al., 2004)*, and *Thermus aquaticus* (Barnes *et al.*, 1973; Stellwagen *et al.*, 1973).

Using electron microscopy and image processing Schurig *et al*. (1995) provided strong evidence that the enolase from *Thermotoga maritima* is arranged as a tetramer of dimers. This was confirmed later by Ehinger *et al*, 2004, when the crystal structure of *Streptococcus pneumonia* enolase was solved.

The reasons for having an octameric versus a dimeric quaternary structure are unknown. Since many of the octameric structures were first isolated from thermophilic species, it was proposed that the reason for having an octameric structure would be to contribute to a higher thermal stability. However, enolases from other thermophilic species have been reported as dimeric, while other nonthermophilic species have shown octameric structure (Brown *et al.*, 1998).

Brown *et al.* (1998) postulated two different evolutionary hypotheses for the quaternary structure of enolase. Their first hypothesis suggests that the ancestral enolase was an octamer and that during the course of the time it had at least three independent evolutionary switches from octamer to dimer. The second hypothesis is that prokaryotic enolases are octameric and eukaryotic enolases are dimeric and that the dimeric *E. coli* enolase is the result of horizontal gene transfer from a eukaryotic species (Brown *et al.*, 1998).

1.3 Multiples roles of enolase

For many years, enolase was considered to be an enzyme abundantly expressed in the cytoplasm and only involved in glycolysis and gluconeogenesis. More recently, surface enolase has been recognized on a variety of eukaryotic epithelial, hematopoetic and neural cell surfaces by fluorescence-activated cell sorting analysis (Redlitz *et al.*, 1995). Surface enolase has also been identified as a plasminogen binding receptor on the cell surfaces of prokaryotes, such as *Streptococcus pneumoniae*, *Streptococcus pyogenes, Streptococcus agalactiae,* as well as a few others (Bergmann *et al.*, 2001; Hughes *et al.*,

2002; Pancholi *et al.*, 1998). The mechanism of enolase translocation to the cell surface is not understood.

Depending on the species, there are other functions that enolase can perform. It has been found that in staphylococci, enolase can act as a laminin-binding protein (Carneiro *et al.*, 2004). Enolase was also found in the cell wall of *Candida albicans.* Supposedly this enolase is involved in cell wall construction and may be an important aspect of *Candida albicans* recognition by the host immune system (Angiolella *et al.*, 1996). In fungal disease, free enolase and anti-enolase antibodies are believed to have the capacity to be useful markers for invasive candidiasis (Pancholi *et al.*, 1998). Enolase has also been identified as a heat-shock protein (Iida *et al.*, 1985). In addition to all these functions, it has been shown that enolase binds to cytoskeletal and chromatin structure, indicating its possible participation in transcription (Pancholi *et al.*, 1998).

Of all of roles mentioned, enolase as a plasminogen receptor has been recently investigated with most interest. Understanding its role as a plasminogen receptor will provide useful information about bacteria and mechanisms of infection.

1.3.1 Plasminogen receptor

The plasminogen system plays a unique role in the host's defences by dissolving fibrin clots and serving as essential role in maintaining homeostasis. Plasminogen is a single-chain glycoprotein with a molecular mass of 92 kDa (Castellino *et al.*, 1981) and is an inactive precursor of plasmin. Its activation involves a tissue plasminogen activator and binding to cell surfaces (Ehinger *et al.*, 2004). The mechanism of plasmin generation from the zymogen plasminogen is crucial in accomplishing fibrinolysis and thrombolysis. Plasmin is generated mainly by the proteolytic action of either tissue-type (tPA) or

urokinase-type (uPA) plasminogen activators (Collen, 2001). Plasminogen possesses a C-terminal binding region consisting of five homologous triple loop kringles and it also has an N-terminal serine protease domain that flanks the Arg-Val site, which is cleaved by tPA and uPA (Cork *et al.*, 2009). Plasmin is a serine-protease that can degrade fibrin directly *in vivo* and can also activate proteolytic systems involved in the degradation of the extracellular matrix (Lopez-Alemany *et al.*, 2003).

Studies have shown that when plasminogen binds to cell surfaces, it is more rapidly activated than soluble plasminogen, and cell-bound plasmin is protected from inactivation by its primary inhibitor, α_2-antiplasmin (Redlitz *et al.*, 1995; Sahoo *et al.*, 2008). In 1991, studies in human cells reported enolase to be on the cell surface. Experiments using ligand blotting show that human enolase is capable of binding plasminogen. This was one of the first experiments suggesting enolase as a plasminogen receptor (Miles *et al.*, 1991). Enolase has been also localized on the surface of several pathogens like fungi, protozoa, and bacteria (Pancholi, 2001). Gram positive bacteria, like *Streptococcus pneumonia,* also bind to plasminogen. The C-terminal domain of enolase in this bacterium functions as a plasminogen-binding site, where it interacts with the kringle domains of plasminogen (Cork *et al.*, 2009). In this case, the bacteria are most likely not involved in dissolving clots. It is believed that bacterial binding to plasminogen may provide a strategy for the bacteria to spread more easily upon plasminogen activation (Bergmann *et al.*, 2001).

1.4 Enolase primary sequence comparison between species

Enolase has been characterized in an extensive variety of species and numerous enolase amino acid sequences can be found in the SWISS PROT database (http://expasy.ch/cgi-bin/sprot-search-de). Both the primary sequence and the tertiary structure are considered to be evolutionarily conserved among species (Hosaka *et al.*, 2003). Figure 2 shows the sequence alignment of enolase from six species: two have been identified as octameric (*Streptococcus pneumonia, Streptococcus pyogenes*), and four with a dimeric quaternary structure (*Enterococcus hirae, Escherichia coli, Saccharomyces cerevisiae,* and lobster).

```
S. pyogenes     MSIITDVYAREVLDSRGNPTLEVEVYTESGAFGRGMVPSGASTGEHEAVELRDGDKSRYL 60
S. pneumoniae   MSIITDVYAREVLDSRGNPTLEVEVYTESGAFGRGMVPSGASTGEHEAVELRDGDKSRYG 60
E. hirae        MSIITDVYAREILDSRGNPTIEVEVYTESGAFGRGMVPSGASTGEYEAVELRDGDKARYG 60
E. coli         MSKIVKIIGREIIDSRGNPTVEAEVHLEGGFVGMAAAPSGASTGSREALELRDGDKSRFL 60
S. cerevisiae   -MAVSKVYARSVYDSRGNPTVEVELTTEKGVF-RSIVPSGASTGVHEALEMRDGDKSKWM 58
Lobster         --SITKVFARTIFDSRGNPTVEVDLYTSKGLF-RAAVPSGASTGVHEALEMRDGDKSKYH 57
                   : .: .* : *******:*.::  . * .  . .*******  **:*:*****:::

S. pyogenes     GLGTQKAVDNVNNIIAPAIIG--YDVRDQQAIDRAMIALDGTPNKGKLGANAILGVSIAV 118
S. pneumoniae   GLGTQKAVDNVNNIIAPAIIG--YDVRDQQAIDRAMIALDGTPNKGKLGANAILGVSIAV 118
E. hirae        GKGVTKAVDNVNNIIAPAIIG--YDVRDQMAIDKAMIALDGTPNKGKLGANAILGVSIAV 118
E. coli         GKGVTKAVAAVNGPIAQALIG--KDAKDQAGIDKIMIDLDGTENKSKFGANAILAVSLAN 118
S. cerevisiae   GKGVLHAVKNVNDVIAPAFVKANIDVKDQKAVDDFLISLDGTANKSKLGANAILGVSLAA 118
Lobster         GKSVFNAVKNVNDVIVPEIIKSGLKVTQQKECDEFMCKLDGTENKSSLGANAILGVSLAI 117
                * .. :**  **. *.  ::    .. :*   *  :  **** **..:******.**:*

S. pyogenes     ARAAADYLEVPLYTYLGGFN-----TKVLPTPMMNIINGGSHSDAPIAFQEFMIMPVGAP 173
S. pneumoniae   ARAAADYLEIPLYSYLGGFN-----TKVLPTPMMNIINGGSHSDAPIAFQEFMILPVGAP 173
E. hirae        ARAAADYLEVPLYHYLGGFN-----TKVLPTPMMNIINGGSHADNSIDFQEFMIMPVGAP 173
E. coli         AKAAAAAKGMPLYEHIAELNGT-PGKYSMPVPMMNIINGGEHADNNVDIQEFMIQPVGAK 177
S. cerevisiae   SRAAAAEKNVPLYKHLADLSKSKTSPYVLPVPFLNVLNGGSHAGGALALQEFMIAPTGAK 178
Lobster         CKAGAAELGIPLYRHIANLAN--YDEVILPVPAFNVINGGSHAGNKLAMQEFMILPTGAT 175
                .:*.*    :*** ::. :          :*.* :*::***.*:.  : :***** *.**

S. pyogenes     TFKEGLRWGAEVFHALKKILKERG--LVTAVGDEGGFAPKFEGTEDGVETILKAIEAAGY 231
S. pneumoniae   TFKEALRYGAEIFHALKKILKSRG--LETAVGDEGGFAPRFEGTEDGVETILAAIEAAGY 231
E. hirae        TFKEALRMGAEVFHALAAILKSRG--LATSVGDEGGFAPNLGSNEEGFEVIIEAIEKAGY 231
E. coli         TVKEAIRMGSEVFHHLAKVLKAKG--MNTAVGDEGGYAPNLGSNAEALAVIAEAVKAAGY 235
S. cerevisiae   TFAEALRIGSEVYHNLKSLTKKRYGASAGNVGDEGGVAPNIQTAEEALDLIVDAIKAAGH 238
Lobster         SFTEAMRMGTEVYHHLKAVIKARFGLDATAVGDEGGFAPNILNNKDALDLIQEAIKKAGY 235
                :. *.:* *:*::* *  : * :       ****** **.:    :..  *  *:: **:

S. pyogenes     EAGENGIMIGFDCASSEFYD-KERKVYDYTKFEGEGAAVRTSAEQVDYLEELVNKYPIIT 290
S. pneumoniae   VPGKD-VFLGFDCASSEFYD-KERKVYDYTKFEGEGAAVRTSAEQIDYLEELVNKYPIIT 289
E. hirae        VPGKD-VVLAMDAASSEFYD-KEKGVY---VLADSGEGEKTTDEMIKFYEELVSKYPIIS 286
E. coli         ELGKD-ITLAMDCAASEFYK-DGKYVL-----AGEGNKAFTSEEFTHFLEELTKQYPIVS 288
S. cerevisiae   D---GKVKIGLDCASSEFFK-DGKYDLDFKNPNSDKSKWLTGPQLADLYHSLMKRYPIVS 294
Lobster         T---GKIEIGMDVAASEFYKQNNIYDLDFKTANNDGSQKISGDQLRDMYMEFCKDFPIVS 292
                    . : :.:* *:***:. .           ..     :  :  .   .: . :**::
```

Figure 2 Alignment of amino acid sequences of enolase from different species. Alignment was created using the web server analysis tool ClustalW2, from the European Bioinformatics Institute, EBI (http://www.ebi.ac.uk/Tools/clustalw2/). Amino acids are colour coded, small hydrophobic amino acids are represented in red, acidic amino acids indicated in blue, basic amino acids shown in magenta, hydroxyl, amine and basic amino acids in green, and other amino acids are indicated in gray. The consensus symbols under the alignments represent: "*" identical amino acids in all sequences of the alignment, ":" conserved substitutions, and "." semi-conserved substitutions.

The percent identity was also compared among species using the alignment tool BLAST, Basic Local Alignment Search Tool, at NCBI (accessed from http://www.ncbi.nlm.nih.gov). A comparison between percentages are shown in Table 1.

	S. pneumoniae	***E. hirae***	***E. coli***	***S. cerevisiae***	**Lobster**
S. pyogenes	93%	80%	58%	49%	48%
S. pneumoniae		83%	58%	49%	49%
E. hirae			65%	49%	50%
E. coli				51%	51%
S. cerevisiae					64%

Table 1 Percent identity between the amino acid sequences of six different enolases

The region where the largest difference is observed in the sequence alignment goes from amino acids 135 to 138, and the region comprising amino acids 244-265 (based on *Streptococcus pyogenes* residue numbers). *S. pyogenes*, *S. pneumoniae* and *E. hirae* possess the same amino acids residues 135-137 (GGFN) and these three enolases share approximately 80% identity, therefore, one would predict that enolase from *E. hirae* is octameric, however the crystal structure of *E. hirae* has been confirmed to be dimeric.

1.5 Overall structure of enolase

There is only one X-ray crystal structure available for octameric enolase. This structure was solved at 2.0 Å resolution from *S. pneumoniae,* by Enhiger *et al.* (2004). Its can be accessed from the Protein Data Bank (http://www.pdb.org) using the PDB entry "1W6T".

The overall structure of enolase from *S. pneumonia* showed high similarity with enolases from yeast (1ONE), lobster (1PDZ), *E. coli* (1E9I) and *Enterococcus hirae* (1IYX). Figure 3 illustrates the superposition of enolase structures from the species mentioned above. The largest difference in structure is observed on loop L3 corresponding to amino acids 244 to 265.

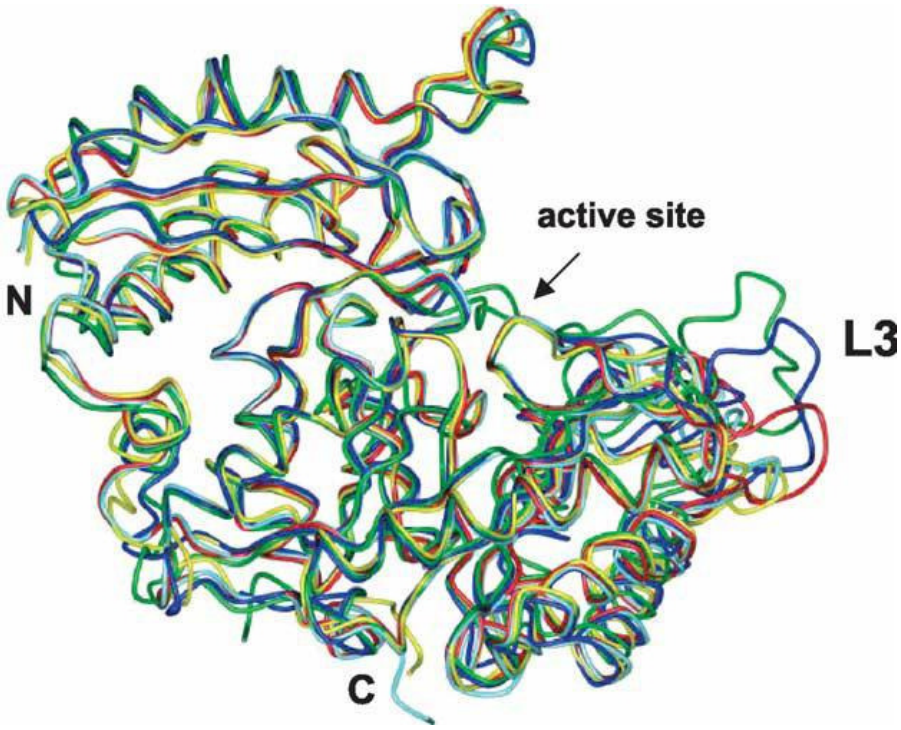

Figure 3 Superposition of enolase structures from different species.
Structures from *S. pneumonia* (red), yeast (green), lobster (blue), *E. coli* (yellow) and *Enterococcus hirae* (cyan) (Ehinger *et al.*, 2004).

All enolase structures reported have similar subunit folding characteristics. Each kidney-shaped monomer of enolase is made up of two domains: the smaller N-terminal domain which in *S. pneumonia* includes residues 1-143 and the larger C-terminal domain comprising residues 144-434 (Ehinger *et al.*, 2004)

1.5.1 The N-terminal domain

Enhiger *et al* (2004) describe a small N-terminal domain from residues 1 to 143 (based on the *S. pneumonia* sequence). It bears a three-stranded antiparallel β-sheet (S1-S3) with tight turns, then continues with four α-helices (H1-H4). After analyzing the PDB text file (1W6T) from the X-ray crystal structure of octameric enolase, a difference

in α-helix and β-sheet numbering was observed as compared with those assigned by Enhiger *et al*. For the purpose of this discussion, the numbering of the α-helices and the β-sheet will follow the same designation provided by Enhiger *et al.* (2004) which is similar to the system employed in publications of enolase from others species. Enhiger *et al.* used a simplified nomenclature counting only the well defined α-helices and the β-sheet.

1.5.2 The C-terminal domain

The C-terminal domain extending from residues 144-434 consists of an eight-stranded mixed α/β-barrel. The eight-stranded α/β-barrel is a frequently occurring folding pattern in many proteins (Hocker *et al.*, 2001). The barrel domain of all members of the enolase superfamily have a distinct $\beta_2\alpha_2(\beta\alpha)_6$ topology (Lebioda *et al.*, 1989). Figure 4 illustrates the topological layout of all enolases. This topology is different from the classical $(\beta\alpha)_8$ found in the TIM barrel. The $(\beta\alpha)_8$-barrel fold, or TIM barrel fold was named for the structure of triose phosphate isomerase (EC 5.3.1.1). The $(\beta\alpha)_8$-barrel structure framework consists of eight β-strands alternating with eight α-helices (Banner *et al.*, 1975). Since the enolase barrel domain has the unusual $\beta_2\alpha_2(\beta\alpha)_6$ topology, α-helix H5 and β-strand S5 of the barrel are exchanged in sequence and arranged antiparallel to the other β-strands and the α-helices as compared to the TIM barrel (Ehinger *et al.*, 2004).

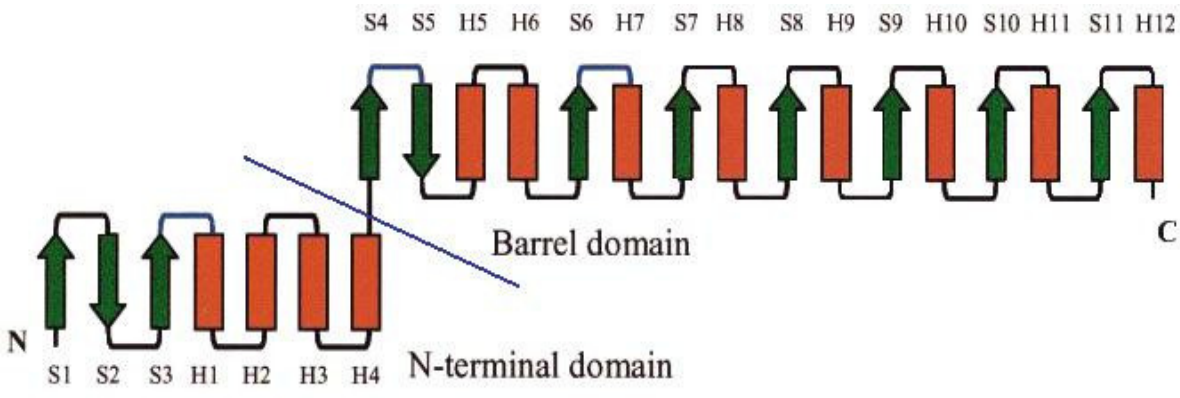

Figure 4 Topology of all enolases.
Arrows represent β-strands (green) with the S notation and the bars (red) represent the α-helices with the H notation. The blue solid line separates the N-terminal domain and the C-terminal domain. Loops that change conformation upon binding of the substrate are labeled blue (between S4 and S5, S6 and H7, and S3 and H1) (Kuhnel *et al.*, 2001).

The major mobile loops of enolase are the loops connecting S3-H1, which closes on the active site, S4-S5 and S6-H7 (shown in blue in figure above). These loops play an important role in the closed and open conformations of the active site (Kuhnel *et al.*, 2001).

1.6 Quaternary structure of enolase

As shown previously, the basic fold of a monomer is the same in all species, however, the quaternary structure can be either dimeric or octameric depending on the organism.

1.6.1 Dimeric enolase

Yeast enolase, along with enolase from other species, has a dimeric quaternary structure with two identical subunits. The quaternary structure resembles that of a butterfly. The crystal structure of yeast enolase is illustrated in Figure 5.

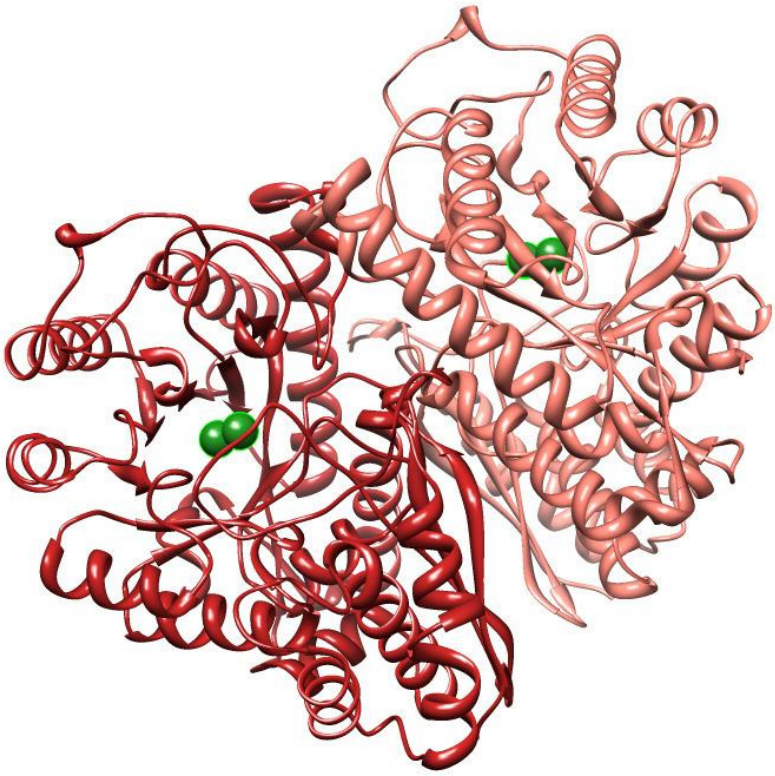

Figure 5 Structure of the dimeric enolase from yeast (1ONE.pdb).
The green spheres represent the Mg^{2+} at the active sites. Figure generated using Chimera (www.cgl.ucsf.edu.chimera/).

One portion of the β-strands of the N-terminus interacts with the large domain of the other subunit. Most of the contacts at the monomer-monomer interface of the dimer are between the atoms of β-strands S1 and S2 of one subunit and the side chains of the last helix (H12) of the barrel domain of the second subunit (Lebioda *et al.*, 1989). Enolase, from all species studied so far has similar subunit contacts at the monomer-monomer interface with a buried surface area of 3575 $Å^2$ (yeast), 3740 $Å^2$ (lobster), 3320 $Å^2$ (*E. coli*). This interaction accounts for 12% or 13% of solvent accessible surface area (Duquerroy *et al.*, 1995; Kuhnel *et al.*, 2001).

1.6.2 Octameric enolase

Crystal structures of enolase from *S. pneumoniae* demonstrate a quaternary structure formed by a tetramer of dimers. The homo-octamer forms a flattened ring like shape; where the N-terminus of each subunit is located towards the center of the ring, while the C-terminal domains form the outer ring (Ehinger *et al.*, 2004). Figure 6 illustrates the quaternary structure of octameric enolase. Figure 6 highlights the dimeric portion, which is similar to the quaternary structure of dimeric yeast enolase.

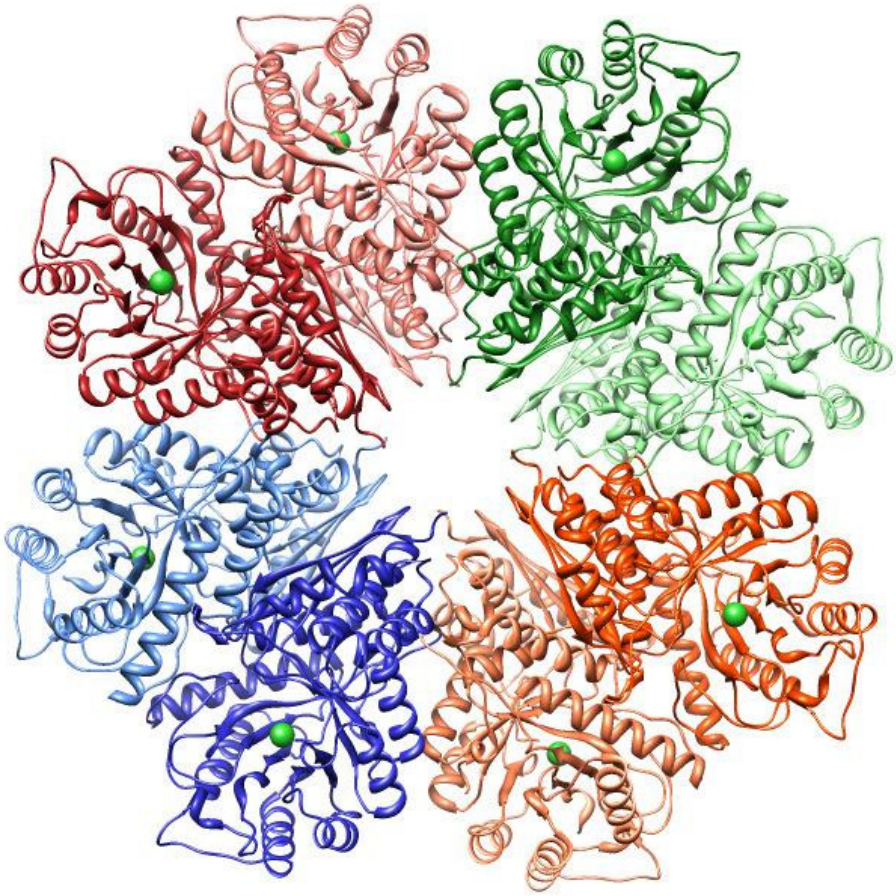

Figure 6 The structure of octameric enolase for *S. pneumoniae* (1W6T.pdb). Dimers are shown in different color. The green spheres represent the Mg^{2+} at the active site. Figure generated using Chimera (www.cgl.ucsf.edu.chimera/).

The monomer-monomer interface has a total buried surface area of 3386 $Å^2$, which is somewhat similar to the one described previously for the dimeric structure. On the other hand, the dimer-dimer interface is smaller burying 2509 $Å^2$ (Ehinger *et al.*, 2004). The dimer-dimer interface is primarily between identical regions of two subunits. Dimer-dimer contacts involve a portion of the N-terminus including: helix 2 (H2, residues 87-99), helix 4 (H4, residues 130-135) and the loop between H4 and strand S4 (H4-S4 loop, residues 136-143). These regions interact with the same region in the nearest subunits. The other points of interaction are at the end of the C-terminal domain involving helix 10 (H10, residues 350-363) which also contacts the same region in the other subunit (Ehinger *et al.*, 2004; Karbassi *et al.*, 2010).

1.7 Dissociation studies

The dissociation of yeast enolase has been studied extensively by different research groups. Most of the methods used to dissociate the dimeric structure produce inactive monomers. Studies have show that the inactive monomers are properly folded and keep most of their secondary structure, even though there is a loss of catalytic activity. Nevertheless, in more recent studies there have been reports of successful dissociation yielding active monomers (Kornblatt *et al.*, 2004).

One of the first methods employed to dissociate the dimers into two monomers was performed by preparing 1 mg/mL enolase in 1 M KCl (a chaotropic salt), in the presence of 2-3 mM EDTA (cation chelator, which remove metal ions from the protein) in the absence of Mg^{2+}. Results from this study have shown the dissociation of the quaternary structure into two inactive monomers. The monomers were identified by

sedimentation equilibrium centrifugation (Brewer *et al.*, 1968). These observations were supported by Gawronski *et al.* (1969). The reversibility of this dissociation was also studied; it was found that enzyme activity was recovered upon the addition of magnesium. This dissociation reversibility was more rapid in the absence of potassium chloride than in its presence (Brewer *et al.*, 1968).

Later in 1971, another research group achieved dissociation of yeast enolase and obtained active monomers by using protein concentrations below 0.7 µg/mL and temperatures above 40 °C. Since physical characterizations are extremely difficult to perform a low concentration, a Sephadex chromatograph was employed to separate monomers and dimers and measure their activity. According to these findings, active monomers were obtained (Keresztes-Nagy *et al.*, 1971). Another research group also used temperature to dissociate yeast enolase into active monomers. According to their results, 50% dissociation was obtained by incubation of 40 µg/mL enolase at 40 ºC. This dissociation was confirmed by determination of the molecular weight using sedimentation equilibrium experiments (Holleman, 1973).

The dissociation of enolase using $NaClO_4$, a weak chaotropic salt, results in inactive monomers (Kornblatt *et al.*, 1996). $NaClO_4$ is believed to perturb the structure of water, this means making the protein's structure less stable by decreasing its hydrophobic interactions and facilitating the hydration of the buried surface area (Collins *et al.*, 1985) or by contributing directly to protein binding thereby favouring the form of the protein with the larger surface area (Arakawa *et al.*, 1982).

Hydrostatic pressure is considered to be a reasonably gentle technique to dissociate dimeric enolase into active monomers (Kornblatt *et al.*, 2004). This technique

was first employed in 1981 when it was used to dissociate yeast enolase and the dissociation was found to be reversible (Paladini *et al.*, 1981). Extensive studies on the dissociation of enolase though hydrostatic pressures have been performed by Kornblatt *et al.* Their experiments confirmed that this dissociation process was fully reversible and the monomers formed by this method were inactive (Kornblatt *et al.*, 1998) or active (Kornblatt *et al.*, 2004) depending on the enzyme used and the presence and identity of divalent metals.

More recently, the dissociation of octameric enolase has been investigated in our lab. This dissociation was examined with $NaClO_4$ which was then monitored by sedimentation velocity. $NaClO_4$ dissociated the octameric structure into inactive monomers without a significant formation of dimers (Karbassi *et al.*, 2010).

1.8 Catalytic mechanism overview

Even though since 1974, enolase from a few species was believed to exhibit an octameric structure, not many studies have been performed in reference to its catalytic mechanism. Since dimeric and octameric enolases share similar monomeric subunits, it is believed that their catalytic reactions must be similar.

1.8.1 Active site

Studies on yeast enolase have shown that the active site is located at the C–terminal end of the β-barrel. The active site also consists of a small portion of the N-terminal domain and two long loops that stick out from the barrel domain forming a wide cavity in that region (Lebioda *et al.*, 1989). The crystal structure of enolase from lobster, *E.coli*, yeast, *E. hirae*, human and *S. pneumoniae* show that the active site is highly

conserved (Duquerroy *et al.*, 1995; Ehinger *et al.*, 2004; Hosaka *et al.*, 2003; Kang *et al.*, 2008; Kuhnel *et al.*, 2001; Lebioda *et al.*, 1989), and in all of these six species the active sites have the same residues involve in metal binding coordination in the same orientation. In octameric enolase from *S. pneumoniae* the high affinity Mg^{2+} site is completely occupied and is octahedrally coordinated by Asp 242, Glu 291, Asp 318 as well as three water molecules (Ehinger *et al.*, 2004).

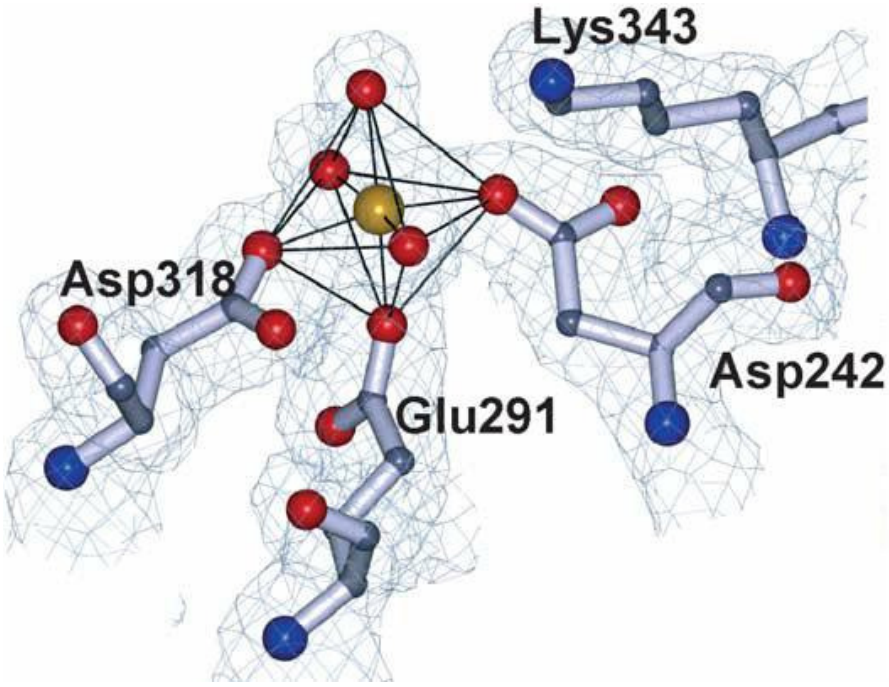

Figure 7 Electron density view of the coordination of Mg^{2+} in *S. pneumoniae* enzyme. Mg^{2+} is represented in yellow. This coordination involved Asp 242, Glu 291, ASP 328 and three water molecules (Ehinger *et al.*, 2004).

1.8.2 Metals as cofactors

As mentioned previously, enolase is a metalloenzyme requiring two divalent ions per active site to produce catalytic activity. Two binding sites have been formally observed by X-ray crystallography (Wedekind *et al.*, 1994; Zhang *et al.*, 1994). One

binding site binds the first metal ion with high affinity (Faller *et al.*, 1977). The binding of this metal ion produces conformational changes in the overall structure of the protein, as demonstrated by absorption spectroscopy and circular dichroism (Brewer *et al.*, 1980; Collins *et al.*, 1982). The presence of the first metal ion allows substrates or substrate analogues to bind, followed by the binding of the second metal ion. The second metal binding to the enzyme is required in order for catalysis to occur. This binding also is followed by conformational changes (Faller *et al.*, 1977). There are many studies which have shown that an elevated concentration of divalent metals inhibits enolase activity (Faller *et al.*, 1977; Vinarov *et al.*, 1999). There are some researchers who propose the presence of a third metal binding site (Brewer *et al.*, 1983; Elliott *et al.*, 1980; Faller *et al.*, 1977), but this theory has been disputed. Other research groups believe that there is no third inhibitory site, but instead their results indicate a classical product inhibition (Poyner *et al.*, 2001).

Metals such as manganese, zinc, cadmium, cobalt, nickel and other divalent metal ions have been found to provide activity and these metals are therefore called 'activators'. In the other hand, metals such as calcium, barium or copper are able to bind but do not produce enzymatic activity, and therefore are called 'non activators' (Brewer *et al.*, 1983).

1.8.3 Enolase mechanism

Early studies in the reaction mechanism suggests that the elimination of water from 2-PGA to give phosphoenolpyruvate proceeds with *anti* stereochemistry (Cohn *et al.*, 1970). For years, the enolase reaction has been intriguing from a mechanism perspective, because it requires the abstraction of a relatively non-acidic proton at

position C-2 (pKa of ~28-32) and elimination of an OH^- which is considered to be a poor leaving group. Experimental data suggest that the dehydration reaction is a stepwise reaction involving two steps. In the first step, a base abstracts the proton from C-2 of 2-PGA to form a carbanion. The second step is the elimination of the hydroxyl group and the formation of a double bond between C-2 and C-3. Finally, the product is released (Dinovo *et al.*, 1971; Lebioda *et al.*, 1991). This stepwise model is shown in Figure 8.

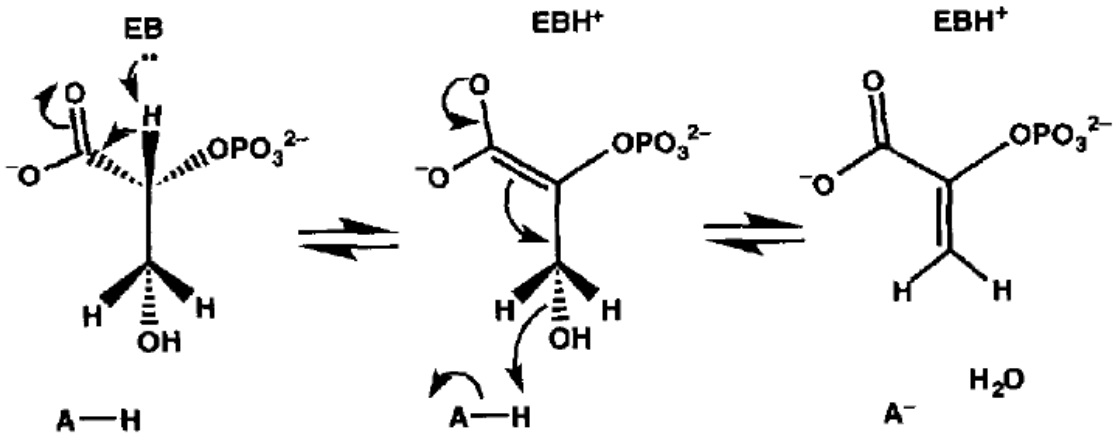

Figure 8 Stepwise mechanism of enolase.
A (acid), EB (enzymatic base) (Reed *et al.*, 1996).

There have been many studies that try to explain the characteristics of the acid/base catalyst in the reaction mechanism of enolase. The proposal that has obtained the most acceptance among investigators is that enolase catalytic scheme involves Lys 345. This proposal emerged from studies in the structure of the enolase complexes with phosphonoacetohydroxamate (PhAH), a tight binding inhibitor. PhAH is known to mimic the structure of the enolase aci-carboxylate intermediate reaction (Anderson *et al.*, 1984). The structure of the PhAH complex shows that the C-2 proton of 2-PGA would be exposed to Lys 345 (Lys 342 in *S. pneumoniae*) if the carboxylate moiety of the

substrate occupied a position analogous to that of the carbonyl oxygen of PhAH in the active site. Also, Lys is located in close proximity to C-2 (Wedekind *et al.*, 1994). This proposal was supported by the experimental data gathered by Poyner *et al.* (1995), when site-directed mutagenesis was performed to change three amino acids [168 (E168Q), 211 (E211Q) and 345(K345A)], proposed previously to be the base catalyst. All three variant proteins showed a significant decrease in their overall activities compared to the wild-type protein. The E168Q and E211Q variants were able to catalyze the C-2 proton exchange of 2-PGA with D_2O, while the K345A variant failed to catalyze this first step of the reaction. Poyner *et al.* (1996) also studied the second step of the reaction by mimicking the addition of OH^- to the C-3 position of PEP in the reverse reaction. Experimental data show that all three proteins were affected in their abilities to carry out this reaction in the following order: E211Q >> E168Q > K345A. Since it is believed that the enolase catalyzed elimination of water from 2-PGA via an *anti*-stereochemistry, it was therefore proposed that the catalytic acid may be the carboxyl side chain of Glu211. Glu211 is on the opposite side to Lys345 and is proximate to the hydroxymethyl group of 2-PGA, facilitating the removal of the C-3-OH. These results evidently implicate Lys 345 in the first step of the reaction and Glu 211 in the second step of the enolase reaction (Poyner *et al.*, 1996).

1.9 Research objectives

Dimeric enolase has been studied for many years, but the investigation of octameric enolase is still its early stages. The recent crystal structure of octameric enolase from *S. pneumoniae* has provided useful information regarding its quaternary

structure, which differs from that of yeast enolase. One of the questions that remains unanswered is why enolase is octameric in some species while dimeric in others.

Brown *et al.* (1998) proposed that four residues (135-138) of yeast enolase prohibit octameric structure formation. Ehinger *et al.* (2004) agreed with the hypothesis above, indicating that the loop connecting helix 4 (H4) and strand 4 (S4) could be responsible for preventing octamer formation in yeast enolase. In the octameric enolase this loop forms the dimer-dimer interface; however, in yeast enolase this loop is shorter due to the presence of an extra turn at the end of H4. Ehinger's research group proposed that substituting an amino acid at the end of H4 in octameric enolase may destroy this dimer-dimer interface and prevent the formation of the octamer. In other words, substituting the second glycine (136) with a bulkier amino acid (for example, aspartic acid, which is present in yeast enolase) and inserting three to five residues at the end of H4, creating an extra turn at the end of H4 that may prevent octamer formation (Ehinger *et al.*, 2004).

The main goal of this project is to better understand if an extra turn at the end of H4 will destroy the dimer-dimer interface and prevent the formation of octameric enolase. Yeast enolase is used as a model, primarily because it is a well-known form of dimeric structure. Figure 9 shows the superimposition of enolases from *S. pneumoniae* and yeast. The amplified section in the figure corresponds to the dimer-dimer interface and the lighter color shows amino acids 135-138 in both structures. In yeast (pink), the amino acid sequence at this specific region comprises alanine, aspartic acid, leucine and serine (ADLS) while the sequence in the octameric enolase (blue) is glycine, glycine, phenylalanine, and asparagine (GGFN). In order to study the effects of this extra turn in

the octameric enolase, site-directed mutagenesis was performed on the loop connecting H4-S4 (amino acid 135-138). These amino acids were changed from GGFN to ADLS, the last four amino acids at the end of Helix 4 in yeast enolase. Also, a second variant was generated using four alanines (AAAA) since alanine is known for its characteristic helix formation and would more likely induce the extra turn in the helix.

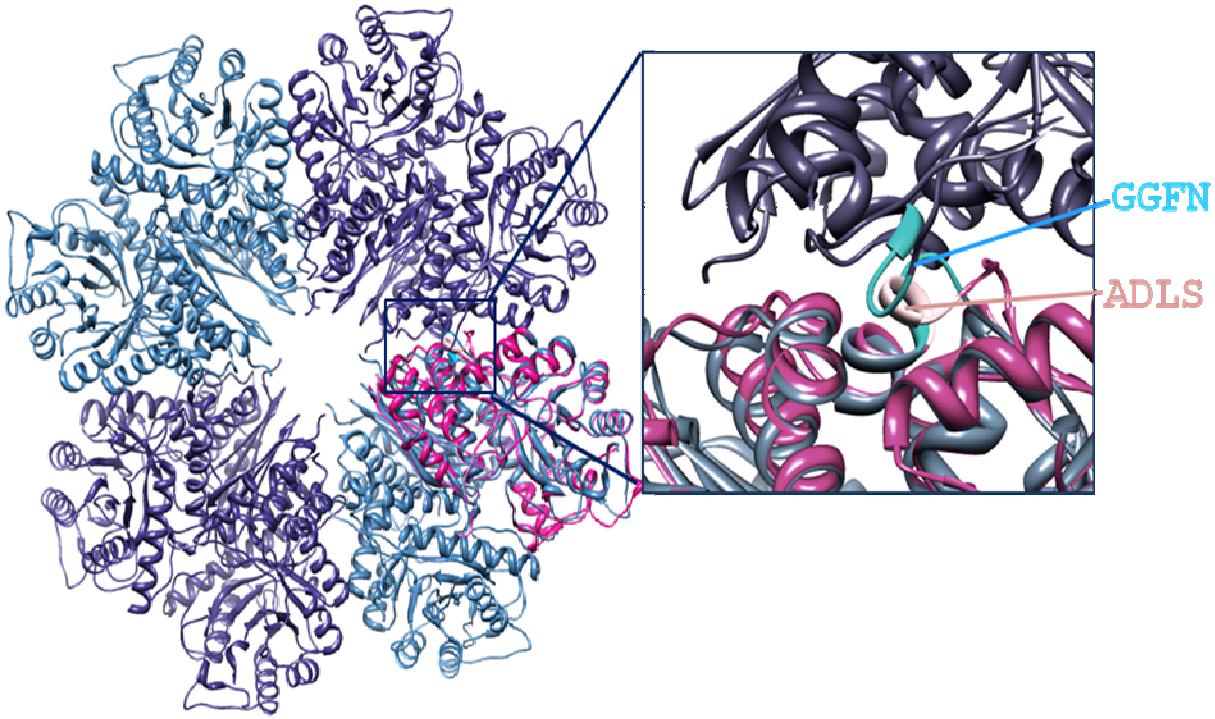

Figure 9 Enolase superimposition from *S. pneumoniae* (blue) and monomer yeast (pink). The dimer-dimer interface is amplified and shown in the right side. Amino acids 135-138 are highlighted in light blue and pink.

The basic characterizations of both wild-type and variant proteins were performed. This characterization included the use of spectroscopic techniques to analyze structural differences and temperature stability, and the use of a chaotropic salt to analyze dissociation.

In our lab, we work with an octameric enolase from *Streptococcus pyogenes*. This gene for enolase had previously been inserted into the pET-14b vector, which carries an N-terminal polyhistidine tag (His-tag). A His-tag is an amino acid motif incorporated into the protein. This motif is usually composed of six or ten histidine (His) residues either at the N or C terminus of the protein. This his-tag may also be followed by an amino acid sequence that facilitates the removal of the tag using proteases. Normally, these tags are included to facilitate protein purification because of their binding affinity to Ni-NTA resin.

The second goal of this project was to determine whether the presence of the His-tag affected the stability of octameric enolase. Since the His-tag is located at the N-terminus, toward the center of the quaternary structure of the protein, it is not accessible for cleavage. To overcome this challenge, the gene of octameric enolase was inserted into a pET-52b(+) vector which carries a C-terminal His-tag with a thrombin recognition cut site, allowing the removal of the tag. In order to analyze stabilization, sodium perchlorate was used to dissociate octameric enolase. This dissociation was monitored by sedimentation velocity using analytical ultracentrifugation (AUC). Also, thermal denaturation studies were performed to compare the N-terminal, C-terminal and No His-tag proteins to determine the effect of the His-tag on protein stability.

Chapter 2 Materials and Methods

2.1 Plasmid

A pET-14b plasmid containing the gene for octameric enolase from *Streptococcus pyogenes* was a generous gift from Dr. Vijay Pancholi (Department of Pathology, Ohio State University, Columbus, Ohio, USA). The resulting plasmid codes for a protein with an N-terminal his-tag, followed by a linker containing a thrombin cleavage site.

E. coli strain XL1-Blue was used for propagation of the plasmid and strain BL21(DE3) was used for expression of the protein.

2.2 Growth medium

Luria broth (LB) was prepared using 1% (*w/v*) tryptone, bacteriological grade, 0.5% yeast extract (Bioshop Canada, Inc.) and 1% NaCl (A.C.S. grade, Fisher Scientific) dissolved in distilled water (dH_2O) and adjusted to pH 7.0 using NaOH. LB plates were prepared using 1.5% (*w/v*) agar (technical grade, Oxoid Ltd.) dissolved in LB. Both LB medium and agar mixture for the plates were sterilized using the liquid 30 cycle program in the autoclave (Amsco® Century™ SV-120 Scientific Prevacuum Sterilizer). After sterilization, the solution of LB and agar for the plates was cooled using a water bath at 53 ºC; ampicillin was then added to a final concentration of 100 µg/mL. This solution was poured into Petri plates next to a flame using sterile techniques. Plates were allowed to solidify and then stored at 4 ºC.

Typically, a 100 mg/mL stock solution of ampicillin was prepared in sterile dH_2O, sterilized by filtration using a 0.45 µm Nalgene syringe filter and stored at -20 ºC.

2.3 Transformation

Transformations of plasmids into *E. coli* BL21(DE3) or XL1-Blue were done by incubating on ice 1 µl of DNA and 100 µL of the desired competent cells for 40 minutes, followed by a 90 second heat shock in a 42 ºC water bath. Sterile LB medium (100 µL) was added and the cells were grown at 37 ºC, 225 rpm for 1.5 hours. Then, 25 µL of culture were plated on LB agar containing 0.1 mg/mL ampicillin. Plates were incubated overnight at 37 ºC. The following morning, plates were checked for colonies and stored at 4 ºC.

2.4 Plasmid DNA extraction

Plasmid DNA was extracted from 10 mL of an overnight culture using the Wizard® *Plus* Minipreps DNA Purification System from Promega. The protocol and solutions used for the plasmid DNA extraction were provided with the system. Once the DNA extraction was completed, the DNA was stored in sterile distilled water at -20 ºC. The DNA concentration was determined by UV absorbance assuming an OD_{260} of 1 corresponds to 50 µg/mL of double stranded DNA. DNA purity was considered to be reasonable when the ratio $OD_{260/280}$ was above 1.7 (Sambrook *et al.*, 1989).

2.5 Restriction enzyme digestion

Restriction enzymes purchased from Fermentas Life Science, Promega, or New England BioLabs were used for different purposes, including the verification of site-directed mutagenesis. DNA (~0.5 µg) was digested in a total volume of 20 µL with 1 µL (10 units) of restriction enzyme and 2 µL of appropriate buffer provided by the supplier

for 1 hour at 37 °C. The restriction enzymes used included: *Bam*HI, *Nde*I, *Sca*I, *Sac*I, *Sac*II, *Nco*I, and *Pci*I.

2.6 Agarose gel electrophoresis

Agarose gel electrophoresis was used to separate and analyze DNA (Sambrook *et al.*, 1989). For a 1% gel, 0.5 g of agarose was weighed (ICM Biomedical) and dissolved in 50 mL 1x TAE buffer, 40 mM Tris (Bioshop Canada, Inc), 20 mM acetic acid (EMD^{TM}), and 1 mM EDTA (Fluka Biochemika) at pH 8.0, by heating for 1 minute in a microwave. After the agarose was dissolved, ethidium bromide was added at a concentration of 1 µg/mL and the gel was allowed to solidify. Samples were diluted using 3.3 µl of 6x blue/orange loading dye (Promega) and loaded into wells. Electrophoresis was carried out in 1x TAE buffer at 90-100 V until the loading dye reached near the end of the gel, approximately 1 hour. Bands were visualized using a UV-transluminator (Alpha Innotech Fluorchem®FC2). The standard molecular marker used was Lambda (λ) DNA (*Eco*RI/*Hind*III) purchased from Fermentas Life Sciences.

2.7 Site-directed mutagenesis

Site-directed mutagenesis was carried out using the QuikChange method from Stratagene (La Jolla, CA, USA). Oligonucleotides were designed as recommended by the QuikChange Site-Directed Mutagenesis Kit (Instruction Manual). Oligonucleotides were synthesized and HPLC purified by BioCorp (Montreal, QC) and resuspended in 250 µl of sterile dH_2O. The concentration of each oligonucleotide was determined by measuring OD_{260}, assuming that OD_{260} of 1 corresponds to 33 µg/mL of oligonucleotide

(Brown, 1991). Table 2 describes the oligonucleotides used to introduce the desired mutation.

Mutations	5' Oligonucleotides 3'	Restriction Enzymes
Leu[137]-Phe	CCTTGGCGGA**T**TCAACACTAAAGTACTTCCAACTCC	*Sca*I
Asn[138]-Ser	CCTTGGCGGACTC**AGC**ACTAAAGTACTTCCAACTCC	*Sca*I
Gly[136]-Asp	CACTTACCTTGGCG**AC**CTCAGCACTAAAGTTCTTCCAACTCC	~~*Sca*I~~
Gly[135]-Ala	CACTTACCTTG**C**CGACCTCAGCACTAAAGTACTTCCAACTCC	*Sca*I
AAAA	CCACTTTACACTTACCTTG**C**CG**CC**GCGGCCACTAAAGTACTTCCAACTCC	*Sac*II

Table 2 Oligonucleotides used for Site-directed Mutagenesis.
Oligonucleotides underlined represent silent mutations where a restriction site was inserted or deleted. Bold letters represent the modified codons.

The thermal cycling was performed using a GeneAmp® PCR System 9700 from Applied Biosystems. The reaction mixture contained 250 ng of each oligonucleotide, 200 ng of double stranded DNA, 200 µM dNTP mix, 1x *Pfu* buffer containing $MgSO_4$ and 5 units of *Pfu* DNA polymerase (Fermentas Life Sciences) in a final volume of 100 µL with water. The *Pfu* was added after the initial denaturation step at 95 ºC. Table 3 shows the temperature, times and cycles used.

Step	Temperature	Time	Number of cycles
Initial denaturation	95 ºC	1.5 min	1
Denaturation	95 ºC	0.5 min	16
Annealing	54 ºC	1.0 min	
Extension	72 ºC	14 min	

Table 3 Cycles and temperatures for the site-directed mutagenesis.

Methylated parental DNA was digested with 10 units of *Dpn*I (Fermentas Life Sciences) for 1 hour at 37 ºC. The digested PCR products were transformed into XL1-Blue *E. coli* competent cells. The transformation procedure was followed as described in section 2.3. Five colonies were selected and inoculated into five different tubes containing 5 mL LB, supplemented with ampicillin to a final concentration of 100 µg/mL. Cells were grown overnight in a shaker incubator at 225 rpm, 37 ºC. Plasmid DNA was extracted using the Wizard® *Plus* Minipreps DNA Purification System (section 2.4).

2.8 Plasmid DNA construction in pET-52b(+) vector

Insert DNA was changed from pET-14b vector to pET-52b(+) which carries a sequence that encodes for a C-terminal His-Tag with a thrombin cleavage site.

2.8.1 Cloning and PCR

The octameric enolase gene in pET-14b vector was amplified by polymerase chain reaction (PCR) using the oligonucleotides in Table 4. This experiment allowed the creation of a DNA sequence with restriction sites that will form sticky ends, which were needed for ligation into the new vector.

Restriction enzyme	**Oligonucleotides**
*Pci*I	GGCAGCCACATGTCAATAATAACTGATG
*Sac*I	CCGGATCGAGCTCTTTTTTTAAGTTATAGAATG

Table 4 Oligonucleotide for PCR.
Restriction enzyme cut site underlined.

The reaction mixture contained 250 ng of each oligonucleotide, 200 ng of template DNA, 200 µM dNTP mix, 1x *Pfu* buffer containing $MgSO_4$ and 5 units of *Pfu* DNA polymerase in a final volume of 100 µL. The *Pfu* was added after the initial denaturation step at 95 ºC. Table 5 shows the temperatures, times and cycles used for PCR.

Step	Temperature	Time	Number of cycles
Initial denaturation	95 ºC	1 min	1
Denaturation	95 ºC	0.5 min	35
Annealing	54 ºC	1.0 min	
Extension	72 ºC	4 min	
Final extension	72 ºC	10 min	1

Table 5 Cycles and temperatures for PCR.

The PCR product was digested with 10 units of *Pci*I (New England BioLab) and *Sac*I (from Fermentas Life Sciences) at 37 °C for 1 hour. The digested samples were separated by agarose gel electrophoresis (Section 2.6).

pET-52b(+) (purchased from Novagen) was digested with 10 units of *Nco*I and *Sac*I at 37 °C for 1 hour. Then, 0.5 µL of CIAP (calf intestinal alkaline phosphatase, Promega) was added to the pET-52b(+) digestion mixture and incubated for another 30 minutes at 37 °C. The digested samples were then separated by agarose gel electrophoresis (Section 2.6).

2.8.2 DNA fragment purification

DNA fragments were purified from agarose gels using the phenol freeze-fracture method (Bewsey *et al.*, 1991) as modified by Dr. Paul Joyce group (Chemistry and Biochemistry Department at Concordia University). After the electrophoresis was complete, the desired DNA fragments were excised from the gel and placed in 1.5 microcentrifuge tube. Then, 500 µl of phenol was added and vortexed vigorously. Tubes were incubated at -80 °C for 30 minutes, followed by a water bath incubation at 37 °C for 30 minutes. The vortexing, freezing and thawing procedures were repeated a second time. Next, 200 µl sterile dH_2O and 20 µl 3M NaOAc (Sodium Acetate) at pH 5.2 was added to the tube and vortexed, followed by a centrifugation at 14,000 x *g*, for 5 minutes at 4 °C. The aqueous solution was transferred into a new microcentrifuge tube. Phenol was added (500 µl), vortexed and centrifuged as before and transferred into another tube, this step was repeated twice. Then, 500 µl of ether was added, vortex, centrifuged and the top layer was discarded, this procedure was performed a second time. Then, the DNA was precipitated by adding two volume of 99% ethanol (EtOH) and storing at -80 °C for at least one hour, and recovered by centrifugation. The pellet was washed using 80% EtOH and the sample was desiccated for 30 minutes. The pellet was then resuspended in 20 µl sterile dH_2O.

2.8.3 Ligation

PCR products digested with *Pci*I and *Sac*I were inserted into pET-52b(+) digested with *Nco*I and *Sac*I. Approximately, 200 ng of the insert and 100 ng of DNA vector were ligated in 1X ligase buffer containing 1 unit of T4 DNA ligase (Fermentas Life Sciences)

to a final 20 µL. The mixture was incubated overnight at 4 °C. The ligation mixture was then transformed into XL1-Blue as described in section 2.3.

2.9 Sequencing of DNA

DNA sequencing was carried out by Bio S&T Inc. (Lachine, Quebec). The sequence obtained was aligned with the parental DNA using the BLAST tool. This alignment was used to verify that the desired changes in the nucleotide sequence were properly introduced, and to verify that there were no additional mutations.

2.10 Glycerol stock

Wild-type and variant DNAs were transformed into XL1-Blue competent cells and 25 µL of transformed cells were plated (LB and ampicillin plates) and grown overnight at 37 ºC. Using sterile technique, one colony was selected and inoculated in 10 mL sterile LB with 100 µg/mL ampicillin. Cells were allowed to grow overnight at 37 ºC in a shaker incubator at 225 rpm. Overnight culture was diluted 100-fold in LB supplemented with ampicillin. Cells were allowed to grow until the OD_{600} of the culture reached 0.6, (approximately 3 hours). Glycerol stocks were prepared by mixing 700 µL of culture with 350 µL of 1:1 sterile LB/glycerol (A.C.S. grade, Fisher Scientific). Glycerol stocks were stored at -80 °C in sterile cryogenic vials.

2.11 Preparation of competent cells

LB plates, without ampicillin, were streaked with a glycerol stock of either BL21(DE3) or XL1-Blue. Plates were incubated at 37 °C, overnight. Using sterile

technique, a single colony was inoculated in 5 mL sterile LB and grown overnight at 37 °C, 225 rpm. The following morning, 2.5 mL of the overnight culture was inoculated into 200 mL sterile LB. Cells were incubated at 37 °C, 225 rpm until the OD_{590} reached 0.65-0.7. Then the cells were incubated on ice for 10 minutes. Cells were centrifuged at 5,000 rpm (JA-20), for 15 minutes at 4 °C using pre-sterilized bottles. The supernatant was thoroughly decanted and the pellet was resuspended in 100 mL $MgCl_2$ (sterile and pre-cooled at 4 °C). Cells were pelleted again at 5,000 rpm (JA-20), for 25 minutes, 4 °C. The supernatant was decanted and the pellet was resuspended in $MgCl_2$ as described previously. Cells were incubated on ice for 25 minutes. Cells were then pelleted a final time as above and the supernatant was decanted. Finally, cells were resuspended in 2.8 mL of 50% glycerol, 1 mL $CaCl_2$ and 6.2 mL of dH_2O (all the solutions used were previously sterilized and pre-cooled at 4 °C). Approximately 200 µl aliquots of cells were placed in sterile cryogenic vials and incubated overnight at 4 °C. The following morning, the tubes were gently vortexed and stored at -80 °C. This protocol was obtained from Dr. Paul Joyce which was modified from Capage *et al.*, (1979); Dagert *et al.*, (1979); and Lederberg *et al.*, (1974).

2.12 Protein expression

Plasmid DNA was transformed into *E. coli* BL21(DE3) and plated onto LB plus ampicillin plates (section 2.3). The next morning, one colony was selected and inoculated into 100 mL of sterile LB supplemented with 400 µg/mL ampicillin. Cells were grown overnight at 225 rpm and 37 °C. The following morning, 10 mL of overnight culture was inoculated into 1 L LB supplemented with 400 µg/mL ampicillin.

Cells were allowed to grow in a shaker incubator at 37 °C. Once the cells reached an OD_{650} nm of 0.6, cells were induced with 0.5 M isopropylthiogalactopyranoside (IPTG) purchased from BioShop Canada, Inc. The temperature was lowered to 29 °C and cells were grown for an additional 4 hours. Cells were harvested by centrifugation at 5,000 rpm (JA-20) for 30 minutes at 4 ºC. The cell pellet was stored at -20 °C until further use.

2.13 Protein purification

The cell pellet was resuspended in 15 mL cold buffer A (20 mM HEPES, 300 mM NaCl, 10 mM imidazole, 1 mM magnesium acetate at pH 7.5) containing 0.003g of DNase I (Roche Diagnostics) and 0.003 g of RNase A (BioShop Canada, Inc). The suspension was sonicated using a Branson sonifier 250 to lyse cell walls. Ten bursts of 30 seconds with a 1 minute cooling time between bursts, were used for a 4 g pellet. The lysate was centrifuged at 14,000 rpm (JA-10) for 30 minutes at 4 °C. The supernatant was applied to a 10 mL Ni-NTA (nickel-nitrilotriacetic acid from Qiagen) chromatography column previously equilibrated with buffer A. After washing the column with 30 volumes of buffer A containing 20 mM imidazole, the protein was eluted with buffer B (20 mM HEPES, 300 mM NaCl, 250 mM imidazole, 1 mM magnesium acetate at pH 7.5). Enzymatically active fractions were dialyzed overnight against 200-volumes of TME buffer (50 mM Tris, 1 mM magnesium acetate, 0.1 mM EDTA at pH 7.4). Fractions with high protein concentration and purity were pooled. Purity was determined by SDS-PAGE and the ratio of $OD_{280/260}$ (ratio above 1.7 was considered acceptable). Proteins were stored at 4 °C after precipitation in 85% ammonium sulfate.

2.14 SDS-PAGE

Denaturing SDS-PAGE was performed using a 12% resolving and 4% stacking polyacrylamide gel (Laemmli, 1970). The stacking gel was prepared using 1.5 mL dH_2O, 650 µL 0.5 M Tris-HCl pH 6.8, 325 µL 30% Acrylamide/Bis, 12.5 µL 10% APS, 25 µL 10% SDS, 5 µL TEMED. The resolving gel contained 1.7 mL dH_2O, 1.25 mL 1.5 M Tris-HCl pH 8.8, 2 mL 30% acrylamide/Bis, 25 µL 10% APS, 50 µL 10% SDS, 5 µL TEMED (Bio-Rad). A stock solution of 30% acrylamide/Bis was prepared using 29.2% of acrylamide (electrophoresis grade, Bioshop Canada, Inc.) and 0.8% of N'N'-bis-methylene-acrylamide (electrophoresis grade, Bio-Rad)

The Bio-Rad Mini-PROTEAN® Tetra electrophoresis system was assembled as described by manufacturer's instructions. Protein samples were diluted 1:1 (*v/v*) in sample loading buffer (12.5 mM Tris-HCl, pH 6.8, 2% glycerol, 4% SDS, 1% 2-β-mercaptoethanol, 0.1% bromophenol blue). Samples were boiled for 1 minute prior to loading. Gel electrophoresis was carried out at 200 V in 1x electrode running buffer (0.3% Tris, 1.44% glycine, 0.1% SDS at pH 8.3). Electrophoresis was stopped when the bromophenol blue tracking dye migrated off the resolving gel. The Bio-Rad low range molecular weight protein bands (phosphorylase b 97400 Da, serum albumin 66200 Da, ovalbumin 45000 Da, carbonic anhydrase 31000 Da, trypsin inhibitor 21500 Da, lysozyme 14400 Da) were used to estimate the molecular weights of proteins in the samples. The gel was stained with PageBlue™ Protein Staining Solution (Fermentas Life Scienes) using the fast staining protocol. The gel was first washed with 100 mL dH_2O and microwaved for a minute; this procedure was repeated three times with 4 minutes interval between washes. Then, 20 mL of stain solution was added and the gel was

heated in the microwave for 20 seconds. After 20 minutes the stain solution was removed and the gel was washed with dH_2O.

2.15 Protein dialysis

Proteins were desalted from ammonium sulfate by dialysis at 4 °C against three 200-fold volume changes of the required buffer. The dialysis tubing (6.4 mm or 15.5 mm wet diameter) with a molecular weight cut off of 8 kDa was purchased from BioDesign. Tubing was boiled two times in dH_2O and stored in 1 mM EDTA at 4 °C. Before use, the tubing was washed thoroughly with dH_2O.

2.16 Determination of protein concentration

Protein concentration was determined from the absorbance at 280 nm. The extinction coefficient was calculated by the ExPASY site (http://ca.expasy.org/cgi-bin/protparam) using the ProtParam application. The extinction coefficient calculated was 43320 $M^{-1}cm^{-1}$ for the wild-type protein.

2.17 ESI-Q-TOF mass spectroscopy

Verification of amino acid substitutions was performed by ESI-Q-TOF mass spectrometry. Samples were dialyzed against 50 mM ammonium bicarbonate (Fluka Biochemika), and then diluted to a final concentration of 5 μM in 50% acetonitrile and 0.2% formic acid. The direct injection method was used for molecular mass determination. The signal from the instrument was deconvulated using MassLynx software (version 4.0, 2003, Micromass Ltd). Mass spectrometric analyses were

performed by the Center for Biological Applications of Mass Spectrometry (CBAMS) of Concordia University.

2.18 Removal of the His-tag

Wild-type enolase with the C-terminal His-tag was treated with thrombin protease to remove the histidine tag. Thrombin (GE Healthcare) was resuspended in 500 µL PBS buffer (140 mM NaCl, 10 mM Na_2HPO_4, 1.8 mM KH_2PO_4, 2.7 mM KCl), and 20 µL aliquots were stored at -80 °C. Purified protein was incubated with thrombin (1 unit of thrombin cleaves 1 µg of protein) for 8 hours in a 15 °C water bath. Protein was transferred to a 50 kDa cut off dialysis tubing and dialyzed against buffer A (section 2.13). After 4 hours of dialysis, the protein was passed through a 1 mL Ni-NTA chromatography column equilibrated with buffer A. Then, protein was dialyzed overnight against 200-volumes of TME. Protein concentration was determined, followed by precipitation in 85% ammonium sulfate and storage at 4 °C.

2.19 Activity assay

Enolase activity was assayed by monitoring the production of PEP at 240 nm using a Varian Carry 1 UV-visible spectrophotometer. Assays were performed on a 1.0 cm quartz cuvette (Hellma) at room temperature. Assay buffer contains 50 mM HEPES (Roche), 1 mM magnesium acetate, pH 7.5, titrated with 2 N KOH. Each assay contained 1 mL of assay buffer and 1 mM 2-PGA. Activity assays were initiated by the addition of enolase. The amount of enzyme in the reaction was determined empirically, producing an optimal slope with approximately 0.1 change in absorbance per minute. All

the assays were performed in duplicate and agree within 5% from each other. Since PGA is not commercially available, it was enzymatically synthesized (Sims *et al.*, 2005) by Dr. M.J. Kornblatt.

2.20 Inactivation using sodium perchlorate

A stock solution of 4 M sodium perchlorate (Fluka Chemika) in TME was prepared and stored at 4 ºC. Enolase was dialyzed in 200-volumes of TME, pH 7.4 exchanging buffer three times. Incubations were performed at concentrations varying from 0 to 0.4 M $NaClO_4$. The final protein concentrations were 2.7 µM. After incubation at 15 ºC for 20-24 hours, aliquots were removed and assayed for activity. Inactivation was determined by the average of duplicates assays.

2.21 Analytical ultracentrifugation

Sedimentation velocity analysis was carried out using a Beckman Optima XL-1 analytical ultracentrifugation. Prior to sedimentation, samples were filtered using 2.0 mL Spin-X® Costar centrifuge tube filters with a cellulose acetate membrane of 0.45 µm. Samples were prepared to a concentration of 23 µM (~1.0 mg/mL) and scanned at 280 nm or 2.7 µM (~0.14 mg/mL) and scanned at 228-230 nm.

Sedimentation coefficients were obtained by fitting the data using SEDFIT, version 11.8 (Schuck, 2000). Buffer density and viscosity were determined using Sednterp (sedimentation interpretation) software, version 1.07 (D. B. Hayes, T. Laue and J. Philo, available at www.bbri.org/RASMB/rasmb.html). These values obtained were

used to calculate $s_{20,w.}$ Analytical ultracentrifugation runs were performed by Dr. M.J. Kornblatt.

2.22 Circular dichroism spectroscopy

Far-UV CD spectroscopy was used to compare the overall secondary structures of wild-type enolase and variant proteins. Samples (80 μL) at a concentration of 1.0 mg/mL were scanned from 180-280 nm with a 0.01 cm quartz cell using a Jasco J-815 spectropolarimeter under continuous nitrogen flow. The temperature was kept constant at 20 °C with the use of a Pelletier water bath accessory. The following parameters were used: 5 scan average, 20 nm/min scan rate, 0.2 nm step resolution, 1 second response, 1 nm bandwidth, and sensitivity set to standard (100 mdeg). Each spectrum was smoothed and normalized for protein concentration. Subtraction of the spectrum of the buffer and smoothing of the spectra were performed using the Jasco Spectra Analysis software (version 1.53.04).

Secondary structure analysis was performed using the DICHROWEB, on-line server for protein circular dichroism spectra deconvolution from Birkbeck College, University of London available at http://dichroweb.cryst.bbk.ac.uk (Lobley *et al.*, 2002; Whitmore *et al.*, 2004). Raw data were loaded onto the web server as JASCO 1.50 (with preview) format. The analysis method used was CDSSTR with Reference Set 6; optimized for 185-240 nm (Manavalan *et al.*, 1987).

2.23 Temperature denaturation

Temperature denaturation was followed by monitoring the changes of the CD signal at 208 nm using the 'Variable Temperature' program. The rate of temperature increase was 15 °C per hour from 40-90 °C. The response time used was 0.25 seconds, bandwidth 1 nm, data pitch at 0.2 °C and sensitivity set to standard. A 0.1 cm cell was used together with a 5 mm spacer. A 400 µL aliquot of protein at a concentration of 0.5 mg/mL in phosphate buffer was used.

2.24 Gel filtration

Fast protein liquid chromatography (FPLC) was used to separate oligomeric forms of the protein. Prior to the filtration experiment, 1 L of dH_2O and 1 L of TME buffer were filtered and degassed. Superdex 200 HR (GE Healthcare) gel filtration column was connected to an ÄKTApurifier™ (Amersham pharma biotech) FPLC system. The Superdex 200 column is normally stored in 20% ethanol. 20% ethanol was washed out with two column volumes (50mL) of dH_2O followed by two column volumes of equilibration buffer (TME) at a flow rate of 0.5 ml/min. Initially, 200 µL of sample was injected into the FPLC system; followed by TME buffer, with a flow rate of 0.40 mL/min with a pressure of 1.50 MPa. Absorbance was monitored at 280 nm and 230 nm. Fractions with a volume of 0.4 mL were collected. This experiment was performed at room temperature. The software used to collect and analyze data was UNICORN 4.12.

2.25 Dynamic Light Scattering

Dynamic light scattering (DLS) was used to measure the hydrodynamic radius of the separated sample from the gel filtration experiment. DLS measurements were performed using a Dyna Pro instrument (Wyatt Technology, Santa Barbara, CA, USA) with the cell compartments regulated to 20 °C. Data was acquired in 10 second intervals for every sample analyzed. Protein concentration varied for each sample eluted from the gel filtration column. Experiments were performed by Dr. M.J. Kornblatt.

2.26 Kinetics studies

Enzymatic activity of the octameric enolase (N-terminal His-tag, C-terminal and no His-tag) were examined by monitoring the production of PEP at 240 nm. The change in absorbance was monitored for 1 minute, but just the linear portion of the curve was employed for rate calculation. All assays were done in duplicate. The buffers used for kinetics experiments were either 100 mM HEPES or 25 mM MES and 25 mM Tris at pH 7.1. Buffers were passed thought a 30 mL column of chelex 100 resin (Bio-Rad). Samples of enolase were also chelated using a 1 mL column. Plastic containers were used instead of glass for storage of buffers in order to reduce contamination by divalent cations. Plastic containers and cuvettes were soaked in 20% nitric acid (Fisher Scientific) for at least 2 hours and rinsed thoroughly with dH_2O prior to use. Several stock concentrations (0.01M, 0.1M, 1M) of $Mg(OAc)_2$ and (1 mM, 10 mM, 100mM, 1M) of $MnCl_2$ were prepared. EnzFitter (Biosoft) was used to fit the kinetic data to the Michaelis-Menten equation or to the modified substrate inhibition equation.

Experiments varying 2-PGA concentrations were performed using 1 mL of buffer at fixed concentrations of metal (50 mM Mg^{2+}, 50 µM Mn^{2+}, and 1 mM Mn^{2+}). Experiments varying the concentration of Mg^{2+} were done at 1 mM 2-PGA. The equation used to analyze 2-PGA and Mg^{2+} kinetics was the Michaelis-Menten equation:

$$v = \frac{V_{max} \times [S]}{K_m} + [S]$$

Kinetic versus Manganese as metal cofactor were analyzed using the modified substrate inhibitor equation:

$$v = \frac{V_{max} \cdot [S] + V_2 \cdot \frac{[S]^2}{K_i}}{K_m + [S] + \frac{[S]^2}{K_i}}$$

Where v is the rate of reaction, [S] is the concentration of the metal ion or substrate, V_{max} is the maximum velocity, V_2 is the residual velocity, K_m is the Michaelis constant and K_i is the inhibition constant.

The turnover rate, k_{cat} was calculated using the following equation:

$$k_{cat} = \frac{V_{max}}{[Enzyme] \cdot \varepsilon_{240} \cdot 60\ sec}$$

Where ε_{240} is the extinction coefficient for PEP determined to be 1.33 $mM^{-1}cm^{-1}$.

2.27 Isothermal titration calorimetry

Isothermal titration calorimetry (ITC) data were collected using a VP-ITC MicroCalorimeter (MicroCal^{TM} Inc.) at 15 °C. Protein was dialyzed in MES/Tris buffer with the appropriate divalent metal. The protein concentration was approximately 40 μM. A solution of an equilibrium mixture of PEP/PGA was prepared by dissolving PEP in buffer (MES/Tris, 1 mM $MnCl_2$) to a final concentration of 1 mM. The actual concentration of PEP was determined by measuring its absorbance at 240 nm. A 5 μL sample of concentrated octameric enolase was added to PEP, and the mixture was incubated overnight at 4 ºC. Absorbance at 240 nm was measured again and the concentration of PEP/PGA was determined. Sample solution and buffer were degassed prior to loading into the sample cell and injection syringe. The first injection was 2 μL of PEP/PGA solution, followed by 69 injections of 3μL. The data were analyzed with Origin software (Northhampton, Mass.) using the one site model.

Chapter 3 Results

3.1 Role of Loop 4 determining quaternary structure

The first part of this project involved the design of two enolase variants. The variants were characterized in order to determine the significance of an extra turn at the end of helix 4 on the determination of quaternary structure of octameric enolase.

3.1.1 Site-directed mutagenesis

The enolase gene from *S. pyogenes* had been previously cloned into the multiple cloning site of pET-14b vector between the restriction enzyme cut sites *Bam*HI and *Nde*I. The complete plasmid containing the gene for the octameric enolase is composed of 5973 bp, where the insert is 1312 bp and the vector is 4661 bp in size.

The protein coded for by this plasmid had two amino acids different from the sequence at the National Center for Biotechnology Information (NCBI: Reference Sequence: NP_268959.1). The sequences differed at positions 137 and 363. Position 363 had been corrected from glycine (G) to glutamic acid (E) by Farhad Karbassi. The second amino acid substitution at position 137 was corrected from leucine (L) to phenylalanine (F) using QuikChange site-directed mutagenesis. Oligonucleotides were designed to introduce a mutation that will change an amino acid and insert a silent mutation nearby to generate a restriction site to identify successful variants. Prior to site-directed mutagenesis, the pET-14b vector and insert contained one *Sca*I restriction site. With the introduction of a second restriction site for *Sca*I, digestion fragments of 1918 bp

and 4055 bp were generated. After this correction, the encoded protein is referred to as 'wild-type'.

A variant octameric enolase was created containing four mutations compared to the wild-type. Residues 135-138 were changed from GGFN to ADLS. Since the original sequence received from Dr. Pancholi already had phenylalanine 137 changed to leucine, this original sequence was used as a template. The other three mutations were performed one at a time and were screened by the insertion or deletion of the *Sca*I restriction enzyme cut site. First asparagine (N) 138 was changed to serine (S) with the insertion of a *Sca*I restriction site. The second mutation involved the conversion of glycine (G) 136 to aspartic acid (D) and the deletion of the *Sca*I cut site. Finally, glycine 135 (G) was mutated to alanine (A) with the reincorporation of the *Sca*I cut site.

The second variant created is referred to as 'AAAA' since the amino acids 135-138 were changed to four alanines (A). These four mutations were introduced using a single oligonucleotide and identified by the introduction of the restriction site for *Sac*II. The pET-14b vector with the insert does not have a *Sac*II restriction site; therefore, digestion of the altered sequence will open the circular DNA and producing a single fragment of 5973 bp. Figure 10 illustrates the plasmids with *Sca*I and Sac II restriction enzyme cut sites used to screen for site-directed mutagenesis.

Figure 11 shows an agarose gel with the plasmid DNA digested by *Sca*I for the ADLS variant and *Sac*II for the AAAA variant. When the *Sca*I site is introduced into the ADLS variant two fragments will be produced, but when the *Sca*I site is removed it will produce a single linear DNA molecule, which will be compared with lane 3.

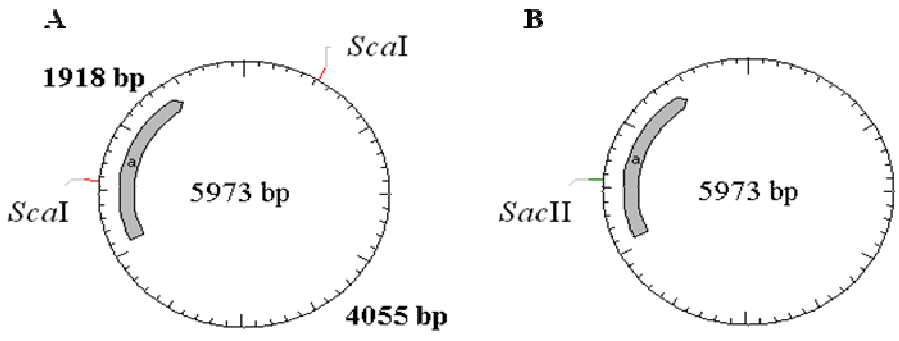

Figure 10 Plasmids showing restriction enzyme cut sites.
Portion in gray illustrate the insert. A) Wild-type and ADLS plasmids show the *Sca*I restriction site. B) AAAA plasmid shows that the new cut site for *Sac*II will linearize the circular plasmid.

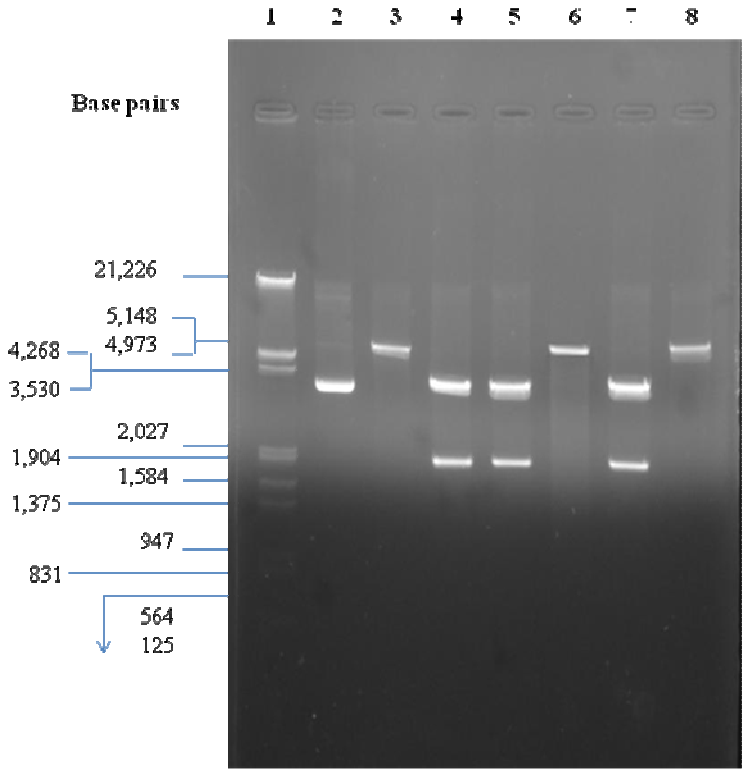

Figure 11 Agarose gel (1%) showing the results of the screening of mutations using restriction enzyme digestion.
Lane 1: Lambda (λ) DNA digested with *Eco*RI and *Hind*III marker, Lane 2: original plasmid uncut, Lane 3: original plasmid digested with *Sca*I, Lane 4: L137F (now wild-type) digested with *Sca*I, Lane 5: N138S digested with *Sca*I (first mutation to create ADLS), Lane 6: G135D digested with *Sca*I, Lane 7: G135A digested with *Sca*I, Lane 8: AAAA variant digested with *Sac*II.

3.1.2 Protein purification

The plasmids for the octameric enolases (wild-type and variants) were transformed into *E. coli,* BL21(DE3) competent cells. The proteins were expressed and harvested according to the procedure described in section 2.12. The proteins expressed contain a (hexa) 6xHis-tag. Purification from the crude extract was achieved using a Ni-NTA (Qiagen) chromatography column as described in section 2.13. NTA occupies four of the six ligand binding sites in the coordination sphere of the nickel ion, leaving two sites free to interact with the 6xHis-tag. The imidazole concentration was increased in order to elute the desired protein. Since the 6xHis-tag proteins can no longer compete against imidazole for the binding site of the Ni-NTA resin, proteins will be eluted. Elution fractions containing protein were monitored by their absorption at 280 nm. Figures 12, 14, and 16 show a characteristic elution profile for wild-type, ADLS and AAAA proteins respectively. The figures show two different plots, where one y-axis is the absorbance at 280 nm and the second y-axis is the enzymatic activity of each fraction collected. As expected, the greater the absorbance at 280 nm, the greater the activity (ΔOD_{240}/min/mL). The elution profiles for all three proteins were relatively similar. Figures 13, 15 and 17 show an SDS-PAGE of the fractions with greatest absorbance at 280 nm for wild-type, ADLS and AAAA proteins. Each fraction was approximately 9 mL in volume, and only the fractions with the highest absorbance, activity, and purity observed by SDS-PAGE and ratio of $Abs_{280/260} > 1.7$ were pooled together. Typically, about 80-100 mg of protein was obtained from a 1 L culture for the wild-type octameric enolase.

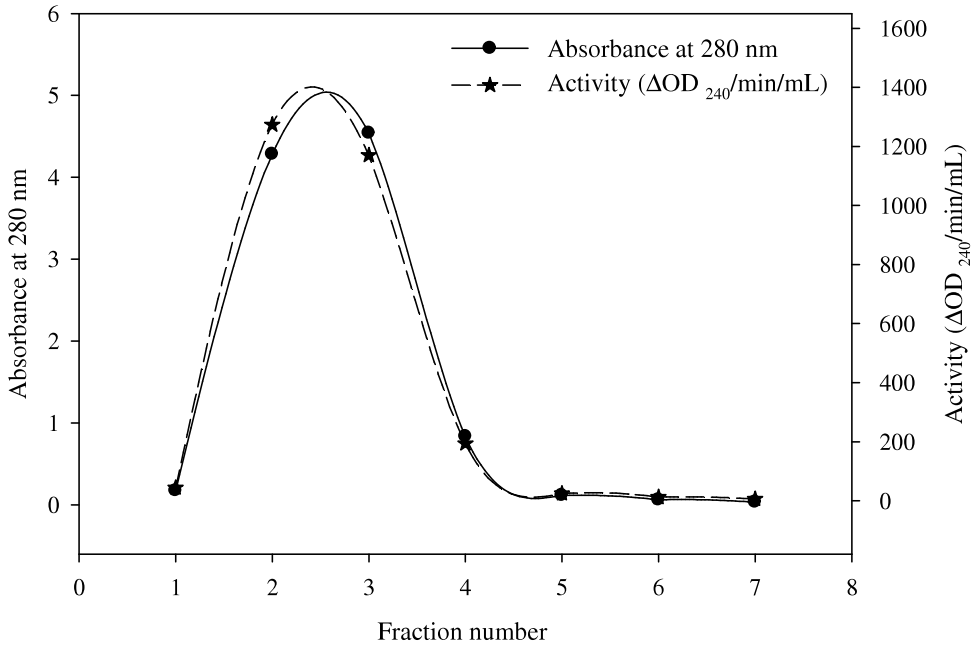

Figure 12 Elution profile of wild-type enolase from the Ni-NTA column.

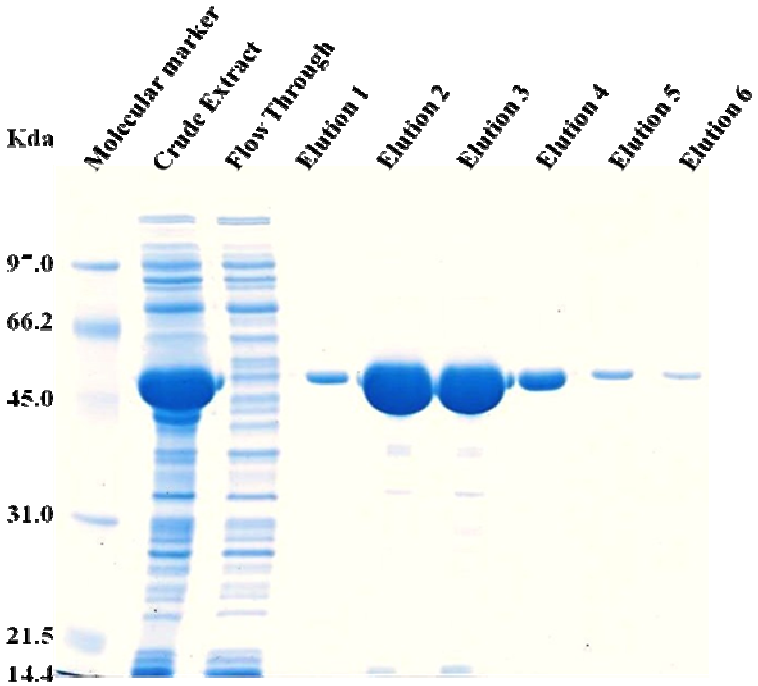

Figure 13 SDS-PAGE of purification fractions of wild-type octameric enolase.
7 µL of samples were loaded into each well. Elution fractions 2 and 3 were pooled together.

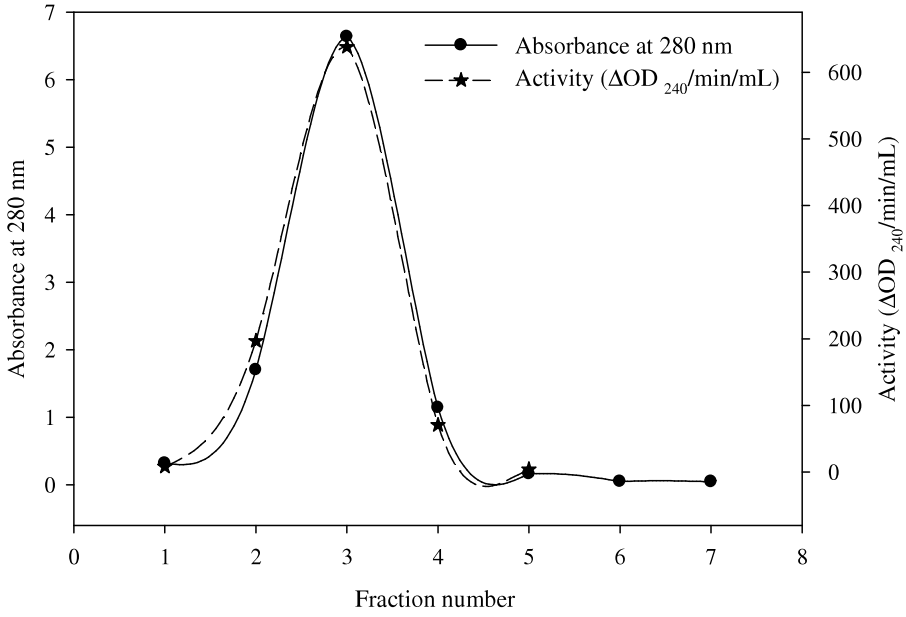

Figure 14 Elution profile of ADLS enolase from the Ni-NTA column.

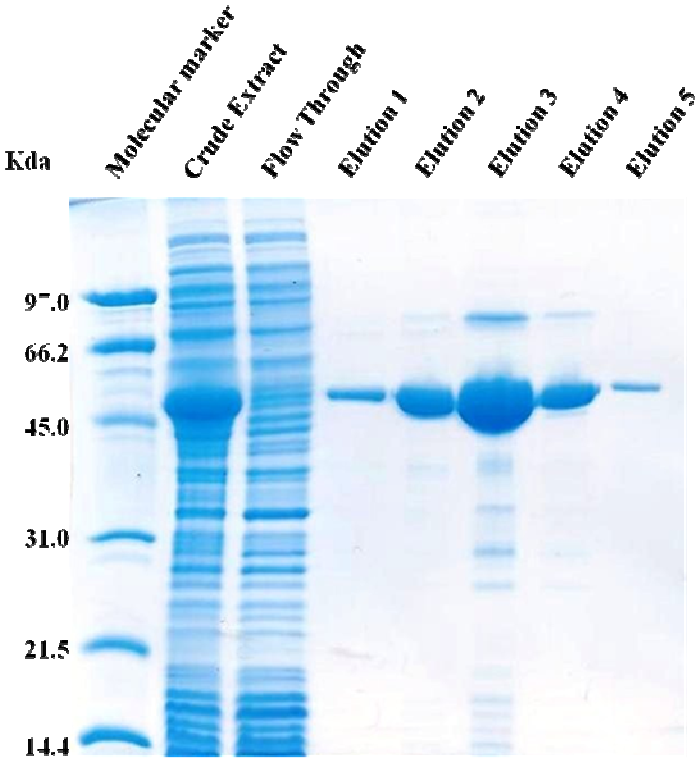

Figure 15 SDS-PAGE of purification fractions of ADLS enolase.
7 µL of samples were loaded into each well. Elution fractions 2, 3 and 4 were pooled together.

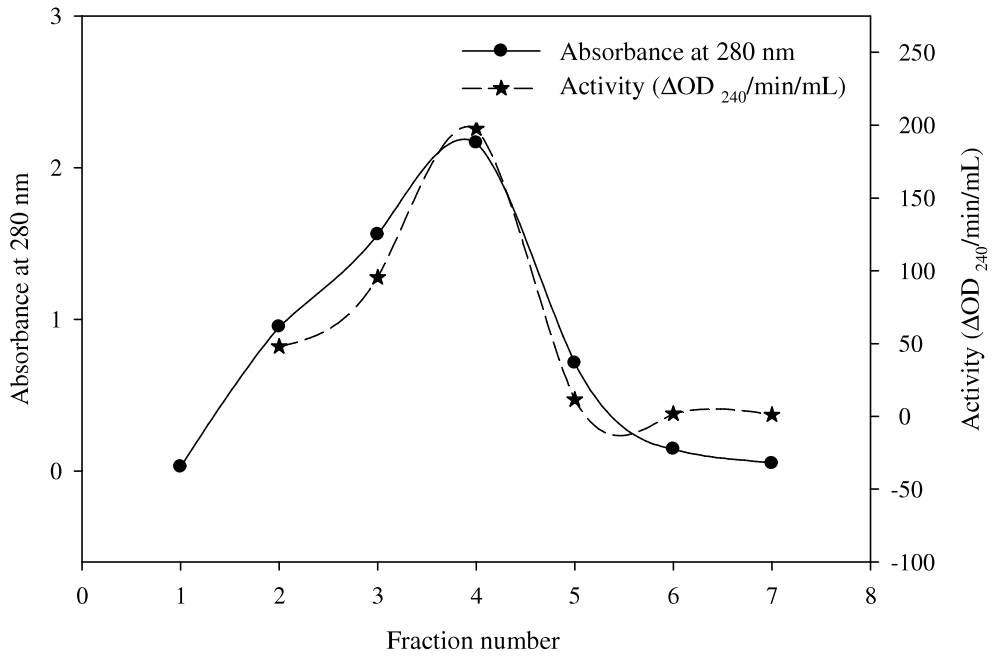

Figure 16 Elution profile of the AAAA variant.

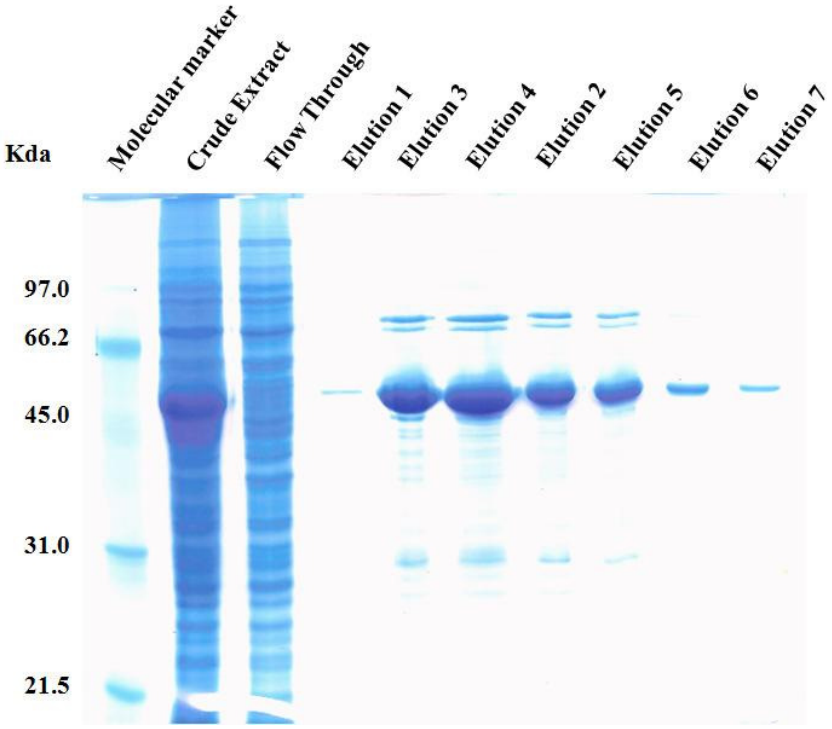

Figure 17 SDS-PAGE of purification of AAAA enolase.
7 µL of samples were loaded into each well. Elution fractions 2, 3 and 4 were pooled together.

3.1.3 Protein mass spectrometry

The purified wild-type, ADLS and AAAA variants were analyzed by ESI-Q-TOF mass spectrometry. The molecular weights were calculated using the ExPASy server with the Compute pI/Mw tool (http://ca.expasy.org/tools/pi_tool.html). Table 6 shows the calculated molecular masses and the experimental molecular masses of wild-type octameric enolase and variants.

Samples	Calculated molecular mass (Da)	Experimental molecular mass (Da)	Difference (Da)
Wild-type	49388.5	49388.0	0.5
ADLS	49399.5	49399.0	0.5
AAAA	49297.4	49295.9	1.5

Table 6 Comparison of the calculated and the experimental molecular masses of the wild-type, ADLS and AAAA octameric proteins.

Figure 18 shows the mass spectra from wild-type, ADLS and AAAA proteins generated by the MassLynx software. Since the molecular masses of the calculated and experimental data are in good agreement, it can be concluded that the correct mutations were introduced in the ADLS and AAAA variants. These data also corroborated the DNA sequencing results.

A)

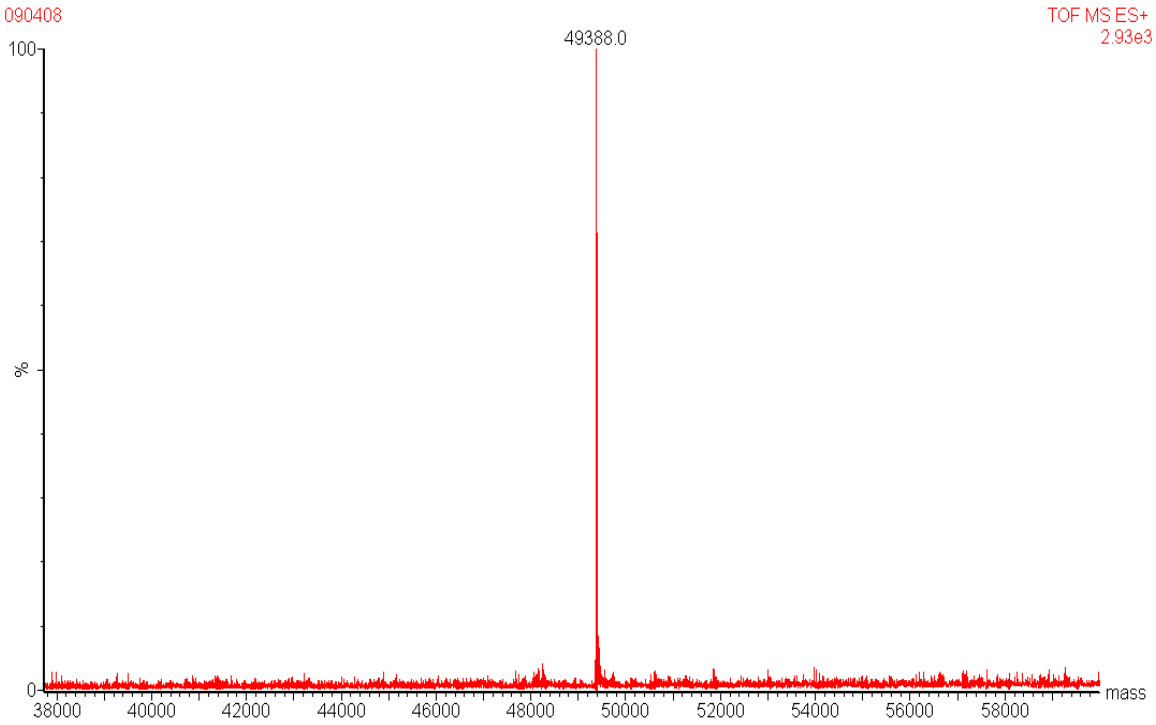
090408
TOF MS ES+
2.93e3
49388.0
100
%
0
38000
40000
42000
44000
46000
48000
50000
52000
54000
56000
58000
mass

B)

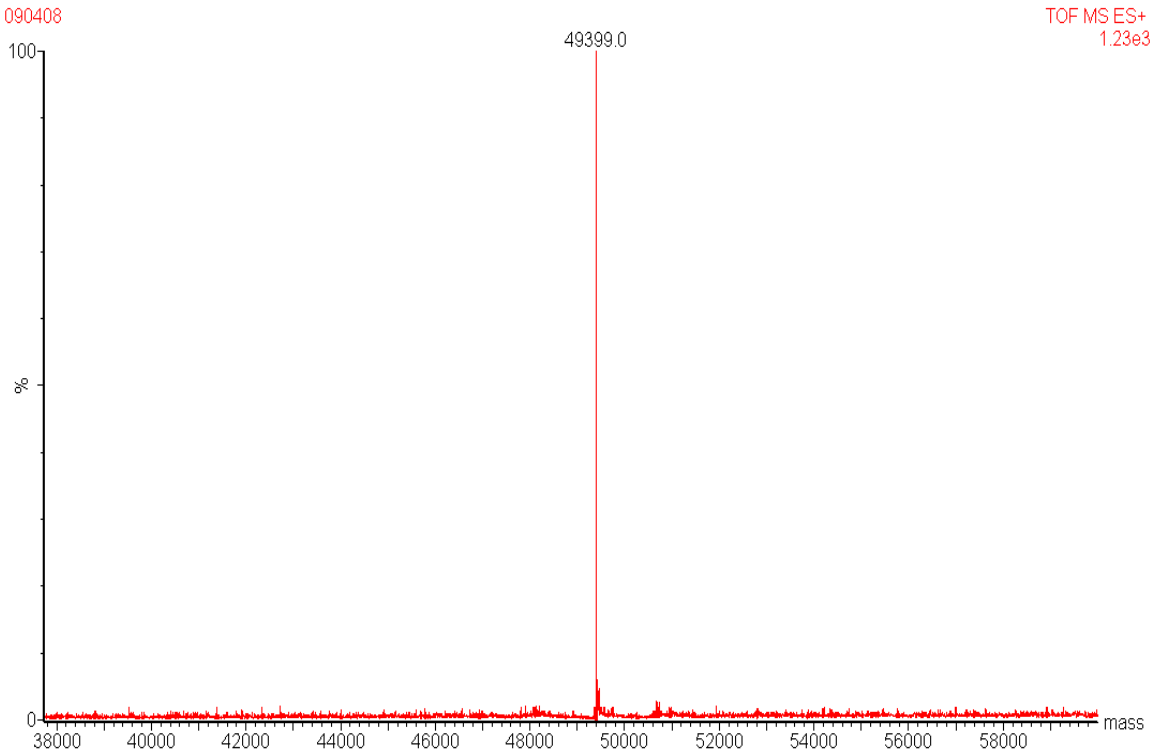
090408
TOF MS ES+
1.23e3
49399.0
100
%
0
38000
40000
42000
44000
46000
48000
50000
52000
54000
56000
58000
mass

C)

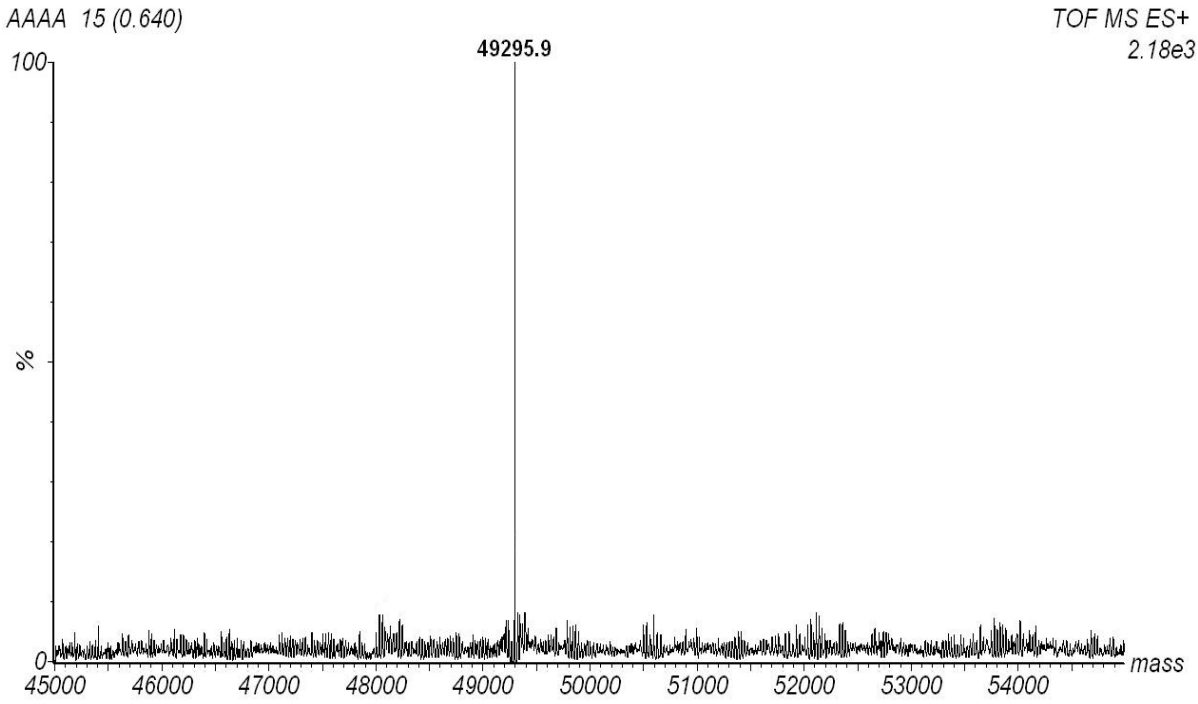

Figure 18 Mass spectrum of purifed octameric enolases.
Signal from ESI-Q-TOF mass spectrometry instrument deconvulated with MassLynx software. A) Wild-type B) ADLS variant C) AAAA variant.

3.1.4 Secondary structure analysis by peptide-bond UV-CD

The peptide-bond UV circular dichroic spectrum of wild-type octameric enolase was compared with those of the two variants. Proteins in solution were monitored in the range of 180-280 nm. Wavelengths from 190 to 230 nm correspond to the difference in absorption between left and right-handed circularly polarized light due to the amide-bond. CD spectra are sensitive to the secondary structural conformation of the protein, such as α-helices, β-strands, and β-turns, which have distinctive patterns (Schmid, 1989). Figure 19 shows the peptide-bond spectra of the wild-type protein and both variants.

These spectra show a double minimum at 208 and 222 nm which is characteristic of a protein with a high α-helical composition. At 190 nm the three samples show a positive intense signal, with a difference in intensity.

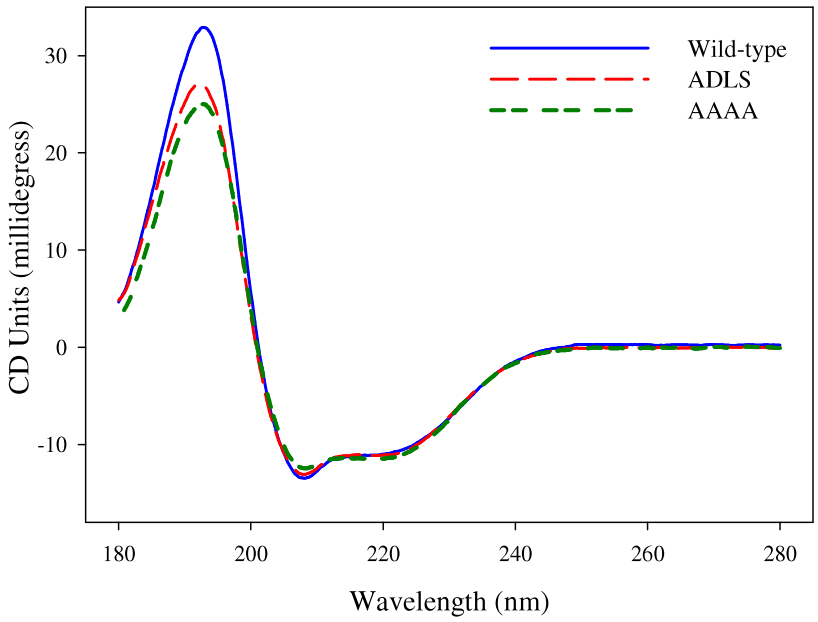

Figure 19 Peptide-bond UV circular dichroic spectra of wild-type, ADLS and AAAA.

Secondary structure determination from the spectra was performed using the DICHROWEB (On-line deconvolution software for protein circular dichroic spectra, available at http://dichroweb.cryst.bbk.ac.uk). Table 7 shows the percentages of α-helices, β-strands, turns and unordered structure.

Samples	α-helices	β-stands	Turns	Unordered
Wild-type	56 %	14 %	12 %	18 %
ADLS	49 %	14 %	16 %	21 %
AAAA	45 %	17 %	14 %	24 %

Table 7 Secondary structure percentages determined with DICHROWEB

3.1.1 Specific activity assay

The activity of the wild-type protein and both variants (ADLS and AAAA) were monitored under similar conditions. Enzymatic activity reactions were performed using 50 mM HEPES buffer with 1 mM 2-PGA and 1 mM of Mg^{2+} as explained in Section 2.19. These concentrations were selected because they provide saturated concentration of both the divalent cation and substrate, which are both required for the optimal activity of the wild-type and variants proteins. It was observed that the activity of ADLS is decreased considerably when compared to the wild-type enzyme. The activity of AAAA decreased even more than that of the ADLS protein. The average specific activity of the wild-type protein was calculated to be 206.8 ΔOD_{240}/min/mg. ADLS activity decreased by 55% compared to the wild-type, with a specific activity of 94.5 ΔOD_{240}/min/mg. The activity of the AAAA variant was calculated to be 30.8 ΔOD_{240}/min/mg, which is an 85% decrease compared to the wild-type protein.

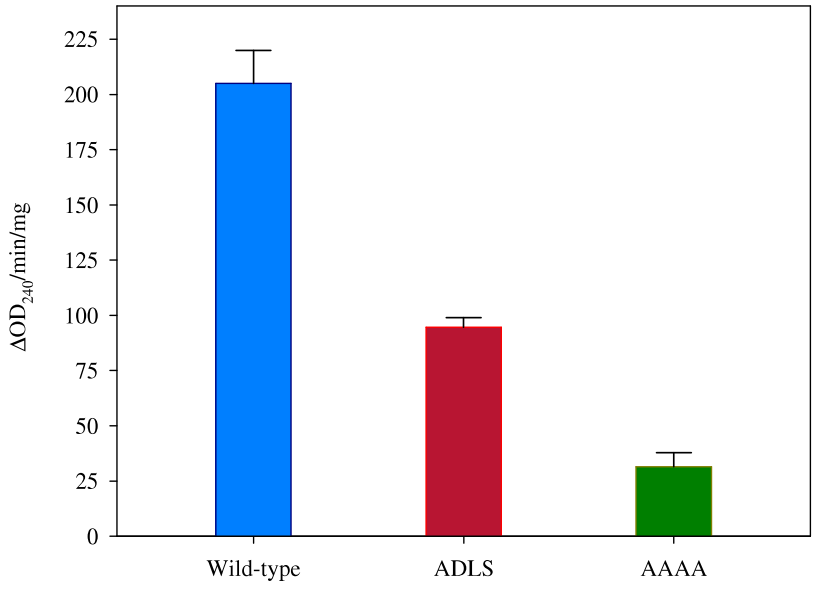

Figure 20 Specific activity under standard assay conditions.

3.1.2 Sedimentation velocity by AUC

Since the main purpose for creating the ADLS and AAAA variants was to test the role of the loop in determining quaternary structure, analytical ultracentrifugation (AUC) was an important technique in order to compare the quaternary structures of wild-type and variant proteins. AUC has the ability to measure the distribution of the sample while it is spinning at high velocity. Sedimentation velocity is an analytical ultracentrifugation method that measures the rate at which molecules move in response to a centrifugal force applied on them. This sedimentation rate provides information about the molecular weight and shape of the species present in the sample (Ralston, 1993). The double-sector cells of the AUC allow the user to take into account solvent absorption. A sample of the protein solution is placed in one sector, and a sample of the solvent is placed in the second sector. All samples were centrifuged under the same condition as described in section 2.21. A comparison of the sedimentation velocities of wild-type protein and the two variants was performed at 23 μM (1 mg/mL).

Figure 21 shows a snapshot comparison of the 25th scan of all three samples. The presence of a single boundary indicates the presence of a single species, as shown in the wild-type. Multiple boundaries suggest the presence of multiple species which sediment at different rates, as in the case of both variants, ADLS and AAAA. The peaks at positions 6.0 and 6.1 cm represent the meniscus of the sample, and they do not overlap due to the fact that the cells were not filled with the same volume, but this difference does not affect the determination of the sedimentation coefficient.

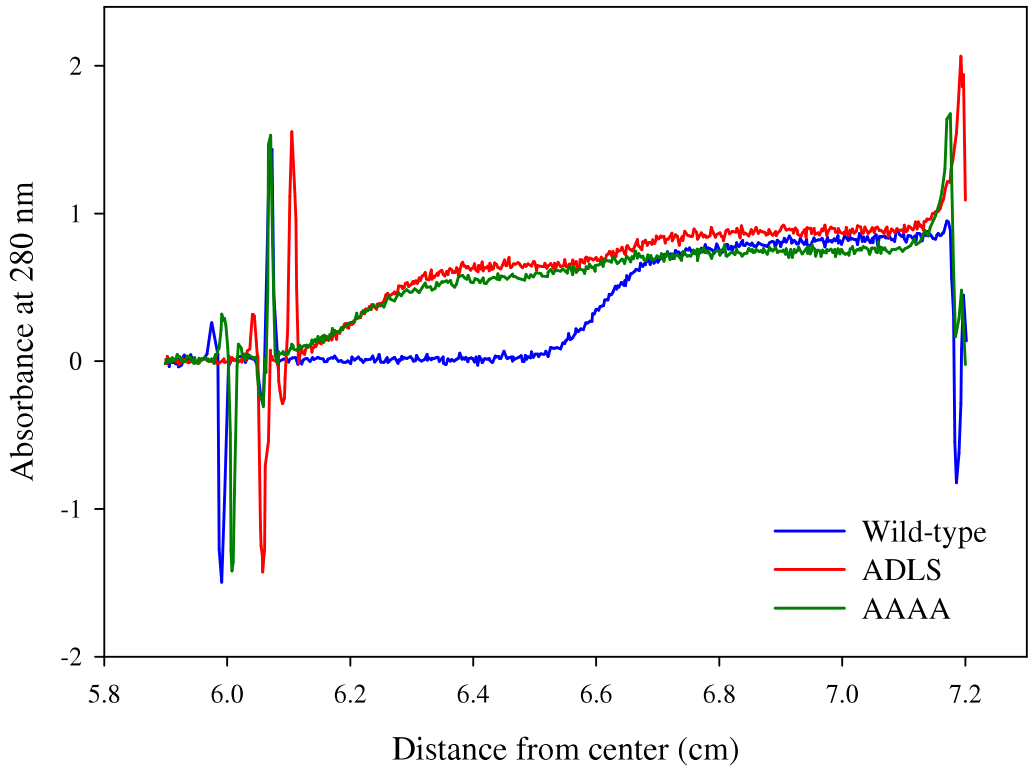

Figure 21 Snapshot of analytical ultracentrifugation run (scan 25).
Three proteins at 23 µM were centrifuged at 32000 rpm (60-Ti- rotor) and 20 °C in a 1.2 cm quartz double compartment cell.

Figure 22 shows the sedimentation coefficient profile obtained by fitting the data using SEDFIT. Table 8 shows the peak integration from Figure 22. Previous results have shown that octameric enolase has an $s_{20,w}$ of 14 (Karbassi *et al.*, 2010) and studies on yeast enolase have shown that the dimeric structure sediments at an $s_{20,w}$ of 5.6 (Zhao *et al.*, 2008).

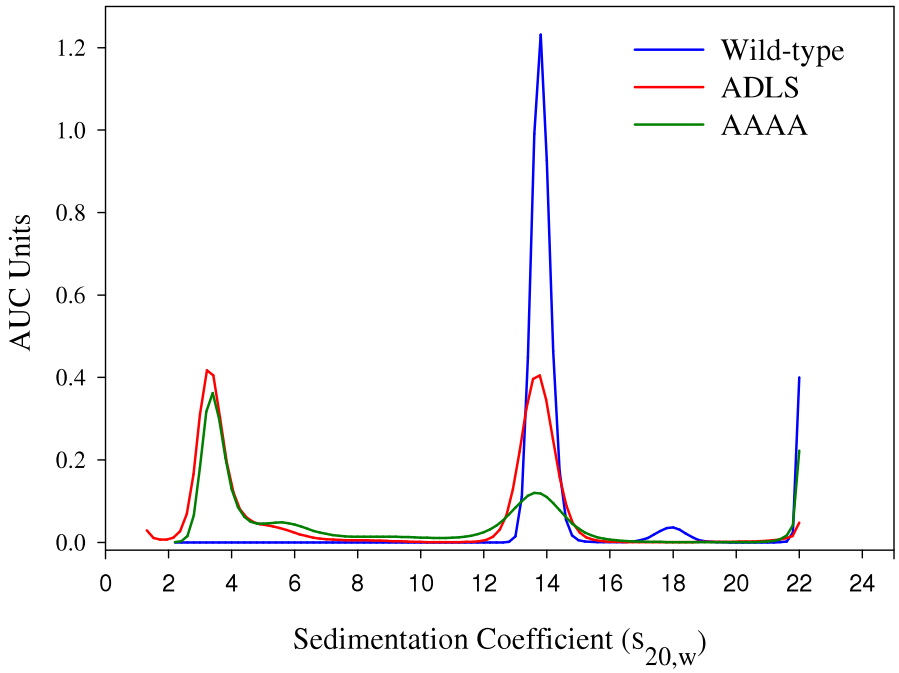

Figure 22 Sedimentation coefficient of wild-type, ADLS and AAAA proteins. Raw data were analyzed using SEDFIT (software use for fitting the data). Density and viscosity were determined using Sednterp software.

	$s_{20,w}$	%	Species
Wild-type	13.81	86.82	octamers
ADLS	3.42	42.14	monomers
	5.66	4.30	dimers
	7.93	1.37	-
	13.75	47.79	octamers
AAAA	3.36	41.42	monomers
	5.26	13.24	dimers
	8.18	7.22	-
	13.71	33.11	octamers

Table 8 Summary for the sedimentation coefficients of wild-type and two variants. Area under the peaks were integrated and the % and $s_{20,w}$ value were determined.

3.1.3 Dissociation of quaternary structure by Sodium perchlorate

Dissociation experiments were carried out using $NaClO_4$, which is a weak chaotropic agent used previously in a number of enolase studies (Karbassi *et al.*, 2010; Kornblatt *et al.*, 1996; Trepanier *et al.*, 1990; Zhao *et al.*, 2008). Studies on yeast enolase have shown that dissociation with $NaClO_4$ proceeds without unfolding and that this dissociation could be followed by a decrease in enzyme activity. It is also known that $NaClO_4$ dissociates octamers into inactive monomers (Karbassi *et al.*, 2010). Enolase at a concentration of 2.7 µM was incubated in TME buffer containing varying concentrations of $NaClO_4$. Samples were assayed for enzymatic activity at 240 nm; followed by analysis of sedimentation velocity using AUC. Figure 23 shows that the loss of activity correlates closely with formation of monomers.

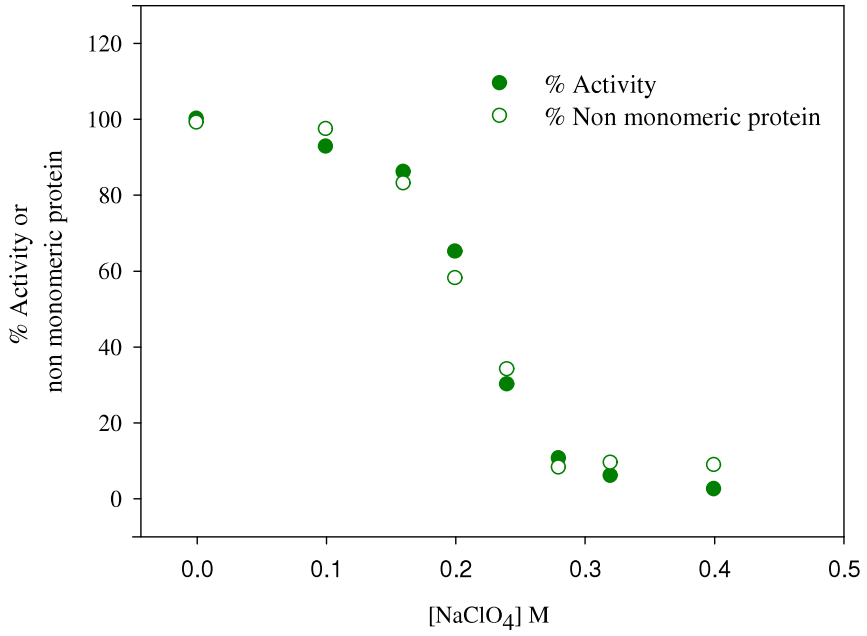

Figure 23 Dissociation and inactivation of wild-type enolase by $NaClO_4$.
Open circles, % activity; closed circles, % non-monomeric protein. % non-monomeric protein calculated as 100% - % monomeric. 0 M $NaClO_4$ is considered as having 100% activity and 100% octameric wild-type enolase.

By varying the $NaClO_4$ concentration from 0 to 0.4 M, a complete dissociation curve for wild-type octameric enolase was obtained. It is clear that increasing $NaClO_4$ concentration results in a gradual loss of enzyme activity. Figure 24 shows that both ADLS and AAAA variants are inactivated at lower concentrations of $NaClO_4$. In the case of the wild-type protein, 0.4 M $NaClO_4$ is required in order to decrease the activity to zero. However, the ADLS variant required approximately 0.1 M $NaClO_4$ to be fully inactive. For the AAAA, complete inactivation occurs even at lower concentrations than the ADLS.

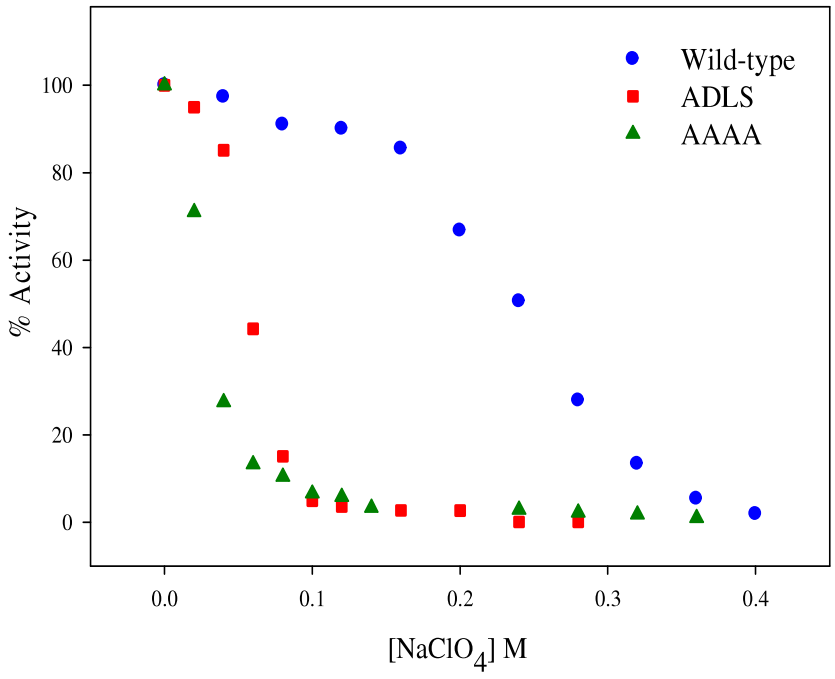

Figure 24 $NaClO_4$ inactivation curve for wild-type, ADLS and AAAA.
Protein concentration was 2.7 µM prepared in TME buffer varying $NaClO_4$ concentration. Enzyme activity was measured in enolase assay buffer by following the production of PEP at 240 nm at room temperature.

3.1.4 Temperature denaturation

In order to compare the thermostability of wild-type and both variant proteins, the loss of α-helical signal at 208 nm as a function of temperature was monitored using circular dichroic spectroscopy. As the temperature increases, a loss in secondary structure occurs. The melting temperature (T_m) is considered to be the midpoint of the transition between native and denatured protein. Temperature denaturation was monitored at pHs, 6.0 and 7.4. Samples were prepared at concentrations of 0.5 mg/mL in phosphate buffer. Phosphate buffer was used instead of Tris buffer, because the pKa of phosphate buffer demonstrates lower variability as a function of temperature. Melting temperatures were determined by calculating the first derivative of the spectra using the Jasco Spectra Analysis software. Wild-type protein at pH 6.0 shows a steep denaturation curve, indicating a cooperative unfolding with a T_m of approximately 68.4 °C. On the other hand, the ADLS and AAAA variants showed a curve with two transition states. The T_m for the ADLS variant was determined to be 34.6 °C at the first inflexion point and 51.6 °C at the second. The T_m for the AAAA variant was estimated to be 30.4 °C and 54.8 °C, at the first and second transition points, respectively. A mixture of species may account for the difference in shape of the denaturation curve observed, since the sample is already partially dissociated prior to temperature denaturation.

Surprisingly, when the temperature denaturations were performed at pH 7.4, all three samples seemed to resist the complete process of denaturation. About 30% of the CD signal was lost, and then the curve plateaued. Wild-type and ADLS show transition points of 62.4 °C and 46.0 °C, respectively; while, AAAA shows two transition points at 34.6 °C and 48.6 °C.

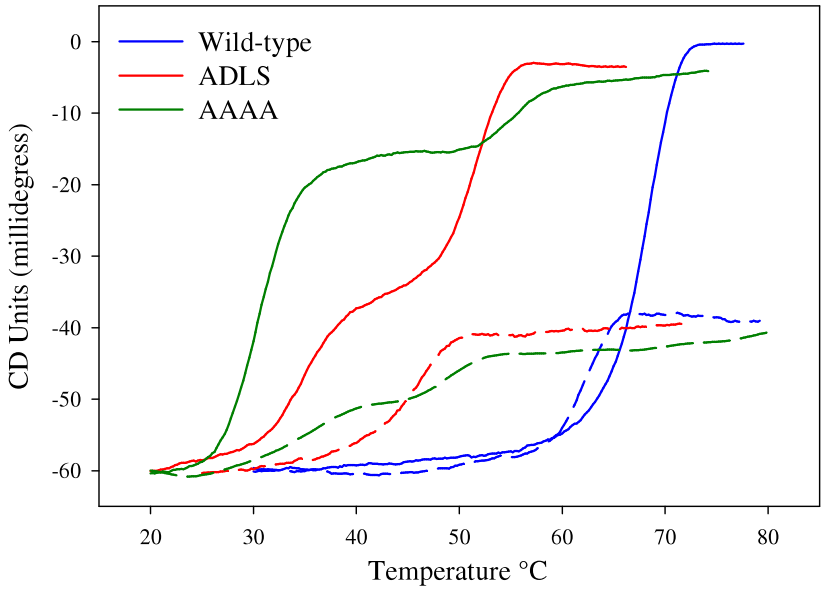

Figure 25 Temperature denaturation detected by circular dichroic spectroscopy. Signal intensity at 208 nm is shown for temperature between 20 °C to 80 °C for all three proteins. Solid line (———) represent samples at pH 6.0 and dashed-lines (- - - - -) represent samples at pH 7.4.

3.1.5 Separation of species in ADLS and AAAA variant proteins

Gel filtration was used to separate the different species of ADLS and AAAA proteins observed in the AUC experiment (section 3.1.2). In each case, 200 µL of protein sample was injected into the FPLC connected to a Superdex 200 column as described in section 2.24. Elution fractions were monitored at 280 and 230 nm.

The gel filtration chromatogram for the ADLS variant (Figure 26) shows two distinct peaks. However, it was observed that the second peak results from very noisy signals; and most likely is due to the presence of an air bubble injected into the system during sample loading. The absorbance at 230 was used in these particular experiments, because the signal at 280 was relatively low and noisy. Fractions with the highest absorbance for each peak (B9 and B2) were selected for enzymatic activity assays, AUC

and DLS analyses. Since gel filtration separates molecules by size, it is expected that the fraction for the first peak (B9) will contain the larger structure, most likely octamers. The protein sample in the second peak (B2) is expected to be dimeric or monomeric.

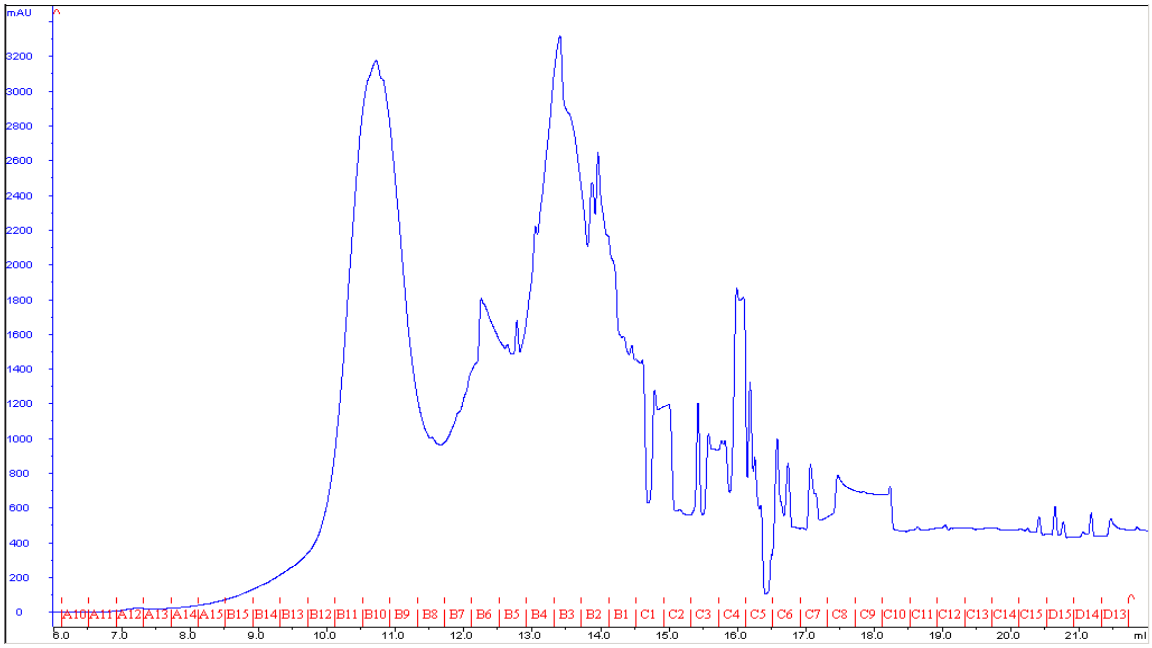

Figure 26 Gel filtration chromatogram of the ADLS variant at A_{230} nm.

The enzymatic activity of the sample loaded into the gel filtration column was 75.3 ΔOD_{240}/min/mg. The B9 fraction's enzymatic activity increased significantly to 127.9 ΔOD_{240}/min/mg suggesting that the sample eluted has a more octameric structure. The activity for B2 decreases considerably compared to the original sample with a value of 4.32 ΔOD_{240}/min/mg, suggesting it is mainly monomeric.

These samples were also analyzed using AUC. Sedimentation velocity analysis indicates that the original ADLS sample was loaded into the column as a mixture of species. Table 9 summarized the $s_{20,w}$ and percentage of each species observed in the fraction selected. For fraction B9, it was observed that 70.9% is octameric in comparison

to the original sample which was only 37.5%. On the other hand, fraction B2 is 83.6% monomeric.

Sample	$s_{20,w}$	%	Species
ADLS Mixture of species	3.4	50.7	monomers
	5.3	11.1	dimers
	8.3	1.7	-
	14.1	37.5	octamers
B9	3.6	18.3	monomers
	6.1	3.5	dimers
	-	-	-
	14.3	70.9	octamers
B2	4.0	83.6	monomers
	-	-	-
	-	-	-
	14.2	4.7	octamers

Table 9 Summary of sedimentation velocities of samples eluted from the FPLC gel filtration column.

After AUC analysis, dynamic light scattering (DLS) experiments were performed on all three samples. In DLS, the signal intensity of large molecules is greater than that of small molecules. An increase in monomers will result in a decrease in signal intensity. Fraction B9 has a hydrodynamic radius measured by DLS of 6.2 nm. This radius was similar to that obtained with previous DLS experiments of octamers which was 6.42 nm (Karbassi *et al.*, 2010). Fraction B2 has a hydrodynamic radius calculated as 3.95 nm. This decrease in signal represents an increase of smaller species. The original ADLS sample has a hydrodynamic radius of 5.85 nm, and a higher percent of polydispersity suggesting that various species are present, corroborating the AUC experimental data.

The same experiment using gel filtration was carried out for the AAAA variant. The chromatogram obtained measuring absorbance at 280 nm for the AAAA variant

(Figure 27) shows two distinct peaks. Again, the fractions at the highest absorbance 280 (B10 and B2) for both the first and second peaks, respectively were used for enzymatic activity and DLS experimental analysis.

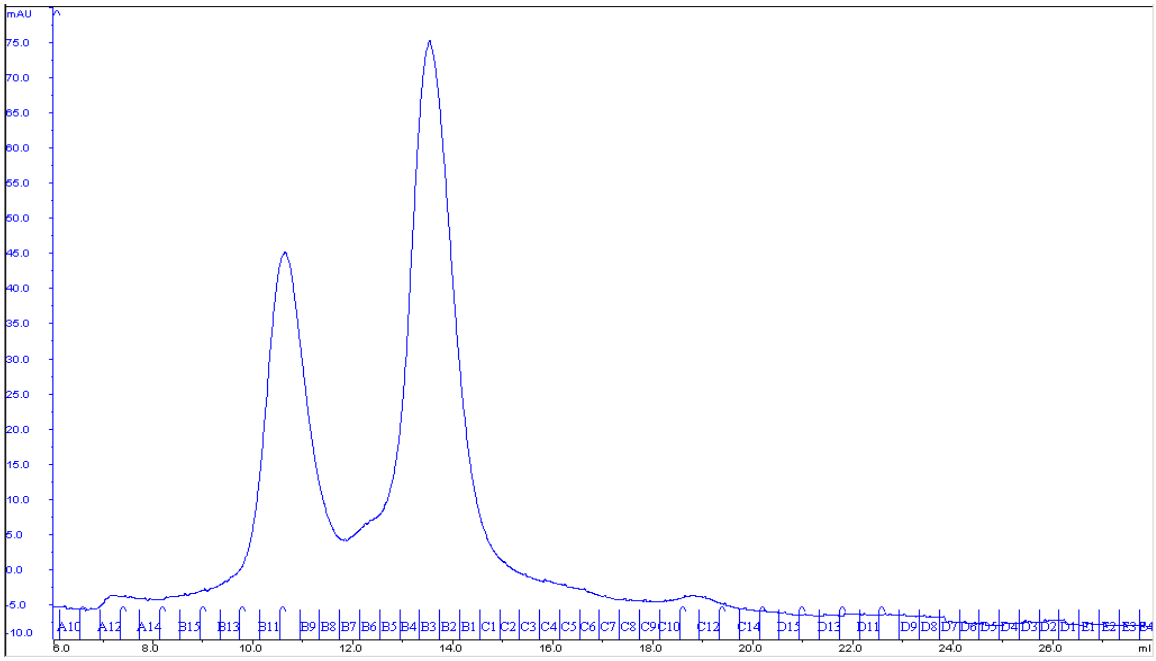

Figure 27 Gel filtration chromatogram of the AAAA variant at A_{280} nm.

Table 10 summarizes the enzymatic activity of fractions B10 and B2 monitored during 48 hours. Fraction B10 initially had a high activity and hydrodynamic radius suggesting that the species in B10 correspond to octamers. After 48 hours, the enzymatic activity decreased by ~68% and the hydrodynamic radius also decreased with an increase of % polydispersity. This means that the sample is smaller in size and less homogeneous. These data suggest that equilibrium between the species is obtained relatively slowly.

	0 hour		24 hours	48 hours	
	Specify activity ΔOD_{240}/min/mg	Hydrodynamic radius (nm)	Specify activity ΔOD_{240}/min/mg	Specify activity ΔOD_{240}/min/mg	Hydrodynamic radius (nm)
B10	150.9	6.2	62.3	48.9	5.8
B2	8.4	3.9	5.8	2.3	3.8

Table 10 Summary of enzymatic activity and hydrodynamic radius for species separated from AAAA variant.

3.2 Stabilization of the quaternary structure by the His-tag

The second part of this project was to study the effects of the His-tag on the stability of octameric enolase. The gene for wild-type octameric enolase (used in the first part of the project) which carries an N-terminal His-tag was inserted into a vector which introduced a C-terminal His-tag. This resulting protein was expressed, purified and treated with thrombin to remove the tag. N-terminal His-tag, C-terminal His-tag and No His-tag proteins were compared in order to determine if the tag affects quaternary structural stability.

3.2.1 pET-52b(+) Vector

The primers used to clone the gene from pET-14b vector into pET-52b(+) vector are listed in section 2.8.1. First, the octameric enolase gene in pET-14b vector was amplified by PCR, with oligonucleotides designed to introduce *Pci*I and *Sac*I restriction sites. This restriction enzyme creates sticky ends which were used later to ligate the insert into the pET-52b(+) vector. *Pci*I and *Sac*I were used to digest the insert DNA, and *Nco*I and *Sac*I were used to digest the vector. *Pci*I cleavage creates the complementary sticky end for the *Nco*I digested DNA. Agarose gels (1%) were used to check the digested insert and vector DNA (Figure 28). The complete plasmid DNA containing the gene is 6433 bp long, where the insert is 1311 bp and the vector is 5122 bp. Fragments from the gel were extracted, purified, and ligated. Successful cloning was verified by DNA sequencing.

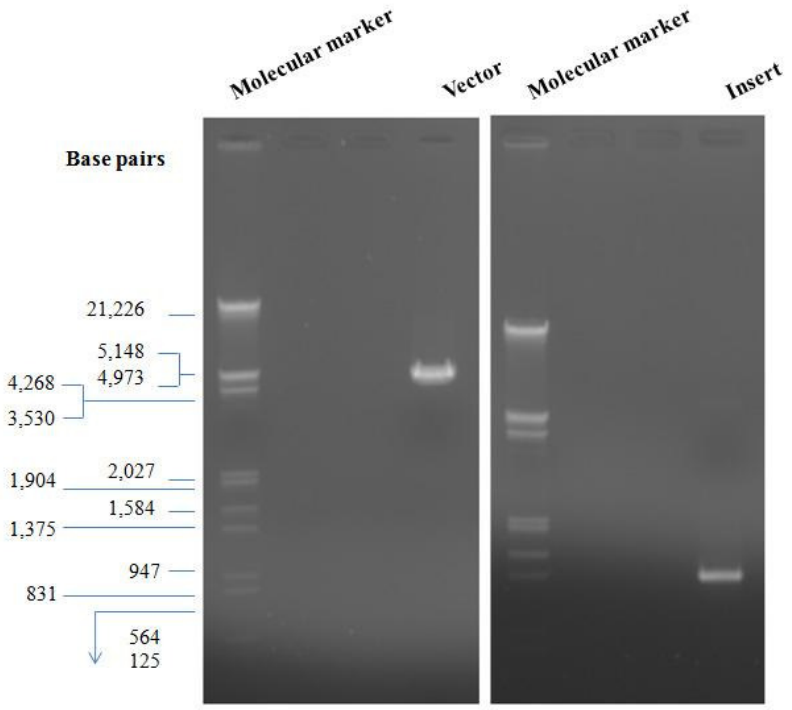

Figure 28 Agarose gels (1%) showing the vector and insert used for ligation.
Vector (left) was digested with *Nco*I and *Sac*I (5122 bp) and insert (right) was digested with *Pci*I and *Sac*I (1311), each gel shows Lambda (λ) DNA digested with *Eco*RI and *Hind*III.

3.2.2 Protein purification and removal of the C-terminal His-tag

The plasmid for octameric enolase carrying the His-tag at its C-terminus was transformed into *E. coli* BL21(DE3) competent cells. The proteins were expressed and purified as described in section 2.12 and 2.13. The elution profile obtained was similar to that of wild-type enolase in the previous section. A total of ~100 mg of protein was obtained per 1L culture.

The purified protein was treated with thrombin protease to remove the histidine tag. Thrombin cleaves the amino acid backbone between proline and arginine in the following sequence: Leu-Val-Pro-Arg-Gly-Ser. After cleavage, protein was dialyzed to

remove thrombin and then passed through a 1 mL Ni-NTA chromatography column to remove the histidine tags and any uncleaved proteins.

Figure 29 shows an SDS-PAGE gel of the three purified proteins to be compared in the second part of this project. The octameric enolase with no His-tag migrated further on the gel, because this protein has 14 fewer amino acids which accounts for the 1.7 kDa difference compared to the C-terminal His-tag protein.

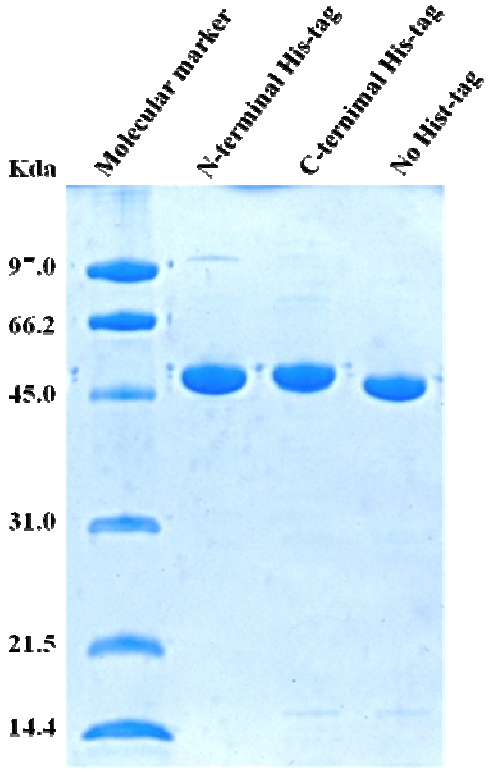

Figure 29 SDS-PAGE of N-terminal His-tag, C-terminal His-tag and No His-tag.
12% SDS-polyacrylamide gel of purified enolases. Lane 1: Low range molecular weight marker. Each sample contains approximately 5 µg of protein.

3.2.3 Protein mass spectrometry

Purified octameric enolase carrying a C-terminal His-tag was subjected to electrospray ionization mass spectrometry to verify its molecular mass. In order to determine the molecular mass, a direct injection method was used as described in Section 2.17. The molecular mass was found to be 49676.7 Da (Figure 30), which is a difference of 1.1 Da compared to the expected molecular mass of 49677.8 Da, calculated from the amino acid composition.

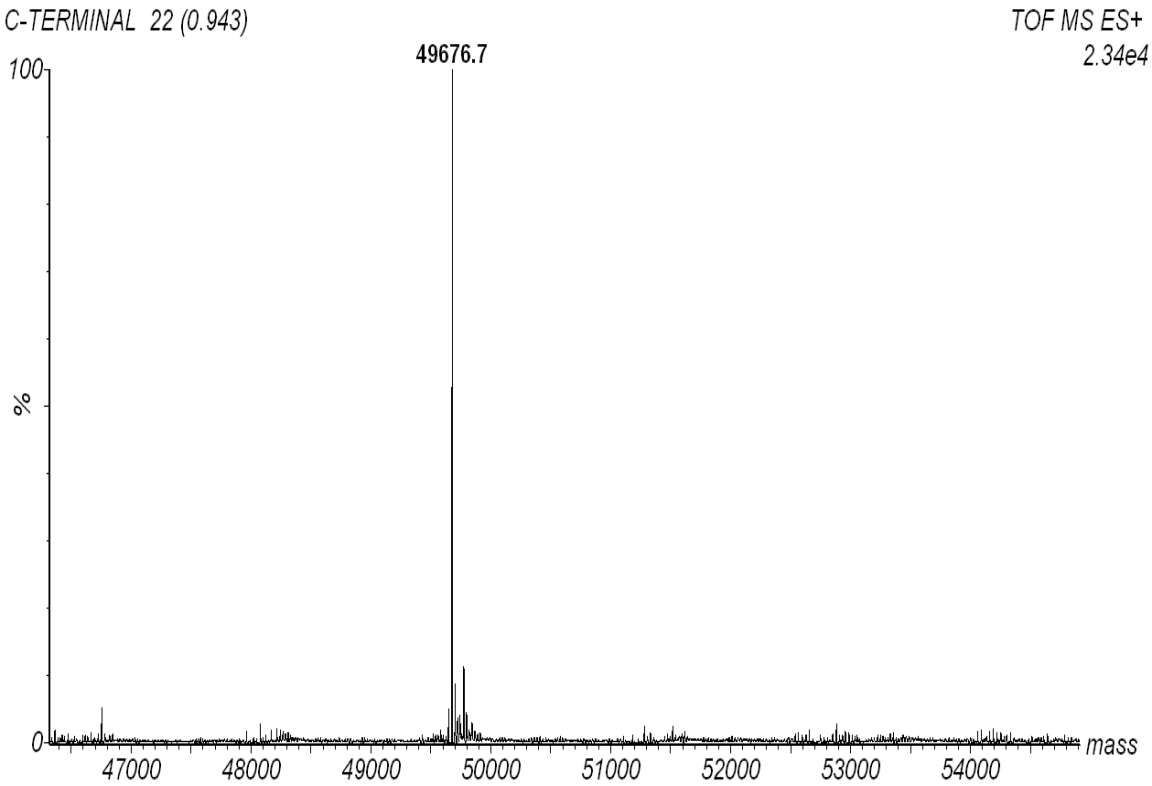

Figure 30 Mass spectrum of octameric enolase expressed with a C-terminal His-tag. Signal from ESI-Q-TOF mass spectrometry instrument deconvoluted with MassLynx software

3.2.4 Secondary structure analysis by CD

Circular dichroic spectra were measured in the far-UV region between 180 and 280 nm. Spectra show a small difference in the intensity of the CD signal at 195 nm between the N-terminal His-tag protein and the C-terminal His-tag protein. This slight variation is most likely due to a small difference in protein concentration (Figure 31).

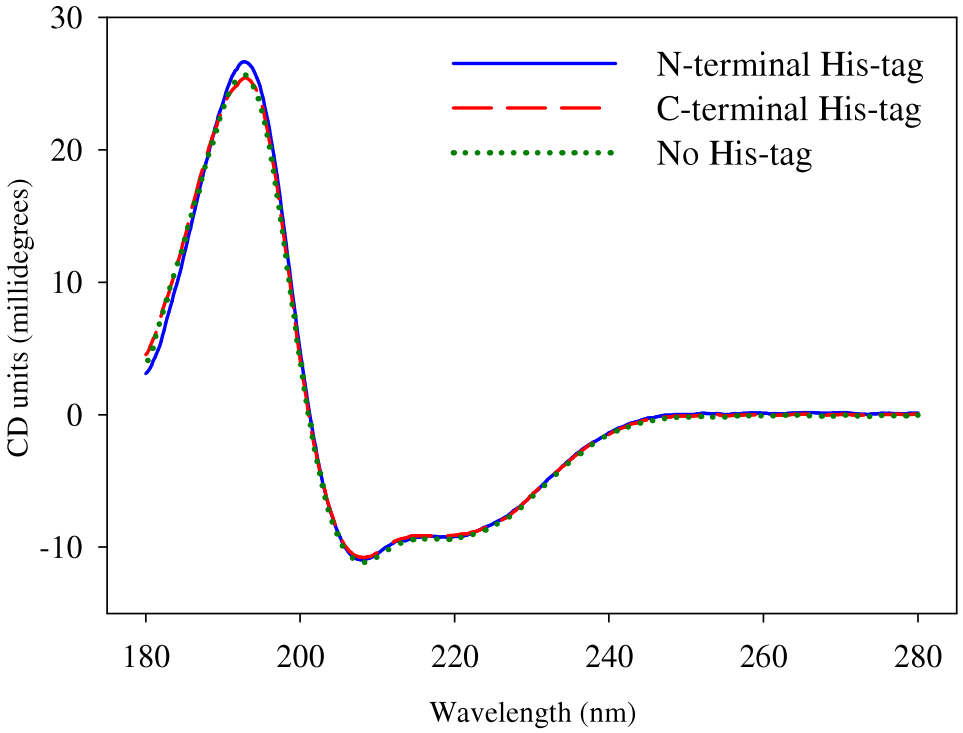

Figure 31 Overlay of the Far-UV Circular dichroism spectra of the three octameric enolases (N-terminal His-tag, C-terminal His-tag and No His-tag).
CD spectra were obtained from 80 µL of sample at a concentration of 1.0 mg/mL in a 0.01 cm cells.

3.2.5 Enolase specific activity assay

Enzyme activity was measured by monitoring the conversion of 2-phosphoglyceric acid (PGA) to phosphoenolpyruvate (PEP) at 240 nm under saturated concentrations of 2-PGA and Mg^{2+} (1 mM 2-PGA and 5 mM of Mg^{2+}). The results obtained demonstrate that the specific activity is not affected by the presence or position (N- or C- terminal) of the His-tag. As shown in the previous section, the average specific activity for the N-terminal His-tag protein was calculated to be 206.8 ΔOD_{240}/min/mg. It was determined to be 204.8 ΔOD_{240}/min/mg for the C-terminal His-tag and 208.0 ΔOD_{240}/min/mg for the No His-tag. There is about a 2% difference in specific activity between these enzymes resulting from experimental error. Figure 32 shows a histogram with the specific activities of the three enzymes.

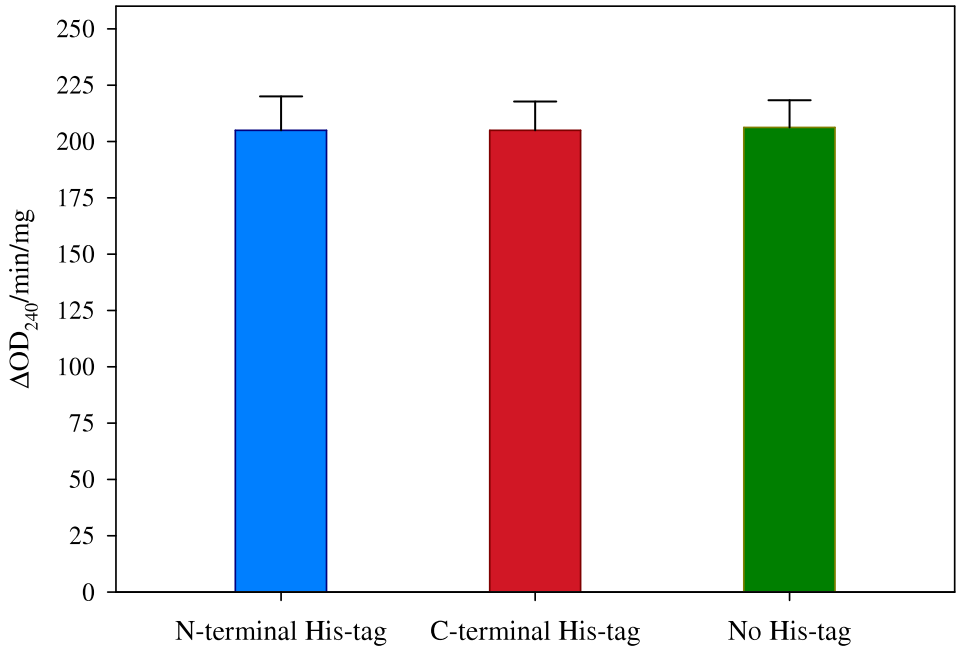

Figure 32 Specify activity of N-terminal His-tag, C-terminal His-tag and No His-tag enolase proteins

3.2.6 Dissociation of quaternary structure by $NaClO_4$

Enolase inactivation by $NaClO_4$ and analytical ultracentrifugation were used to compare stabilities of the three proteins (N-terminal His-tag, C-terminal His-tag and No His-tag). As shown previously, the enzymatic inactivation by this chaotropic agent correlates with the quaternary structure dissociation. Therefore, after incubation in $NaClO_4$, samples were tested for enzymatic activity at 240 nm and then analyzed by AUC (following section). The enzymatic activity data show that the C-terminal His-tag and No His-tag require lower concentrations of $NaClO_4$ than the N-terminal His-tag for complete inactivation. These results suggest a stabilization of the N-terminal His-tagged protein.

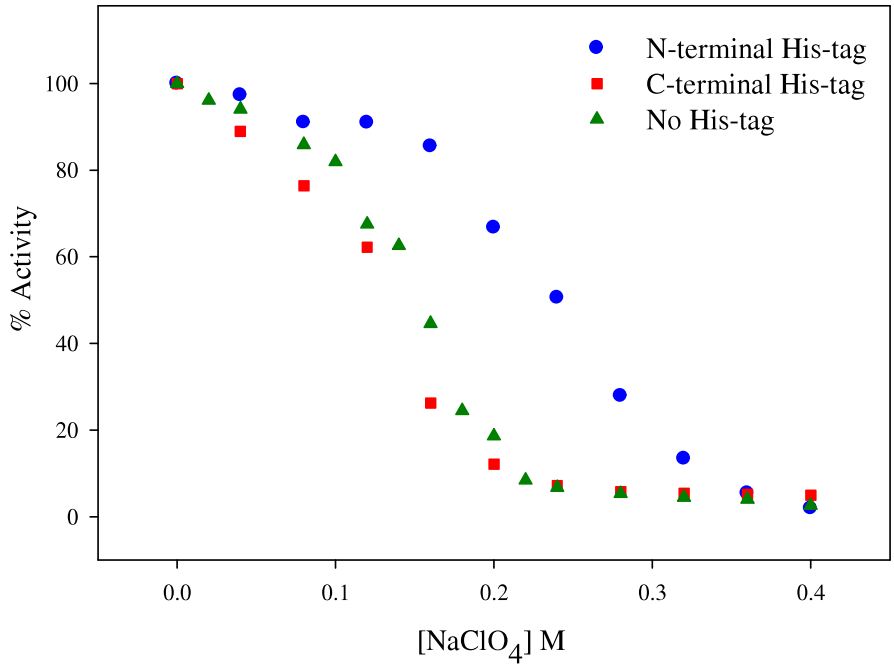

Figure 33 $NaClO_4$ inactivation curve of the three proteins at pH 7.4.
~ 2.7 µM protein samples were incubated for 18-24 hours at increasing concentrations of $NaClO_4$ (from 0 M to 0.4 M) at pH 7.4.

The same experiment was also performed at pH 8.6 for all three proteins. Proteins were incubated in $NaClO_4$ at pH 8.6, and then measured for enzymatic activity. The results from this experiment show that there is no difference between the No His-tag protein at pH 8.6 and 7.4. On the contrary, the stabilization effect observed at pH 7.4 for the N-terminal His-tag protein appears to be lost when the pH was raised to 8.6.

Figure 34 shows the inactivation curve for the N-terminal His-tag and No His-tag at both pHs 7.4 and 8.6. The C-terminal His-tag was observed to have the same inactivation curve as the No-tag at both pHs (data not shown).

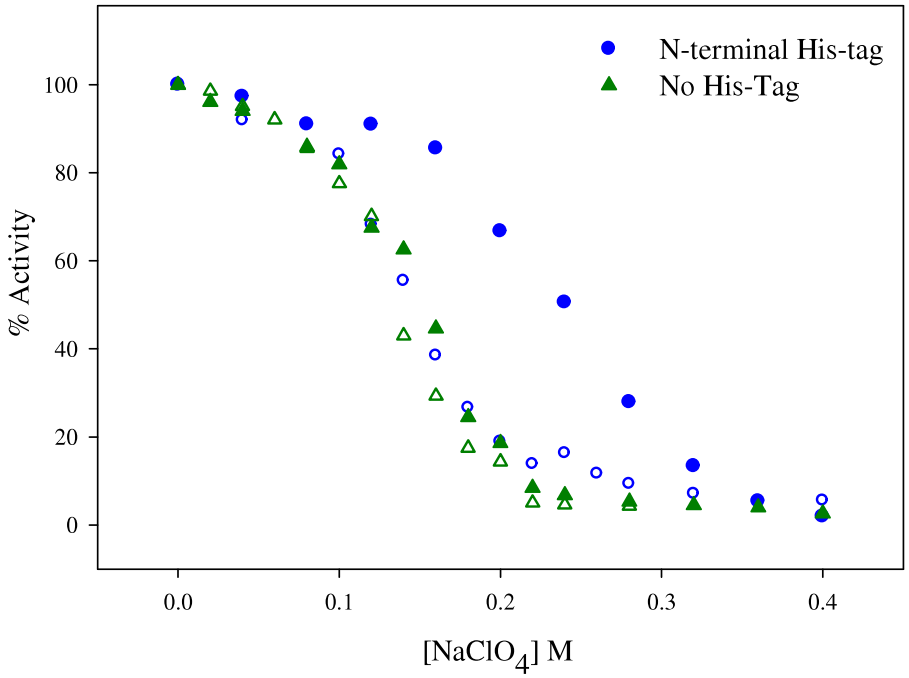

Figure 34 $NaClO_4$ inactivation curve at pHs 7.4 and 8.6.
Closed symbols represent samples at pH 7.4, open symbols at pH 8.6. Proteins were incubated in $NaClO_4$ for 18 to 24 hours prior to the enzyme activity measurements.

3.2.7 Sedimentation velocity by AUC

After the samples had been incubated in $NaClO_4$ and assayed for enzymatic activity, analytical ultracentrifugation was performed to determine quaternary structure. Analysis of AUC sedimentation velocity data using SEDFIT showed that at 0 M $NaClO_4$ there is only one species present, and it is octameric. N-terminal His-tag protein at 0.24 M $NaClO_4$ is mainly monomeric, however approximately 15% still is octameric. In contrast the C-terminal His-tag protein is 100% monomeric at 0.24 M $NaClO_4$. Similar results were observed for the No His-tag protein as those obtained for the C-terminal His-tag. Figure 35 shows the sedimentation coefficients for the N-terminal His-tag and C-terminal His-tag at 0 M and 0.24 M $NaClO_4$.

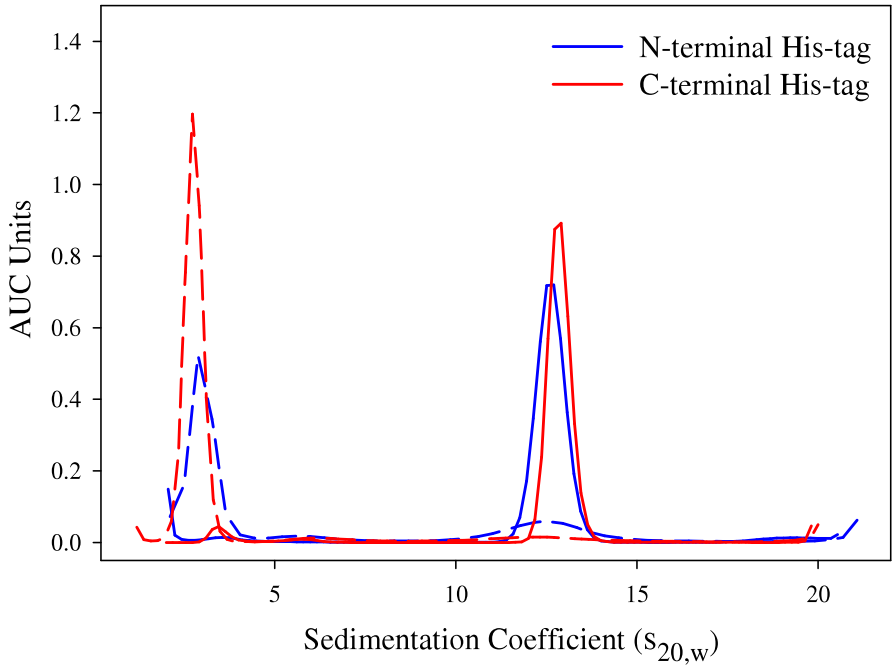

Figure 35 Comparison of the sedimentation velocity at different [$NaClO_4$].
Solid line (———) represents samples incubated at 0 M $NaClO_4$ and dashed-lines (– – – ·) represent samples in 0.24 M $NaClO_4$.

This result indicates that the N-terminal His-tag is more resistant to $NaClO_4$ dissociation as compared to the C-terminal His-tag and No His-tag. Figure 36 shows the correlation between $NaClO_4$ inactivation and the lost of quaternary structure. The peak areas were integrated in order to obtain the percentage of monomeric and octameric protein.

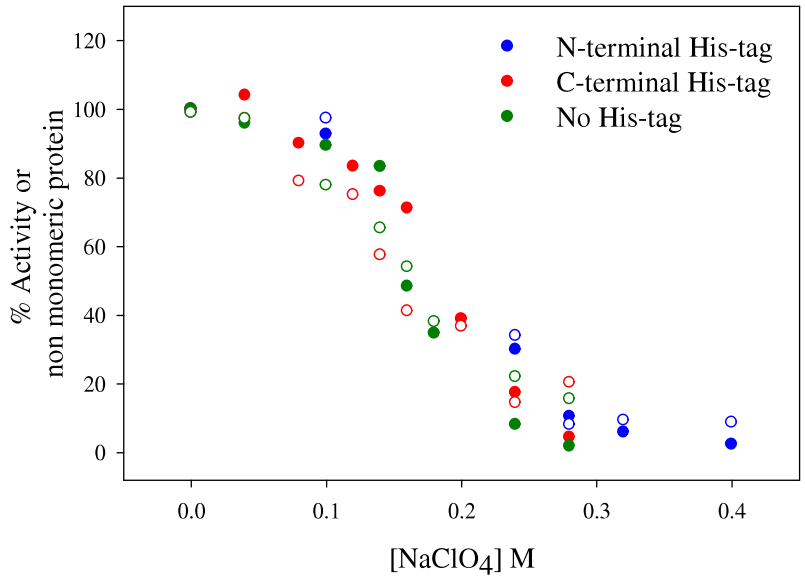

Figure 36 Dissociation and inactivation of octameric enolase by $NaClO_4$.
Open symbols, % activity, closed symbols % non-monomeric protein. % non-monomeric protein is calculated as 100% - % monomeric.

The purpose of Figure 36 is to show that the percent activity and percent non-monomeric protein follow the same trend. Most of the points between samples are close to each other. However, there are a few points where dissociation and inactivation do not seem to correlate. This could be explained by the approximately 5% error in the activity measurements and the 5-10% error in the analysis of the sedimentation coefficients.

3.2.8 Temperature denaturation

In order to determine whether or not the presence and position of the His-tag produces a decrease in temperature stability of the enzyme, temperature denaturation experiments were performed on all three proteins (N-terminal His-tag, C-terminal His-tag and No-tag). The temperature scan was performed in potassium phosphate buffer at two different pHs, 6.0 and 7.4. Figure 37 shows the curves obtained at both pHs for all three proteins studied.

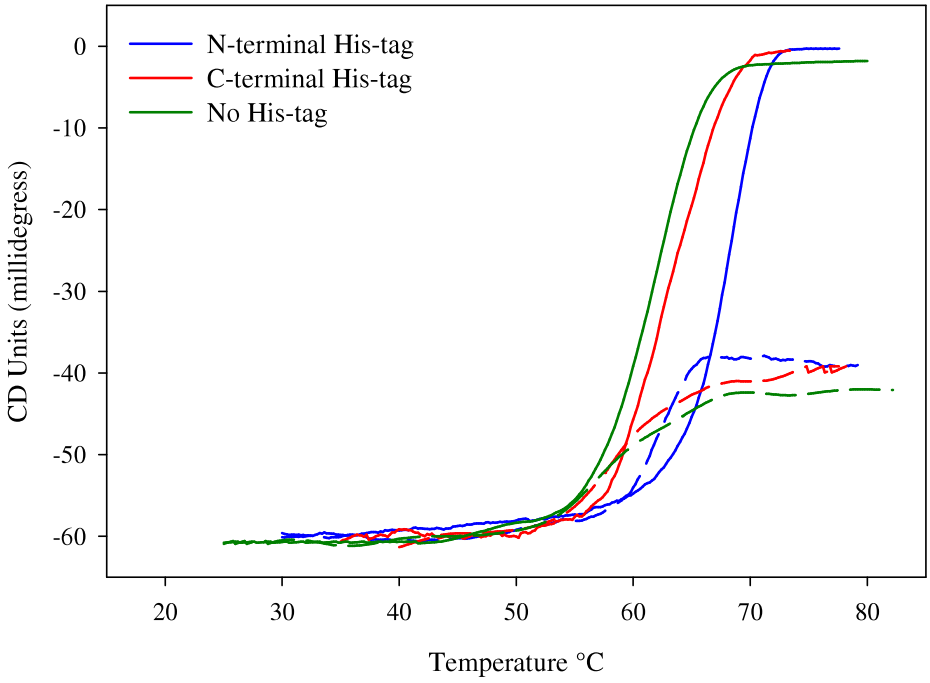

Figure 37 Temperature denaturation by circular dichroism spectroscopy.
Signal intensity at 208 nm is shown for all three proteins. Solid line (———) represents samples at pH 6.0 and dashed-lines (– – – – –) represents samples at pH 7.4.

The shape of all curves at pH 6.0 demonstrate a cooperative unfolding process for all three proteins. The small difference in ellipticity observed at the beginning of the measurement results from small variations in enzyme concentration between samples.

By taking the first derivative of the ellipticity signal, the melting temperatures at pH 6.0 were determined to be 68.4 °C, 62.8 °C and 61.8 °C for the N-terminal His-tag, C-terminal His-tag, and no His-tag proteins, respectively. This result suggests that beside resistance to dissociation by $NaClO_4$ there is also thermal stabilization of the N-terminal His-tag protein.

Temperature denaturation studies at pH 7.4 provided results similar to those in the as in previous section, where the proteins seem to partially denature and then plateau, keeping a significant amount of the ellipticity signal. Table 11 summarizes the T_m values calculated for all samples at both pH.

Enzyme	T_m pH 6.0	Difference from N-terminal His-tag	T_m pH 7.4	Difference from N-terminal His-tag
N-terminal His-tag	68.4 °C	-------	62.4 °C	-------
C-terminal His-tag	62.6 °C	- 5.6 °C	58.0 °C	- 4.4 °C
No His-tag	61.8 °C	- 6.6 °C	56.6 °C	- 5.8 °C

Table 11 Melting temperatures of N-terminal His-tag, C-terminal His-tag and No His-tag. Determined by taking the first derivative of the ellipticity values using the Jasco Spectra Analysis software.

3.3 Kinetics and binding studies

There are not many kinetics studies published on octameric enolase. In this part of the project, kinetic constants were determined and binding studies were performed using ITC. The enzymatic activities of octameric enolase (N-terminal His-tag, C-

terminal His-tag and No His-tag) were examined by monitoring the production of PEP at 240 nm and varying the concentrations of the divalent metal and 2-PGA.

3.3.1 Determination of kinetic constants when varying Mg^{2+}

Activity assays were performed while increasing the magnesium concentration (from 0.25 mM to 5 mM) in metal free buffer (HEPES or MES/Tris) at a concentration of 1 mM 2-PGA . Change in absorbance was monitored for 1 minute. EnzFitter software was used to fit the data to the Michaelis-Menten equation provided in section 2.26. The results obtained by comparing the N-terminal His-tag, C-terminal His-tag and No His-tag, suggest that there is no significant variation between the kinetic parameters. No inhibition was observed at high concentrations of Mg^{2+}.

The kinetic parameters obtained are summarized in Table 12. Figure 38 shows the fit of the data from all three enzymes to the Michaelis-Menten model. In all three samples, the fitted data are in good agreement with the raw data.

Enzyme	K_m [µM]	V_{max} (ΔOD_{240}/min)	k_{cat} s^{-1}
N-terminal His-tag	329.1 ± 16.4	0.151 ± 0.002	193.9 ± 3.1
C-terminal His-tag	308.8 ± 9.1	0.121 ± 0.001	151.5 ± 1.8
No His-tag	271.8 ± 8.9	0.142 ± 0.001	174.3 ± 1.4

Table 12 Kinetic parameters for Mg^{2+} of octameric enolase.
Experiments performed in 100 mM HEPES and 1 mM 2-PGA. A protein concentration of ~0.01 µM was used.

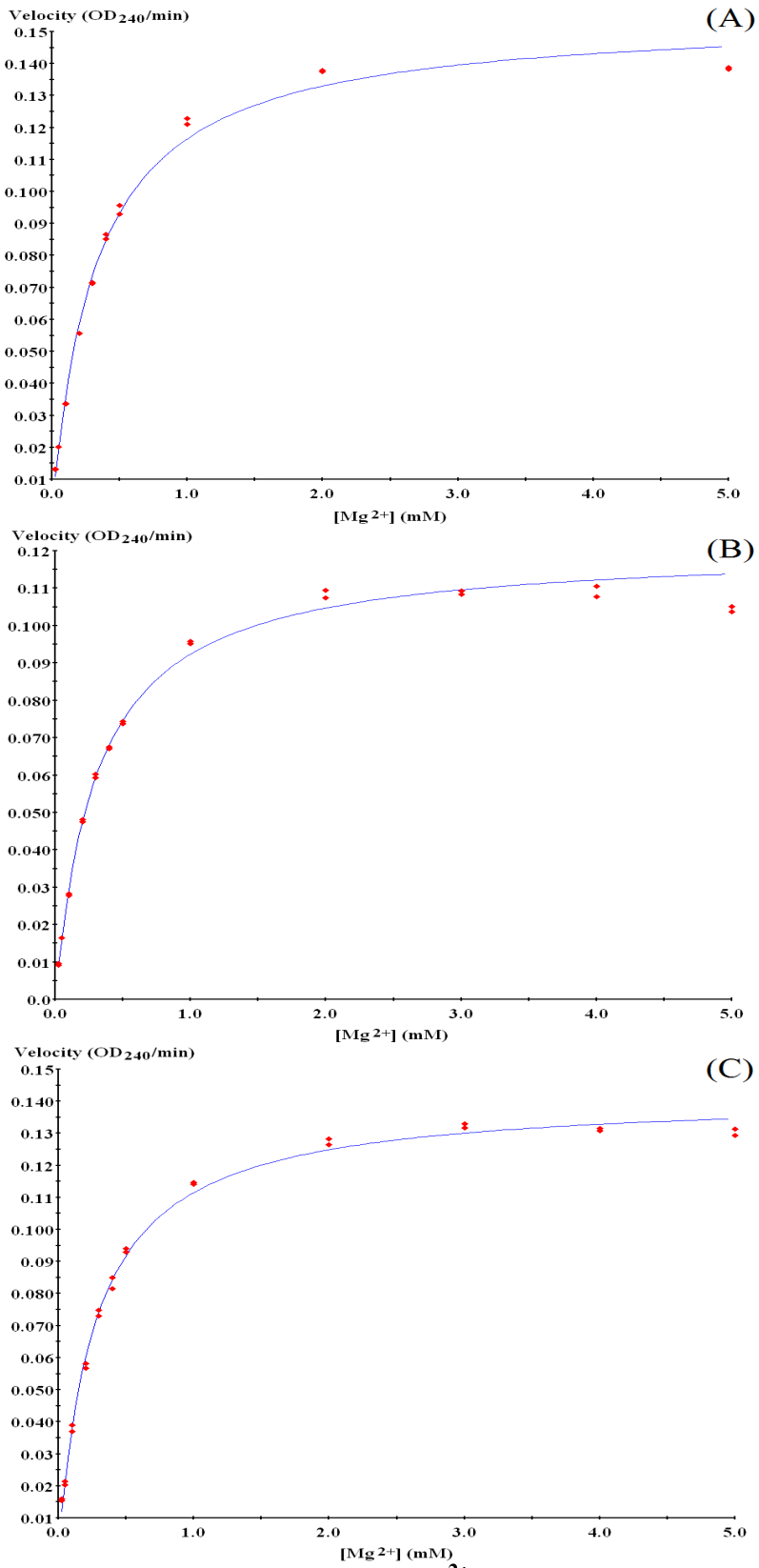

Figure 38 Kinetics studies with increasing [Mg^{2+}] at saturated 2-PGA.
A) N-terminal His-tag, B) C-terminal His-tag C) No His-tag.

3.3.2 Determination of kinetic constants when varying Mn^{2+}

Kinetic studies varying manganese concentrations were also performed. Manganese has been investigated as a cofactor in numerous experiments with yeast enolase. In yeast enolase, Mn^{2+} is the cation which gives in the highest activity after Mg^{2+}. Kinetic assays were performed in the same buffer and 2-PGA concentration as described in section 3.3.1. Table 13 displays the kinetic parameters obtained by fitting the raw data to the modified substrate inhibition equation noted in section 2.26. There are no significant differences between the parameters obtained for the N-terminal His-tag, C-terminal His-tag or No His-tag.

Enzyme	Metal	K_m [µM]	K_i [µM]	Vmax (ΔOD_{240}/min)	kcat s^{-1}
N-terminal His-tag	Mn^{2+}	4.2 ± 0.4	612.1 ± 88.3	0.117 ± 0.008	46.3 ± 3.3
N-terminal His-tag*	Mn^{2+}	3.2 ± 0.2	422.5 ± 43.5	0.090 ± 0.002	36.5 ± 0.7
C-terminal His-tag	Mn^{2+}	3.1 ± 0.1	392.2 ± 34.4	0.114 ± 0.002	33.8 ± 0.5
No His-tag	Mn^{2+}	6.2 ± 0.28	353.9 ± 29.8	0.130 ± 0.002	53.6 ± 1.0

Table 13 Kinetic parameters for Mn^{2+} of octameric enolase.
Samples were assayed in 100 mM HEPES or 50 mM MES-Tris. (*) represents samples analyzed in MES-Tris buffer. A protein concentration of ~0.03 µM was used for all samples.

Samples analyzed in MES-Tris buffer shows similar results compared to those analyzed in HEPES. Samples were analyzed in MES-Tris buffer because experiments for ITC were performed in this buffer.

Figure 39 A, B and C shows the fit for the N-terminal His-tag, C-terminal His-tag and No His-tag to the modified substrate inhibition. The raw data correlate well with the fitted data.

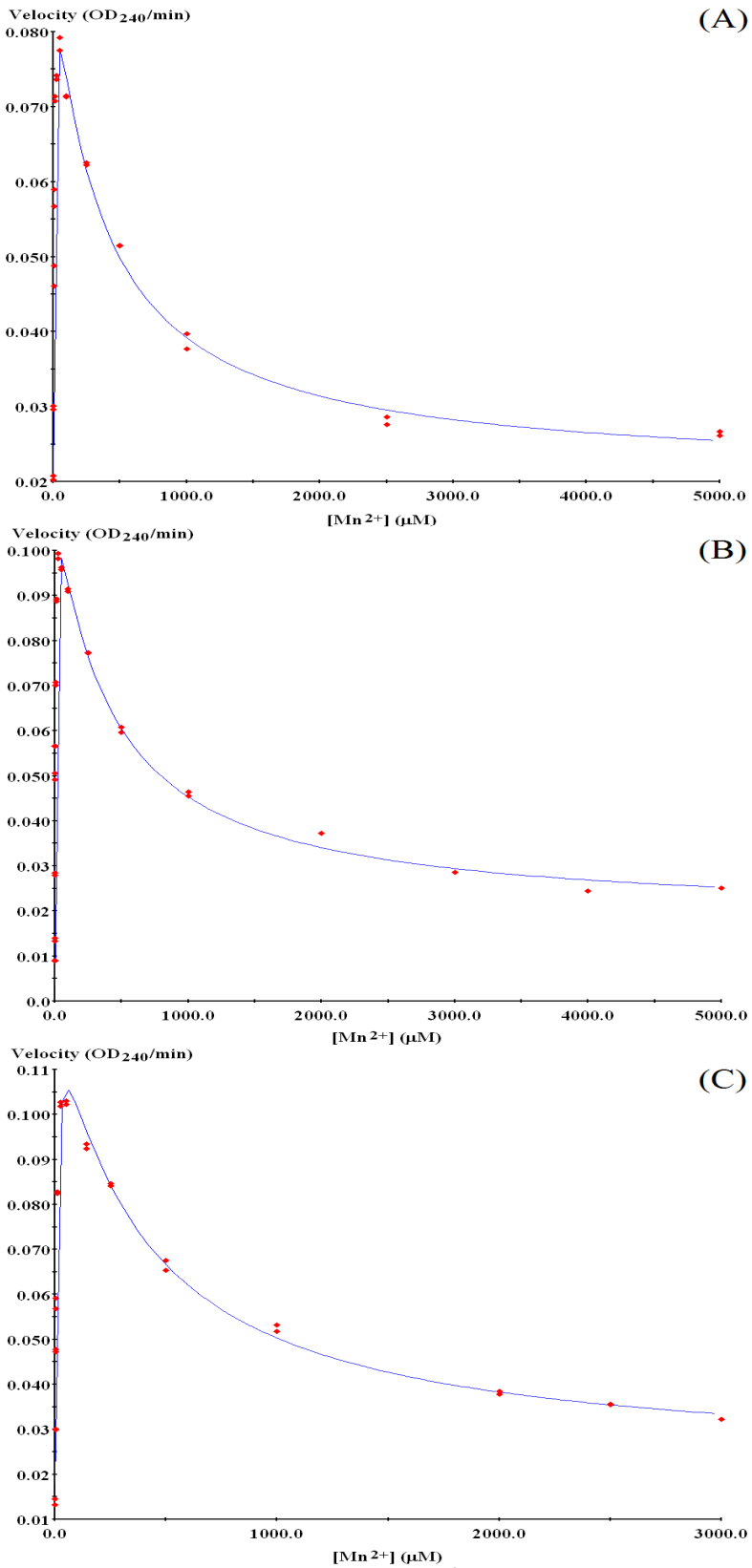

Figure 39 Kinetics studies with increasing [Mn^{2+}] at saturated 2-PGA.
A) N-terminal His-tag, B) C-terminal His-tag, C) No His-tag.

3.3.3 Determination of kinetic constants when varying [2-PGA]

Kinetic studies on the effect of 2-PGA concentration on enzyme activity were performed at a fixed concentration of Mg^{2+} or Mn^{2+}. Enzymatic activity was monitored in the same form as described in section 3.3.1 and 3.3.2. Table 14 summarizes the kinetic constants obtained varying 2-PGA concentration. No inhibition was observed at high concentrations of 2-PGA. As expected, higher K_m and k_{cat} values were obtained at fixed concentrations of Mg^{2+} compared to Mn^{2+}. Similar values were obtained for the kinetic constants when comparing all three proteins, suggesting that the presence or position of the his-tag does not affect the catalytic activity of the protein.

Enzyme	Metal	K_m [µM]	V_{max} (ΔOD_{240}/min)	k_{cat} s^{-1}
N-terminal His-tag	5 mM Mg^{2+}	97.9 ± 3.9	0.115 ± 0.009	136.9 ± 1.1
C-terminal His-tag	5 mM Mg^{2+}	61.3 ± 3.4	0.114 ± 0.001	140.6 ± 1.6
No His-tag	5 mM Mg^{2+}	57.6 ± 1.4	0.143 ± 0.008	176.1 ± 1.1
N-terminal His-tag	50 µM Mn^{2+}	24.8 ± 1.6	0.092 ± 0.001	38.5 ± 0.5
N-terminal His-tag *	50 µM Mn^{2+}	21.4 ± 1.0	0.080 ± 0.080	33.5 ± 0.4
N-terminal His-tag *	1 mM Mn^{2+}	17.0 ± 0.7	0.063 ± 0.004	12.0 ± 0.1

Table 14 Kinetic parameters for 2-PGA of octameric enolase.
Samples were assayed in 100 mM HEPES or 50 mM MES-Tris. (*) represents sample analyzed in MES-Tris buffer. A protein concentrations of ~0.015µM for 5 mM Mg^{2+}, 0.0301 µM for 50 µM Mn^{2+} and ~0.0656 µM 1 mM Mn^{2+} were used.

In order to have comparable data for ITC experiments, kinetic parameters for enolase at varying concentration of 2-PGA at two concentrations of Mn^{2+} were employed. Similar K_m values were obtained at 50 µM, and 1 mM Mn^{2+} concentrations while k_{cat} decreased at saturated concentration of 1 mM Mn^{2+}, probably due to the fact that at this concentration there is a large degree of inhibition.

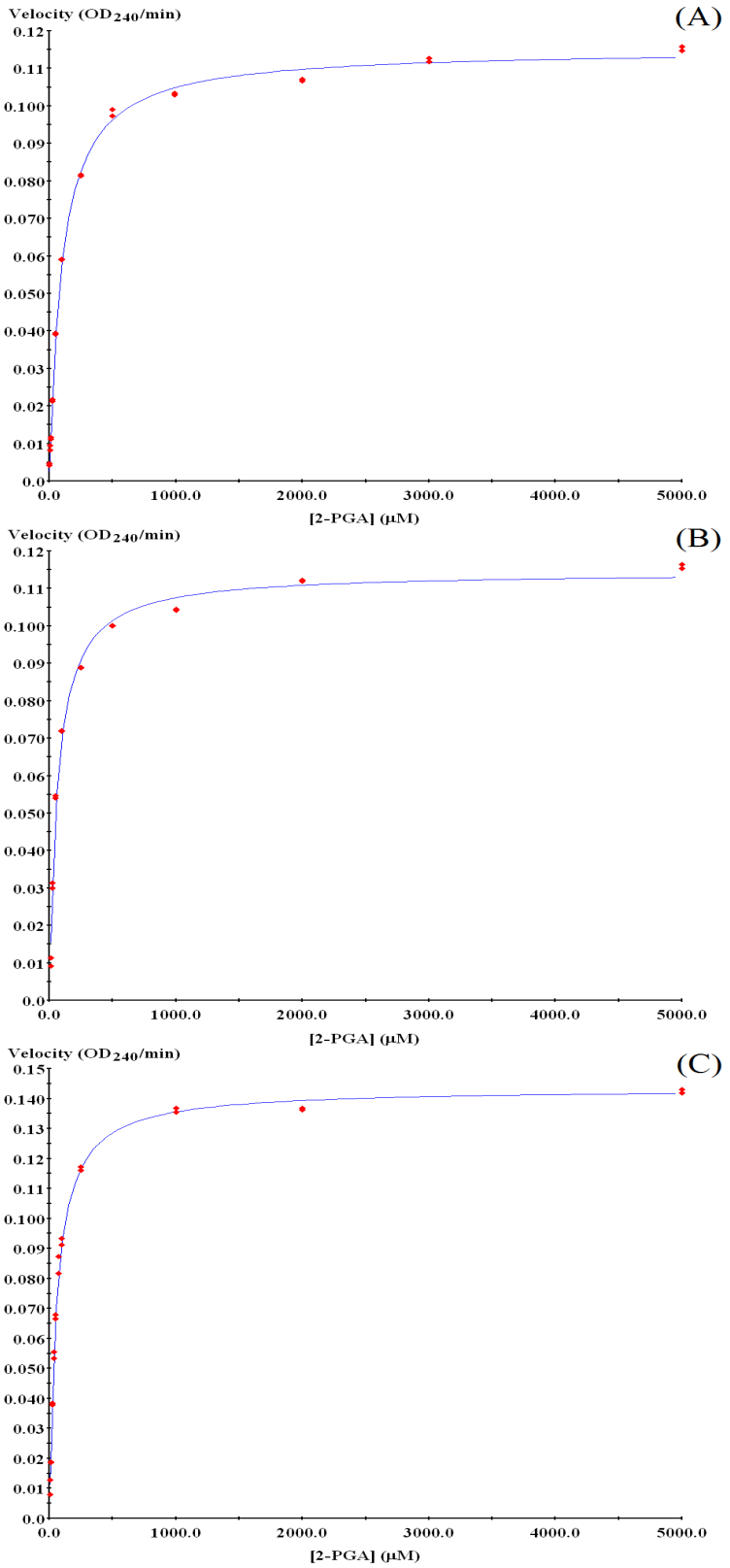

Figure 40 Kinetics studies with increasing [2-PGA] at 5 mM Mg^{2+}
A) N-terminal His-tag, B) C-terminal His-tag, C) No His-tag.

3.3.4 Binding experiments using ITC

Isothermal Titration Calorimetry (ITC) was used to determine binding parameters including enthalpy (ΔH), entropy (ΔS), reaction stoichiometry (n), and binding constants (K) for N-terminal His-tag octameric enolase. This experiment requires the monitoring of the heat changes upon a titrated substrate binding to the enzyme. The calorimetric titration was performed in 50 mM MES-Tris buffer with 1 mM Mn^{2+}. The substrate binding constant was obtained using an equilibrium mix of PEP/PGA. A protein concentration of 44.3 μM was used and a concentration of 0.637 μM for PEP.

MicroCal Origin software was used to integrate the raw data and the cumulative heat was plotted against substrate concentration. The results were fitted to a one binding site model because a better fit and lower standard errors are obtained. Table 15 lists the results obtained for the titration of substrate to the N-terminal His-tag protein.

	Value	units
Chi-squared	2541	
N	0.9479 ± 0.009	
K	$1.62 \times 10^6 \pm 2.52 \times 10^5$	K^{-1}
ΔH	-1252 ± 17.98	cal/mol
ΔS	24.21	cal/K

Table 15 Binding parameters for the N-terminal His-tag determined by ITC.

The K_d was determined to be 0.61 μM which is considerably lower than the Km values obtained for enolase varying [2-PGA] in the presence of Mn^{2+}. Figure 41 displays the raw and fitted data from the ITC experiment.

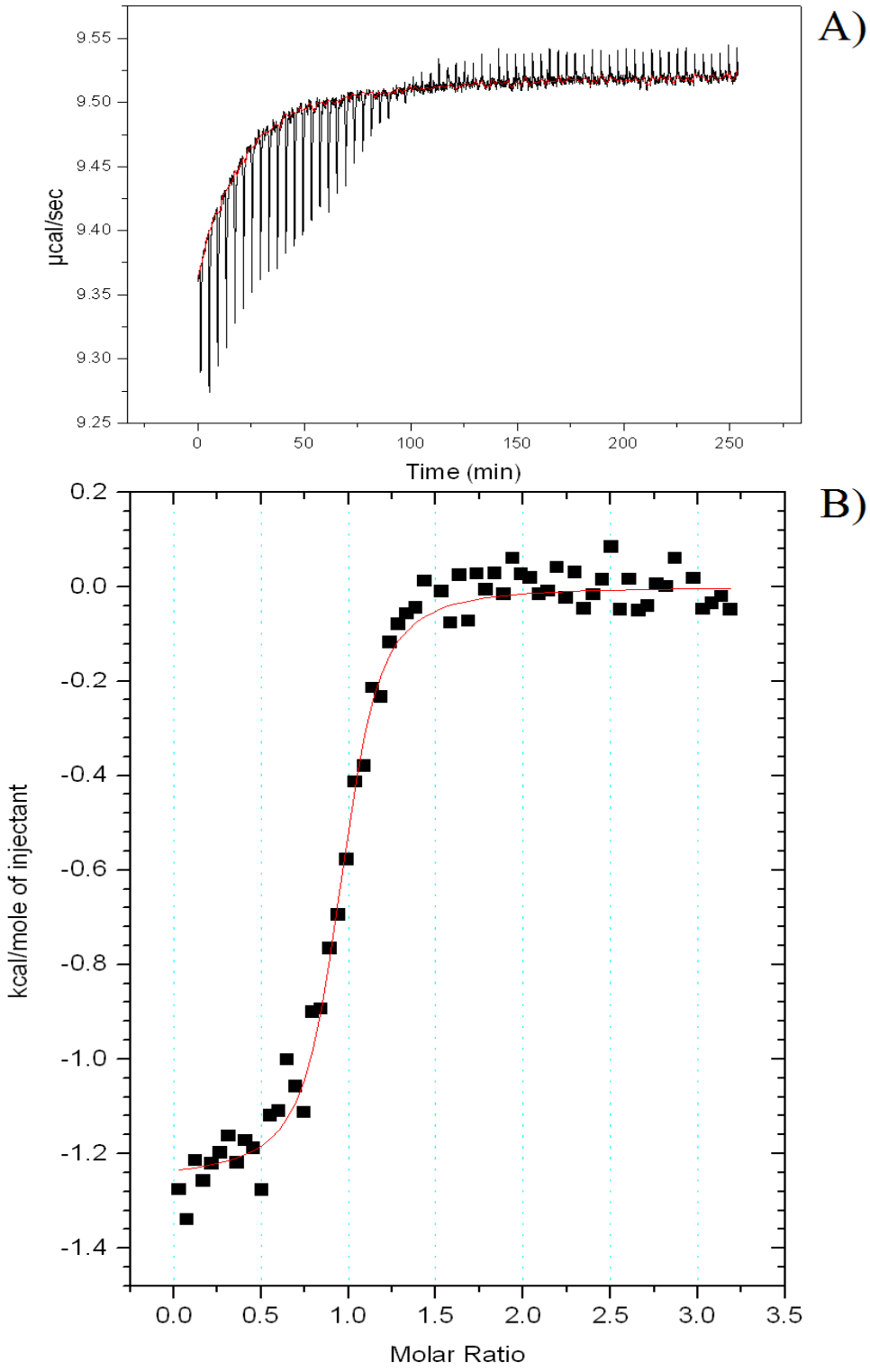

Figure 41 ITC graph of PEP/PGA mixture titration.
A) Raw ITC data, B) Binding isotherm fitted to a one site model. Graph was generated using MicroCal Origin software.

Chapter 4 Discussion

4.1 Design of two variants to explore the influence of the loop connecting H4-S4 in determining quaternary structure.

As mentioned earlier, X-ray crystal structure of *S. pneumonia* enolase has shown that a loop connecting H4-S4 is involved in the dimer-dimer interaction (Ehinger *et al.*, 2004). Structural superimposition of yeast dimeric enolase and *S. pneumonia* octameric enolase (Figure 9) demonstrates that in yeast enolase there is one extra turn at the end of H4, and that the H4-S4 loop is shorter by 3-5 amino acids compared to the same loop in octameric enolase. Ehinger *et al.* (2004) proposed that creating an extra turn at the end of H4 in octameric enolase may prevent the formation of octamers. In order to test this hypothesis, two variant proteins were successfully created. The first variant was called ADLS, since amino acids 135-137 (GGFN) were changed to ADLS (the amino acid sequence in yeast enolase). In the second variant the same amino acids were changed to four alanines, which are known to have a high helical propensity.

Wild-type, ADLS and AAAA enolase proteins were prepared using QuikChange site-directed mutagenesis. DNA sequence analysis showed that the desired substitutions had indeed been introduced, and unwanted mutations had not been incorporated. The recombinant proteins were correctly expressed and purified using Ni-NTA chromatography column. In general, approximately 100 mg of wild-type octameric enolase was obtained per 1 L culture. The level of purity of the wild-type protein was higher than what was obtained for both ADLS and AAAA proteins. The purification of both variants was improved by increasing the concentration of imidazole in the wash

buffer from 20 mM (used for wild-type) to 35 mM, and by also increasing the volume of the washes. Although, protein purity was significantly improved, there were still other small bands of protein visible in the SDS-PAGE (Figure 15 and 17).

The wild-type and variant proteins were examined using spectroscopic techniques such as circular dichroism (CD) and analytical ultracentrifugation (AUC). Although the CD spectra of wild-type and both variants appear to be identical in the 200-280 nm region, differences become noticeable when the circular dichroic absorbance is measured at lower wavelengths (Figure 19). An overlay of the CD spectra from wild-type, ADLS and AAAA variants show that the biggest difference in CD signal intensity is apparent at 190 nm. DICHROWEB was used to analyze the CD spectra obtained. DICHROWEB is a web server which enables on-line analysis of CD spectroscopic data, providing a calculated estimate of secondary structure content and graphical analysis comparing calculated structures and experimental data (Whitmore *et al.*, 2004). According to this analysis, there is a difference in the percent of α-helices. The percent of α-helical content decreased from 56% in the wild-type protein to 49% in the ADLS variant; this percent decrease was even more pronounced for the AAAA, 45%. On the other hand, in both variants the percent of unordered structure increased from 18% (wild-type) to 21% and 24% for ALDS and AAAA variants. Since both variants are partially dissociated, this may account for the difference in the percent α-helical content and unordered structure. The DICHROWEB results reported in yeast enolase, indicate that a small increase in unordered structure is related to a dissociation of quaternary structure (Zhao *et al.*, 2008).

The 56% α-helical content observed in the wild-type was higher than expected. According to the crystal structure of *S. pneumoniae* (1W6T.pdb), octameric enolase is

composed of 40% α-helices and 14% β-strands. Similar composition values were anticipated for octameric enolase from *S. pyogenes*, since both enolases share 93% sequence identity. Wild-type protein shows a 16% discrepancy between the DICHROWEB analysis and the crystal structure. A drawback to this software is that a slight variation in the experimental determination of the protein concentration will provide a large difference in the resulting α-helical and β-strand percentages obtained from the software. However, a 16% discrepancy seems relatively high to be a product of an error in protein concentration. At this point the reason for this difference is unknown, especially because studies on yeast enolase have shown good agreement between the DICHROWEB analysis and the theoretical data from the crystal structure. One possible reason for this discrepancy could be from imidazole contamination of the sample from the purification process. It has been shown previously that imidazole absorbs in the far-UV region (Kelly *et al.*, 2005). Another hypothesis could be that the His-tag might contribute to the difference in absorbance. Clearly, more experiments must be done in order to determine whether there is really a difference in secondary structure, or whether there are other factors altering the CD spectra.

4.1.1 The effect of the ADLS and AAAA mutations on enzymatic activity and protein stability

The enzymatic activities of both variants were found to be dramatically decreased compared to the wild-type. About 65% of enzymatic activity was lost when the ADLS mutations were introduced to octameric enolase and approximately 85% of enzymatic activity was lost for the AAAA variant. The sedimentation velocity data collected

provided useful information on the proteins. The AUC experimental data showed that both variants, ADLS and AAAA, are partially dissociated (Figure 22). Only, 50% of the quaternary structure in the ADLS protein is octameric and only 34% in the AAAA variant. It seems that only the octameric and dimeric species have enzymatic activity. Despite the fact that these mutations were performed at the dimer-dimer interface, most of the species observed in the sedimentation velocity experiment are either monomeric or octameric, with a low dimeric percentage.

Previous experiments using sedimentation velocity have show that incubation with $NaClO_4$ produces changes in the quaternary structure and that this dissociation correlates with inactivation of *S. pyogenes* enolase (Karbassi *et al.*, 2010). Both variants were more susceptible to inactivation by $NaClO_4$ compared to the wild-type protein. This inactivation was follow by sedimentation velocity experiments and both variants were more easily dissociated than the wild-type. One possible reason for the ADLS and AAAA to be more sensitive to inactivation is that these proteins are already partially monomeric and dimeric; therefore, in order to obtain complete dissociation a lower concentration of $NaClO_4$ is required. Interestingly, all three proteins including the wild-type octameric enolase in the presence of $NaClO_4$ seem to dissociate directly into monomers with a very low percentage of dimers. Together with other experiments in our lab, we have observed that weakening the dimer-dimer interface of this protein also weakened the monomeric interface. These results suggest that the dimeric form of *S. pyogenes* is unstable.

The temperature denaturation curve at pH 6.0 of wild-type enolase demonstrates a cooperative unfolding process, while the ADLS and AAAA variants unfold in a more

gradual process with two phases. Even though, both ADLS and AAAA proteins show a two-step unfolding process, there is a difference in the temperature at which melting occurs. In the first phase of the curve, ADLS lost 50% in its CD signal with a T_m of 34.6 ºC, followed by the complete loss of CD signal with a T_m of 51.6 ºC. On the other hand, the AAAA protein lost approximately 70% of the CD signal in the first part of the curve and only 30% in the second portion of the curve, with corresponding T_m of 30.4 ºC and 54.8 ºC, respectively. In both ADLS and AAAA the percent unfolded protein in the first phase correlates closely with the percentage of smaller species (monomers and dimers) observed by sedimentation velocity experiments, while the percent unfolded for the second phase correlates with the percentage of octamers.

4.1.2 Equilibrium between species from the variants

FPLC gel filtration was used to separate the species in both variant proteins. High performance gel filtration chromatography provided an excellent means for separating dimers/monomers from octamers according to their differences in size. Separated samples were analyzed for quaternary structure using AUC and DLS. Sedimentation velocity experiments show that the first sample eluted from the column was mainly octameric. On the other hand the second sample eluted was mostly monomeric. These results were also confirmed by DLS, which provided a similar hydrodynamic radius of 6.2 nm for the octamers compared to the previous published value of 6.4 nm for the *S. pyogene* octameric enolase (Karbassi *et al.*, 2010). The monomeric fraction has a smaller hydrodynamic radius, which is indicative of smaller species. The fact that we observe discrete species in the AUC experiments indicates that equilibration among the species is slow. The enzymatic activity of the AAAA variant was monitored over 48 hours.

During the first 24 hours the enzymatic activity of the sample, which was mainly octameric, had decreased 60% compared to time zero. After 48 hours the activity had decreased approximately 70%. This suggests that the majority of the equilibrium among species occurs slowly, during the first 24 hours. These experiments provided a rough picture regarding the equilibrium among species, but more experiments should be done. It would be interesting to monitor samples eluted from the gel filtration FPLC for enzymatic activity, sedimentation velocity and DLS every twelve hours for longer periods of time, in order to obtain more information about this equilibrium.

In summary, it was not possible to create dimeric enolase from octameric enolase. However, it was possible to prevent the complete formation of octamers by changing the amino acid sequence. It is clear that amino acids 135-138 play an important role in octamer formation. Nevertheless, with the information obtained it is not possible to be certain that an extra turn at the end of H4 was actually introduced. The disruption of octameric enolase could be result from an extra turn at the end of H4, or it could be also result from the presence of bulkier amino acids. Two tandem glycines were substituted by alanine and aspartic acid; aspartic acid in particular is a bulkier amino acid, which may be causing some kind of steric effect and preventing the formation of octamers.

4.2 Stabilization by the N-terminal His-tag

One of the most commonly used tags to purify and detect recombinant proteins is the polyhistidine tag (Yip *et al.*, 1989). Protein purification employing polyhistidine tags relies on the affinity of histidine residues for immobilized metals such as nickel, which permits selective protein purification (Hutchens *et al.*, 1990). Although it is frequently

assumed that the introduction of a His-tag has little or no effect on stability, this is not always confirmed experimentally. We have show that the N-terminal His-tag stabilizes the octameric enolase from *S. pyogenes*.

The first approach employed to explore the effects of the tag on stability was to clone octameric enolase into pET-3a. This vector expresses proteins that do not require a Ni-NTA chromatography column for its purification. Since this protein does not have a His-tag, the purification procedure is more complicated and requires two different columns for purification (hydrophobic Interaction Chromatography/Phenyl Sepharose and Q-Sepharose), with a total yield of purified protein from this technique much lower than with the His-tagged protein. Only 3 mg of protein were obtained per litre of culture.

The second approach used to remove the tag was to cleave peptide bond located after the His-tag using thrombin. The N-terminus is located inside of the ring-like structure and is found to be buried preventing the cleavage of the tag using thrombin. The N-terminal his-tagged protein was treated with thrombin, but after more than 24 hours of incubation, thrombin began to digest other parts of the protein, but not the tag.

The final approach was to clone the gene encoding octameric enolase into pET-52b(+) vector. This allow expression of a C-terminal his-tagged protein. The C-terminal his-tag was more accessible than the N-terminal His-tag for thrombin digestion; cleavage was completed within 8 hours.

Sodium perchlorate experiments at pH 7.4 have shown that the His-tag in octameric enolase stabilizes the quaternary structure. One of the reasons for this stabilization could be that the histidines in the tag, located at the N-terminus, might be interacting with each other, making it more resistant to $NaClO_4$ dissociation. On the

other hand, incorporation of the polyhistidine tag in the C-terminus of octameric enolase does not seem to stabilize the quaternary structure. Similar results were observed for the octameric enolase without the His-tag. It was necessary to use higher concentrations of $NaClO_4$ for the N-terminal His-tag in order to obtain complete enzymatic inactivation compared to the C-terminal His-tagged and no His-tagged protein (Figure 24). Similar experiments were performed at pH 8.6 instead of 7.4. Surprisingly, the stabilization of the N-terminal His-tagged protein observed at pH 7.4 appears to be lost at pH 8.6. The pKa of histidine is approximately 6.0 (Nelson *et al.*, 2004), above the pKa deprotonation occurs. It appears that the stabilization is lost when the protein is less protonated. It seems more likely that, if the His-tags would interact together to stabilize the octamer, it would be in neutral form of histidine, not its charged form, because all the charged histidines would repel one another. However, other studies suggest that histidine-histidine pairs may play a role in protein stability and protein-protein interactions under acidic conditions (Heyda *et al.*, 2010). There are many questions raised from this finding. Since it is not understood how His-tags interact in order to improve quaternary structure stability, it would be worth performing experiments under acidic conditions to observe if the strength of this stabilization would be affected.

Stabilization of the N-terminal His-tagged protein was also observed in the temperature denaturation experiments. The resulting curves for all three proteins at pH 6.0 (N-terminal, C-terminal and No His-tagged) reflected a steep transition without any intermediates (Figure 37). Abruptness in the denaturation is indicative of a cooperative transition (Creighton, 1993). The calculated T_m for the N-terminal His-tagged protein was 6.6 ºC more stable than the no His-tagged protein and 5.6 ºC more stable than the C-

terminal His-tagged protein. Although the temperature denaturation curves at pH 7.4 do not go to completion for all three enolases, N-terminal His-tagged protein has a T_m which is 5.8 ºC more stable than the no His-tagged protein, and 4.4 ºC more stable than the C-terminal His-tagged protein.

4.1.1 Kinetics and Binding Studies

Kinetic studies were performed in order to obtain a general idea of whether the kinetics of octameric enolase compare to those of yeast enolase. Also, a comparison of the proteins with differences in the presence and position of the His-tag was examined to observe whether the affinity for the divalent metals (Mg^{2+} and Mn^{2+}) or substrate (2-PGA) was affected by the His-tag. All the proteins, regardless of the position or absence of the His-tag, show similar substrate/metal ion affinities (K_m), and turnover number (k_{cat}). Previous kinetic studies on yeast enolase preformed in our lab, show that the K_m for Mg^{2+} is 10-fold lower in yeast compared to octameric enolase. Kinetic studies for Mn^{2+} in yeast and octameric enolase show inhibition and similar K_m and k_{cat} for both proteins. However, K_i of Mn^{2+} was 12-fold higher in the octameric enolase than yeast enolase. Substrate kinetic studies show similar affinities for 2-PGA in both yeast and octameric enolase in the presence of either Mg^{2+} or Mn^{2+}.

Binding studies were performed using isothermal titration calorimetry (ITC). ITC has become an important method to determine binding for biological processes, including protein-ligand binding. This technique provides a direct method to measure the heat change during complex formation. This technique involves one binding partner, in our case the ligand, which is titrated into a solution containing the protein, thereby generating or absorbing heat. This heat can be directly observed and quantified by the calorimeter

(Perozzo *et al.*, 2004). The heats of single substrate addition to the enzyme are integrated and plotted against the molar ratio of the substrate. Binding experiments were performed at 40 μM protein concentration and 1 mM of Mn^{2+}. When lower concentrations of Mn^{2+} were used, we were unable to obtain good data and a smaller ΔH was obtained. However, experiments with yeast enolase have been performed at much lower concentrations (50-1000 μM) and the values for the equilibrium dissociation constant (K_d) and ΔH were not affected. This seems to suggest that the binding of Mn^{2+} is much weaker in octameric enolase.

The dissociation constant, K_d, is a measure of how tightly an enzyme binds to the enzyme-substrate complex. For some enzymes, the enzymatic reactions exhibit simple Michaelis-Menten kinetics in which product formation is the rate-limiting step. Therefore, K_m is similar to $K_{d,}$. For those enzymes, K_m can be referred to as an approximate measure of binding affinity of a substrate to an enzyme. However, equilibrium dissociation constant for the octameric enolase was found to be 0.61 μM which is 30-fold lower than the K_m, suggesting that the rate of the catalytic step is different than the substrate binding rate. Therefore, nothing can be said about the enzyme affinity from the Michaelis constant alone.

4.1.2 Temperature denaturation at pH 7.4

While studying the stabilization of the His-tag protein surprising temperature denaturation curves were observed at pH 7.4. Temperature denaturation at pH 6.0 occurs in a cooperative manner. Interestingly, when similar experiments were performed at pH 7.4 about one third of the CD signal was lost, and then a plateau was present up to 100 ºC. Preliminary experiments performed in our lab have also showed similar results at pH

7.0. From pH 6.0 to 7.0 there is just a difference of one pH unit, which causes a significant variation in the manner that octameric enolase is denatured.

Protein unfolding has been conventionally believed to be a cooperative process, where only the native and unfolded states are stable. It has been shown that a variety of proteins under certain conditions demonstrate conformations that are neither fully folded nor fully unfolded (Creighton, 1993). One of the explanations for this observation can be that a higher pH (7.4) increasing temperature leads to dissociation into monomers, which changes into a highly stable conformation that does not denature. More experiments are necessary in order to obtain more information about the unfolding process of octameric enolase at higher pH.

The use of affinity tags is preferred for purification since it can be quick, simple, efficient, and used for large scale purification. However, many have taken for granted that these tags have little effect on native protein structure. Other studies have indicated that, a His-tag has either a destabilizing or functional effect on proteins. Comparison of the lipase protein with and without the His-tag has been reported (Horchani *et al.*, 2009). Studies on this protein have shown that purified protein production was improved by 8 - 15 fold when using the pET14b vector which carries an N-terminal His-tag. However, their results reveal that the hexahistidine-tag, when placed at the N-terminus, negatively affects the specific activity and thermostability of lipase (Horchani *et al.*, 2009). Other studies using the terminase enzyme from bacteriophage λ have shown that the His-tag has an effect on DNA-binding (Hang *et al.*, 1999). On the other hand, many other experiments using various proteins have shown no effect at all of the His-tag on protein function (Dabrowski *et al.*, 1998; Dabrowski *et al.*, 2003; Mason *et al.*, 2002).

Conclusion

Most of the goals planned at the beginning of this research project were accomplished. We obtained important information about octameric enolase from *S. pyogenes*, however, as scientific investigation the more results obtained, the more questions emerged.

For the first part this project examines the hypotheses presented by Brown *et al.* and Ehinger *et al.* They suggested that an extra turn at H4 may destroy the dimer-dimer interface and prevent octamer formation. The ADLS and AAAA variants show that amino acids at the end of H4 and at the beginning of the loop connecting H4 and S4 (135-138) play an important role in the quaternary structure of octameric enolase. Introducing those four amino acid substitution, it was possible to significantly decrease the formation of octamers. ADLS and AAAA variants exist as a mixture of octamers, monomers, dimers, and possibly other intermediates. Enolase octameric formation is not based exclusively on those amino acids. As previous observations, when the dimer-dimer interface is weakened, it will also cause weakening of the monomeric interface. Therefore, the way that the octameric structure is held together is more complex than just a loop at the dimer-dimer interface.

Temperature denaturation of the ADLS and AAAA variants show two phases for the unfolding process. It seems that in the first phase of temperature denaturation the monomers and dimers unfold first, followed by the unfolding of the octamers.

From the second part of the project we conclude that the His-tag at the N-terminus of octameric enolase stabilizes the protein structure. This stabilization occurs at pH 7.4 but not at 8.6, therefore it appears that this stabilization occurs when the histidines are

protonated. The His-tag at the N-terminus stabilizes the octameric structure in a manner that is pH dependent; when the pH is increased the stabilization is lost. According to the $NaClO_4$ experiments, there is no difference in stability between the C-terminal His-tag and the absence of the tag. Temperature denaturation at pH 6.0 shows that the N-terminal His-tag is approximately 6 ºC more stable than the C-terminal and no His-tagged protein. Although the addition of the His-tag is a simple and well established approach to facilitate purification, there results suggest the need to remove the tag before characterization of some proteins.

Temperature denaturations at pH 6.0 demonstrate a cooperative unfolding process, but temperature denaturations performed at pH at 7.4 demonstrate a partial denaturation process, indicating a more stable conformation. This new conformation did not denature even when the temperature reached 100 ºC, this was observed for all proteins studied.

Kinetic studies performed on wild-type enolase show that there is inhibition at high concentrations of Mn^{2+}. The kinetic parameters obtained for 2-PGA are similar for octameric enolase from *S. pyogenes* and dimer enolase from yeast. The equilibrium dissociation constant (K_d) for PEP was found to be 30-fold lower than the K_m for the octameric enolase.

Future Work

ADLS and AAAA variant proteins were created with the purpose of forming an extra turn at the end of Helix 4. Therefore, to determine if indeed this mutation creates an extra turn, X-ray crystallography of the variants will provide information about any structural changes that may have occurred. Also X-ray crystallography of the wild-type octameric enolase with the His-tag in the N-terminus will provide substantial details about how the histidines interact together to create a more stable quaternary structure. Results from the first crystallization trials of the wild-type are promising, but optimizations of the crystallization conditions are required.

Since we have observed that the His-tag stabilized the quaternary structure at pH 7.4 but not 8.6, experiments at pH 6.0 should provide some information about whether or not the stabilization occurs when the protein is protonated. $NaClO_4$ dissociation experiments will be a more convenient approach to compare the results obtained in this project.

Secondary structure analysis using DICHROWEB showed discrepancies between the percentage of α-helices calculated from the CD spectra and the percentage calculated from the crystal structure. In order to confirm that this difference is not due to imidazole or nickel contamination resulting from the Ni-NTA chromatography column for purification, more experiments should be performed using wild-type octameric enolase in pET-3a which was not expressed with a His-tag. Even though the process of protein purification is complicated, experiments on this protein could help to understand the differences in the content of α-helices.

Another aspect that is worth investigating is the pH dependence of temperature denaturation. Complete temperature denaturation occurs at pH 6.0 but the protein does not appear to complete the unfolding process at 7.4. Useful information would be obtained from a complete denaturation profile between pHs 6.0 and 7.0 (by increments of 0.1 pH units) in order to determine at which pHs the shift occurs between complete and partial denaturation. Another experiment that would be worth pursuing is chemical denaturation at different pHs in order to determine if it would prevent complete denaturation at higher pHs as observed with temperature, or if it would follow a different pattern.

References

Anderson, V. E., Weiss, P. M., & Cleland, W. W. (1984). Reaction intermediate analogues for enolase. *Biochemistry, 23*(12), 2779-2786.

Angiolella, L., Facchin, M., Stringaro, A., Maras, B., Simonetti, N., & Cassone, A. (1996). Identification of a glucan-associated enolase as a main cell wall protein of candida albicans and an indirect target of lipopeptide antimycotics. *The Journal of Infectious Diseases, 173*(3), 684-690.

Arakawa, T., & Timasheff, S. N. (1982). Preferential interactions of proteins with salts in concentrated solutions. *Biochemistry, 21*(25), 6545-6552.

Banner, D. W., Bloomer, A. C., Petsko, G. A., Phillips, D. C., Pogson, C. I., Wilson, I. A., Corran, P. H., Furth, A. J., Milman, J. D., Offord, R. E., Priddle, J. D., & Waley, S. G. (1975). Structure of chicken muscle triose phosphate isomerase determined crystallographically at 2.5 Ångstrom resolution using amino acid sequence data. *Nature, 255*(5510), 609-614.

Barnes, L. D., & Stellwagen, E. (1973). Enolase from the thermophile *Thermus* X-1. *Biochemistry, 12*(8), 1559-1565.

Berg, J., Tymoczko, J., & Stryer, L. (2002). *Biochemistry* (Fifth ed.) W.H. Freeman and Company.

Bergmann, S., Rohde, M., Chhatwal, G. S., & Hammerschmidt, S. (2001). Alpha-enolase of *Streptococcus pneumoniae* is a plasmin(ogen)-binding protein displayed on the bacterial cell surface. *Molecular Microbiology, 40*(6), 1273-1287.

Bewsey, K. E., Johnson, M. E., & Huff, J. P. (1991). Rapid isolation and purification of DNA from agarose gels: The phenol-freeze-fracture method. *BioTechniques, 10*(6), 724-725.

Brewer, J. M. (1985). Specificity and mechanism of action of metal ions in yeast enolase. *FEBS Letters, 182*(1), 8-14.

Brewer, J. M., & Collins, K. M. (1980). Studies of the role of catalytic and conformational metals in producing enzymatic activity in yeast enolase. *Journal of Inorganic Biochemistry, 13*(2), 151-164.

Brewer, J. M., & Ellis, P. D. (1983). 31P-nmr studies of the effect of various metals on substrate binding to yeast enolase. *Journal of Inorganic Biochemistry, 18*(1), 71-82.

Brewer, J. M., & Weber, G. (1968). The reversible dissocation of yeast enolase. *Proceedings of the National Academy of Sciences of the United States of America, 59*(1), 216-223.

Brewer, J. M., Carreira, L. A., Collins, K. M., Duvall, M. C., Cohen, C., & DerVartanian, D. V. (1983). Studies of activating and nonactivating metal ion binding to yeast enolase. *Journal of Inorganic Biochemistry, 19*(3), 255-267.

Brown, C. K., Kuhlman, P. L., Mattingly, S., Slates, K., Calie, P. J., & Farrar, W. W. (1998). A model of the quaternary structure of enolases, based on structural and evolutionary analysis of the octameric enolase from *Bacillus subtilis*. *Journal of Protein Chemistry, 17*(8), 855-866.

Brown, T. A. (1991). *Molecular biology LabFax*. San Diego, USA: Academic Press Inc and Bios Scientific Publishers Ltd.

Capage, M., & Hill, C. W. (1979). Preferential unequal recombination in the glyS region of the *Escherichia coli* chromosome. *Journal of Molecular Biology, 127*(1), 73-87.

Carneiro, C. R., Postol, E., Nomizo, R., Reis, L. F., & Brentani, R. R. (2004). Identification of enolase as a laminin-binding protein on the surface of staphylococcus aureus. *Microbes and Infection / Institut Pasteur, 6*(6), 604-608.

Castellino, F. J., & Powell, J. R. (1981). Human plasminogen. *Methods in Enzymology, 80 Pt C*, 365-378.

Chin, C. C., Brewer, J. M., & Wold, F. (1981). The amino acid sequence of yeast enolase. *The Journal of Biological Chemistry, 256*(3), 1377-1384.

Cohn, M., Pearson, J. E., O'Connell, E. L., & Rose, I. A. (1970). Nuclear magnetic resonance assignment of the vinyl hydrogens of phosphoenolpyruvate. stereochemistry of the enolase reaction. *Journal of the American Chemical Society, 92*(13), 4095-4098.

Collen, D. (2001). Ham-wasserman lecture: Role of the plasminogen system in fibrin-homeostasis and tissue remodeling. *Hematology / the Education Program of the American Society of Hematology.American Society of Hematology.Education Program,* , 1-9.

Collins, K. D., & Washabaugh, M. W. (1985). The Hofmeister effect and the behaviour of water at interfaces. *Quarterly Reviews of Biophysics, 18*(4), 323-422.

Collins, K. M., & Brewer, J. M. (1982). Circular dichroism (CD) studies on yeast enolase: Activation by divalent cations. *Journal of Inorganic Biochemistry, 17*(1), 15-28.

Cork, A. J., Jergic, S., Hammerschmidt, S., Kobe, B., Pancholi, V., Benesch, J. L., Robinson, C. V., Dixon, N. E., Aquilina, J. A., & Walker, M. J. (2009). Defining the structural basis of human plasminogen binding by streptococcal surface enolase. *The Journal of Biological Chemistry, 284*(25), 17129-17137.

Creighton, T. E. (1993). *Proteins: Structures and molecular properties* (Second ed.). New York: W.H. Freeman and Company.

Dabrowski, S., & Kiaer Ahring, B. (2003). Cloning, expression, and purification of the His6-tagged hyper-thermostable dUTPase from *Pyrococcus woesei* in *Escherichia coli*: Application in PCR. *Protein Expression and Purification, 31*(1), 72-78.

Dabrowski, S., & Kur, J. (1998). Recombinant his-tagged DNA polymerase. I. cloning, purification and partial characterization of *Thermus thermophilus* recombinant DNA polymerase. *Acta Biochimica Polonica, 45*(3), 653-660.

Dagert, M., & Ehrlich, S. D. (1979). Prolonged incubation in calcium chloride improves the competence of *Escherichia coli* cells. *Gene, 6*(1), 23-28.

Dinovo, E. C., & Boyer, P. D. (1971). Isotopic probes of the enolase reaction mechanism. *Journal of Biological Chemistry, 246*(14), 4586-4593.

Duquerroy, S., Camus, C., & Janin, J. (1995). X-ray structure and catalytic mechanism of lobster enolase. *Biochemistry, 34*(39), 12513-12523.

Ehinger, S., Schubert, W. D., Bergmann, S., Hammerschmidt, S., & Heinz, D. W. (2004). Plasmin(ogen)-binding alpha-enolase from S*treptococcus pneumoniae*: Crystal structure and evaluation of plasmin(ogen)-binding sites. *Journal of Molecular Biology, 343*(4), 997-1005.

Elliott, J. I., & Brewer, J. M. (1980). Binding of inhibitory metals to yeast enolase. *Journal of Inorganic Biochemistry, 12*(4), 323-334.

Faller, L. D., Baroudy, B. M., Johnson, A. M., & Ewall, R. X. (1977). Magnesium ion requirements for yeast enolase activity. *Biochemistry, 16*(17), 3864-3869.

Garret, R., & Grisham, C. (2005). *Biochemistry* (Third ed.) Thomson-Brook/Cole.

Gawronski, T. H., & Westhead, E. W. (1969). Equilibrium and kinetic studies on the reversible dissociation of yeast enolase by neutral salts. *Biochemistry, 8*(11), 4261-4270.

Hang, Q., Woods, L., Feiss, M., & Catalano, C. E. (1999). Cloning, expression, and biochemical characterization of hexahistidine-tagged terminase proteins. *The Journal of Biological Chemistry, 274*(22), 15305-15314.

Heyda, J., Mason, P. E., & Jungwirth, P. (2010). Attractive interactions between side chains of histidine-histidine and histidine-arginine-based cationic dipeptides in water. *The Journal of Physical Chemistry.B, 114*(26), 8744-8749. doi:10.1021/jp101031v

Hocker, B., Jurgens, C., Wilmanns, M., & Sterner, R. (2001). Stability, catalytic versatility and evolution of the (beta alpha)(8)-barrel fold. *Current Opinion in Biotechnology, 12*(4), 376-381.

Holland, M. J., Holland, J. P., Thill, G. P., & Jackson, K. A. (1981). The primary structures of two yeast enolase genes. homology between the 5' noncoding flanking regions of yeast enolase and glyceraldehyde-3-phosphate dehydrogenase genes. *The Journal of Biological Chemistry, 256*(3), 1385-1395.

Holleman, W. H. (1973). The use of absorption optics to measure dissociation of yeast enolase into enzymatically active monomers. *Biochimica Et Biophysica Acta, 327*(1), 176-185.

Horchani, H., Ouertani, S., Gargouri, Y., & Sayari, A. (2009). The N-terminal his-tag and the recombination process affect the biochemical properties of *Staphylococcus aureus* lipase produced in *Escherichia coli. Journal of Molecular Catalysis B: Enzymatic, 61*(3-4), 194-201.

Hosaka, T., Meguro, T., Yamato, I., & Shirakihara, Y. (2003). Crystal structure of *Enterococcus hirae* enolase at 2.8 A resolution. *Journal of Biochemistry, 133*(6), 817-823.

Hughes, M. J., Moore, J. C., Lane, J. D., Wilson, R., Pribul, P. K., Younes, Z. N., Dobson, R. J., Everest, P., Reason, A. J., Redfern, J. M., Greer, F. M., Paxton, T., Panico, M., Morris, H. R., Feldman, R. G., & Santangelo, J. D. (2002). Identification of major outer surface proteins of *Streptococcus agalactiae*. *Infection and Immunity, 70*(3), 1254-1259.

Hutchens, T. W., & Yip, T. T. (1990). Differential interaction of peptides and protein surface structures with free metal ions and surface-immobilized metal ions. *Journal of Chromatography, 500*, 531-542.

Iida, H., & Yahara, I. (1985). Yeast heat-shock protein of mr 48,000 is an isoprotein of enolase.*315*(6021), 690.

Kang, H. J., Jung, S. K., Kim, S. J., & Chung, S. J. (2008). Structure of human alpha-enolase (hENO1), a multifunctional glycolytic enzyme. *Acta Crystallographica.Section D, Biological Crystallography, 64*(Pt 6), 651-657.

Karbassi, F., Quiros, V., Pancholi, V., & Kornblatt, M. J. (2010). Dissociation of the octameric enolase from *S. pyogenes* - one interface stabilizes another. *PloS One, 5*(1), e8810.

Kelly, S. M., Jess, T. J., & Price, N. C. (2005). How to study proteins by circular dichroism. *Biochimica Et Biophysica Acta, 1751*(2), 119-139.

Keresztes-Nagy, S., & Orman, R. (1971). Dissociation of yeast enolase into active monomers. *Biochemistry, 10*(13), 2506-2508.

Kornblatt, M. J., Al-Ghanim, A., & Kornblatt, J. A. (1996). The effects of sodium perchlorate on rabbit muscle enolase--spectral characterization of the monomer. *European Journal of Biochemistry / FEBS, 236*(1), 78-84.

Kornblatt, M. J., Lange, R., & Balny, C. (1998). Can monomers of yeast enolase have enzymatic activity? *European Journal of Biochemistry / FEBS, 251*(3), 775-780.

Kornblatt, M. J., Lange, R., & Balny, C. (2004). Use of hydrostatic pressure to produce 'native' monomers of yeast enolase. *European Journal of Biochemistry / FEBS, 271*(19), 3897-3904.

Kuhnel, K., & Luisi, B. F. (2001). Crystal structure of the *Escherichia coli* RNA degradosome component enolase. *Journal of Molecular Biology, 313*(3), 583-592.

Laemmli, U. K. (1970). Cleavage of structural proteins during the assembly of the head of bacteriophage T4. *Nature, 227*(5259), 680-685.

Lebioda, L., & Stec, B. (1988). Crystal structure of enolase indicates that enolase and pyruvate kinase evolved from a common ancestor. *Nature, 333*(6174), 683-686.

Lebioda, L., & Stec, B. (1991). Mechanism of enolase: The crystal structure of enolase-Mg2(+)-2-phosphoglycerate/phosphoenolpyruvate complex at 2.2-A resolution. *Biochemistry, 30*(11), 2817-2822.

Lebioda, L., Stec, B., & Brewer, J. M. (1989). The structure of yeast enolase at 2.25-Å resolution. An 8-fold β + α-barrel with a novel ββαα $(\beta\alpha)_6$ topology. *The Journal of Biological Chemistry, 264*(7), 3685-3693.

Lederberg, E. M., & Cohen, S. N. (1974). Transformation of *Salmonella typhimurium* by plasmid deoxyribonucleic acid. *Journal of Bacteriology, 119*(3), 1072-1074.

Liti, G., Peruffo, A., James, S. A., Roberts, I. N., & Louis, E. J. (2005). Inferences of evolutionary relationships from a population survey of LTR-retrotransposons and telomeric-associated sequences in the *Saccharomyces sensu stricto* complex. *22*(3), 177-192.

Lobley, A., Whitmore, L., & Wallace, B. A. (2002). DICHROWEB: An interactive website for the analysis of protein secondary structure from circular dichroism spectra. *Bioinformatics (Oxford, England), 18*(1), 211-212.

Lopez-Alemany, R., Longstaff, C., Hawley, S., Mirshahi, M., Fabregas, P., Jardi, M., Merton, E., Miles, L. A., & Felez, J. (2003). Inhibition of cell surface mediated plasminogen activation by a monoclonal antibody against alpha-enolase. *American Journal of Hematology, 72*(4), 234-242.

Manavalan, P., & Johnson, W. C.,Jr. (1987). Variable selection method improves the prediction of protein secondary structure from circular dichroism spectra. *Analytical Biochemistry, 167*(1), 76-85.

Mason, A. B., He, Q. Y., Halbrooks, P. J., Everse, S. J., Gumerov, D. R., Kaltashov, I. A., Smith, V. C., Hewitt, J., & MacGillivray, R. T. (2002). Differential effect of a his tag at the N- and C-termini: Functional studies with recombinant human serum transferrin. *Biochemistry, 41*(30), 9448-9454.

Miles, L. A., Dahlberg, C. M., Plescia, J., Felez, J., Kato, K., & Plow, E. F. (1991). Role of cell-surface lysines in plasminogen binding to cells: Identification of alpha-enolase as a candidate plasminogen receptor. *Biochemistry, 30*(6), 1682-1691.

Nelson, D. L., & Cox, M. M. (2004). *Lehninger Principles of Biochemistry* (Fourth ed.) W. H. Freeman.

Paladini, A. A.,Jr, & Weber, G. (1981). Pressure-induced reversible dissociation of enolase. *Biochemistry, 20*(9), 2587-2593.

Pancholi, V. (2001). Multifunctional alpha-enolase: Its role in diseases. *Cellular and Molecular Life Sciences : CMLS, 58*(7), 902-920.

Pancholi, V., & Fischetti, V. A. (1998). Alpha-enolase, a novel strong plasmin(ogen) binding protein on the surface of pathogenic *Streptococci*. *The Journal of Biological Chemistry, 273*(23), 14503-14515.

Perozzo, R., Folkers, G., & Scapozza, L. (2004). Thermodynamics of protein-ligand interactions: History, presence, and future aspects. *Journal of Receptor and Signal Transduction Research, 24*(1-2), 1-52.

Poyner, R. R., Cleland, W. W., & Reed, G. H. (2001). Role of metal ions in catalysis by enolase: An ordered kinetic mechanism for a single substrate enzyme. *Biochemistry, 40*(27), 8009-8017.

Poyner, R. R., Laughlin, L. T., Sowa, G. A., & Reed, G. H. (1996). Toward identification of acid/base catalysts in the active site of enolase: Comparison of the properties of K345A, E168Q, and E211Q variants. *Biochemistry, 35*(5), 1692-1699.

Pryde, F. E., Huckle, T. C., & Louis, E. J. (1995). Sequence analysis of the right end of chromosome XV in *Saccharomyces cerevisiae*: An insight into the structural and functional significance of sub-telomeric repeat sequences. 11(4), 371-382.

Ralston, G. (1993). *Introduction to Analytical Ultracentrifugation*. Beckman Instruments: Fullerton.

Redlitz, A., Fowler, B. J., Plow, E. F., & Miles, L. A. (1995). The role of an enolase-related molecule in plasminogen binding to cells. *European Journal of Biochemistry, 227*(1-2), 407-415.

Reed, G. H., Poyner, R. R., Larsen, T. M., Wedekind, J. E., & Rayment, I. (1996). Structural and mechanistic studies of enolase. *Current Opinion in Structural Biology, 6*(6), 736-743.

Sahoo, G. C., Dikhit, M. R., Sahoo, G. C., & Das, P. (2008). Homology modeling of *Mycoplasma pneumoniae* enolase and its molecular interaction with human plasminogen. *Bioinformation, 3*(1), 18-23.

Sambrook, J., Fritsch, E. F., & Maniatis, T. (1989). *Molecular cloning. A laboratory manual* (Second Edition) Cold Spring Harbor Laboratory Press.

Schmid, F. X. (1989). Circular dichroism. In T. E. Creighton (Ed.), *Protein structure: A practical approach* (2nd ed., pp. 251-285). Oxford: IRL Press.

Schuck, P. (2000). Size-distribution analysis of macromolecules by sedimentation velocity ultracentrifugation and lamm equation modeling. *Biophysical Journal, 78*(3), 1606-1619.

Schurig, H., Rutkat, K., Rachel, R., & Jaenicke, R. (1995). Octameric enolase from the hyperthermophilic bacterium *Thermotoga maritima*: Purification, characterization, and image processing. *Protein Science.* 4(2), 228-236.

Sims, P. A., & Reed, G. H. (2005). Method for the enzymatic synthesis of 2-phospho-d-glycerate from adenosine 5′-triphosphate and d-glycerate via d-glycerate-2-kinase. *Journal of Molecular Catalysis B: Enzymatic, 32*(3), 77-81.

Stec, B., & Lebioda, L. (1990). Refined structure of yeast apo-enolase at 2.25 A resolution. *Journal of Molecular Biology, 211*(1), 235-248.

Stellwagen, E., Cronlund, M. M., & Barnes, L. D. (1973). A thermostable enolase from the extreme thermophile *Thermus aquaticus* YT-1. *Biochemistry, 12*(8), 1552-1559.

Trepanier, D., Wong, C., & Kornblatt, M. J. (1990). The salt-induced dissociation and inactivation of a mammalian enolase: Evidence for the formation of active monomers. *Archives of Biochemistry and Biophysics, 283*(2), 271-277.

Veronese, F. M., Schiavon, O., Boccu, E., Benassi, C. A., & Fontana, A. (1984). Enzymatically active subunits of *Bacillus stearothermophilus* enolase bound to sepharose. *International Journal of Peptide and Protein Research, 24*(6), 557-562.

Vinarov, D. A., & Nowak, T. (1999). Role of His159 in yeast enolase catalysis. *Biochemistry, 38*(37), 12138-12149.

Wedekind, J. E., Poyner, R. R., Reed, G. H., & Rayment, I. (1994). Chelation of serine 39 to Mg2+ latches a gate at the active site of enolase: Structure of the bis(Mg2+) complex of yeast enolase and the intermediate analog phosphonoacetohydroxamate at 2.1-A resolution. *Biochemistry, 33*(31), 9333-9342.

Westhead, E. W., & McLain, G. (1964). A purification of brewers' and bakers' yeast enolase yielding a single active component. *The Journal of Biological Chemistry, 239*, 2464-2468.

Whitmore, L., & Wallace, B. A. (2004). DICHROWEB, an online server for protein secondary structure analyses from circular dichroism spectroscopic data. *Nucleic Acids Research, 32*(Web Server issue), W668-73.

Wold, F. (1957). Studies on the enzyme enolase. II. kinetic studies. *The Journal of Biological Chemistry, 227*(1), 313-328.

Yip, T. T., Nakagawa, Y., & Porath, J. (1989). Evaluation of the interaction of peptides with Cu(II), Ni(II), and Zn(II) by high-performance immobilized metal ion affinity chromatography. *Analytical Biochemistry, 183*(1), 159-171.

Zhang, E., Hatada, M., Brewer, J. M., & Lebioda, L. (1994). Catalytic metal ion binding in enolase: The crystal structure of an enolase-Mn2+-phosphonoacetohydroxamate complex at 2.4-A resolution. *Biochemistry, 33*(20), 6295-6300.

Zhao, S., Choy, B. S., & Kornblatt, M. J. (2008). Effects of the G376E and G157D mutations on the stability of yeast enolase--a model for human muscle enolase deficiency. *The FEBS Journal, 275*(1), 97-106.